ГОСУДАРСТВЕННЫЙ КОМИТЕТ РОССИЙСКОЙ ФЕДЕРАЦИИ ПО ВЫСШЕМУ ОБРАЗОВАНИЮ

Известия высших учебных заведений

РАДИОФИЗИКА

ежемесячный научно-технический журнал

Издается с апреля 1958 г.

Том XXXIX N 1 Нижний Новгород 1996

Содержание

Лекции и доклады II Международной школы
"ФИЗИКА КОСМИЧЕСКОЙ ПЛАЗМЫ",
представленные для публикации

ВТОРАЯ МЕЖДУНАРОДНАЯ ШКОЛА ПО ФИЗИКЕ КОСМИЧЕСКОЙ ПЛАЗМЫ

Мы начинаем выпуск нашего журнала в 1996 году с материалов Второй Международной Летней Волжской Школы по Физике Космической Плазмы, организованной Научно-Исследовательским Радиофизическими Институтом (Нижний Новгород, Россия) и Институтом Космической Физики (Уппсала, Швеция) в тесном сотрудничестве с Отделом Физики Космоса Института Прикладной Физики Российской Академии Наук (Нижний Новгород, Россия).

Основная задача школы состояла в стремлении ввести научную молодежь в курс актуальных направлений физики плазмы ближнего и дальнего космоса, провести с участием научной молодежи обсуждение ведущими специалистами, исследующими различные астрофизические объекты, общих физических проблем.

В связи с этим, на школе не было отдельных секций, а официальные дискуссии по возможности строились таким образом, чтобы представлять интерес для большого числа участников. Рабочий язык Школы — английский. Для иностранных участников, однако, были организованы неформальные уроки русского языка.

На школе традиционно освещались различные проблемы физики астрофизической плазмы, возможности моделирования динамических процессов в плазме при использовании ближайших к нам космических объектов, наиболее полно диагносцируемых дистанционными методами и с помощью космических аппаратов. Особое внимание при этом было уделено моделированию в условиях ионосферы, возмущенной мощными пучками радиоволн.

Материал освещался в общих лекциях, в лекциях, посвященных конкретным проблемам, в оригинальных сообщениях и стендовых докладах. О характере прочитанных лекций можно составить впечатление из следующего ниже неполного списка их названий:

- C. E. Alissandrakis *(Greece)* "The Magnetic Field of the Solar Corona"
- E. Ergma *(Estonia)* " Millisecond pulsars and low mass X-ray binaries"
- L. M. Erukhimov *(Russia)* "Low-Frequency Turbulence in Space Plasma"
- D. T. Farley *(Germany)* "Probing a Plasma with Incoherent Scatter Radar: Techniques and Limitations"
- J. C. Foster *(USA)* "Ionosphere-Magnetosphere Coupling Phenomena at Mid Latitudes: Incoherent Scatter Radar and Satellite Techniques and Results"

- V. L. Ginzburg *(Russia)* "Radiation by Uniformly Moving Sources"
- E. Mjoelhus *(Norway)* "The Theory of Electrostatic Excitations in Ionospheric Radio Experiments"
- M. J. Rycroft *(France)* "Some Current Challenges in Space Plasma Physics"
- P. Stubbe *(Germany)* "Stimulated Electromagnetic Emission near Gyroharmonics, and its Physical Implications"
- B. Thidé *(Sweden)* "Using the Earth's Ionosphere as a Space Plasma Laboratory for Controlled Excitation of Radio Emission"
- D. A. Varshalovich and A. Potekhin *(Russia)* "Astrophysical Testing Possible Variability of Fundamental Physical Constants over Cosmological Time-scale"
- L. Vlahos *(Greece)* "Particle Acceleration and Radiation from Complex Active Regions and Turbulent Flows"
- V. V. Zheleznyakov *(Russia)* "Plasma Envelopes of Magnetic White Dwarfs"

- H. Aurass *(Germany)* "Solar Decimeter and Meter Wave Spectroscopy — Recent Results about Energy Storage and Particle Acceleration in Small- and Large Scale Structures of the Corona"
- P. A. Bespalov and Yu. V. Chugunov *(Russia)* "The Planetary Generator Effect in Space Plasma"
- W. Boeck *(USA)* "Observations of Lightning Induced Optical Phenomena in the Mesosphere and the Lower Ionosphere"
- A. D. Danilov *(Russia)* "Plasma Physics Problems in Ionospheric Studies"
- N. S. Erokhin *(Russia)* "Long-Term Resonant Wave-Particle Interaction in Inhomogeneous Plasma"
- G. B. Gelfreikh *(Russia)* "Problems of Magnetospheres of the Solar Active Regions as Based on Microwave Observation"
- E. Gromov and V. Talanov *(Russia)* "High-Frequency Pulses in Nonhomogeneous Plasma with Pondermotive Nonlinearity"
- A. V. Gurevich and K. P. Zybin *(Russia)* "Isolated Striations Developed During Ionospheric Modification"
- V. I. Klyatskin *(Russia)* "Statistical Topography of Random Processes and Fields in Application to Wave Propagation in Random Media"

- M. E. Koepke *(USA)* "Signatures of processes responsible for spectral broadening of ion cyclotron waves"
- G. Z. Machabeli and A. D. Rogava *(Georgia)* "Surprises of the Centrifugal acceleration"
- W. Manheimer *(USA)* "Possible New Applications of Near Space for Remote Sensing"
- C.-V. Meister *(Germany)* and V. A. Lierovsky *(Russia)* "Wave Generation by Moving Ionospheric Plasma Clouds"
- H. O. Rucker *(Austria)* "Non-Thermal Planetary Radio Emission"
- V. Yu. Trakhtengerts *(Russia)* "Wave-Wave Interactions in Whistler Frequency Range in Space Plasma"
- V. V. Vaskov *(Russia)* "Excitation of LF Waves in the Upper Ionosphere in Heating Experiments by Beams of Accelerated Suprathermal Electrons"
- A. W. Wernik *(Poland)*"Chaotic *vs* stochastic behavior of the high-latitude density fluctuations"
- Yu. M. Yampolsky and P. V. Bliokh *(Ukraine)* "Interaction between ELF and HF signals in the Earth's Ionosphere"
- L. M. Zelenyi *(Russia)* "Regular and Chaotic Dynamics of Magnetotail Plasma"
- и другие

Естественно, что далеко не все лекции публикуются в выпусках журнала. По возможности в публикуемых материалах Школы освещены основные оригинальные результаты, которые, кроме того, еще не опубликованы в других журналах. Первый выпуск посвящен результатам исследований в астрофизике и физике Солнца, второй, и частично, третий в большей степени посвящены физике околоземной и ионосферной плазмы.

Мы надеемся, что в публикуемых статьях читатель найдет полезные для него сведения. Мы также пользуемся случаем, чтобы пригласить читателей принять участие в Третьей Международной Летней Волжской Школе, которая состоится в начале июня 1997 г.

Мы будем рады Вашему участию.

Председатели Школы: Лев Ерухимов

Бу Тидé

SOME CURRENT CHALLENGES IN SPACE PLASMA PHYSICS

M. J. Rycroft

An overview of the subject of space plasma physics is attempted. This encompasses a discussion of various ground-based and satellite studies of the near-Earth space environment, with its marked temporal and spatial variations, theoretical investigations and numerical simulations.

The important distinction is drawn between (passive) studies of elements of the natural system, aimed at the difficult task of understanding the self-consistent evolution of some natural processes, and (active) investigations, which either probe or modify natural processes, in order to improve understanding of cause and effect (e.g. of energy transformations) within the system. Linear, nonlinear and chaotic processes can occur.

Attention is paid to:

(a) Energetic events on the Sun,

(b) Large scale features of the interplanetary medium, both observed directly and via scintillations of distant radio stars,

(c) The magnetosphere in general, and the aurora in particular,

(d) Wave-particle interactions, especially cyclotron resonance phenomena, and

(e) The ionosphere, particularly when heated by powerful radio waves.

The approach adopted is to place these special topics in the context of the Solar Terrestrial Energy Program (STEP) of ICSU's SCOSTEP. Finally, mention is made of some benefits to humanity of studies of space plasma physics phenomena.

1. INTRODUCTION

Space plasma physics is basically an experimental subject. Remote observations of the near-Earth space environment have been made from the ground for over seventy years (e.g. using high frequency (HF, 3 – 30 MHz) radio waves to sound the ionosphere). Direct observations of plasma properties, energetic charged particles and electric and magnetic fields (both direct current (DC) and alternating current (AC)) have been carried out using instruments aboard Earth-orbiting satellites or interplanetary spacecraft for half that time. The field has therefore now reached a certain maturity.

The theoretical foundations of plasma physics have been developed, in parallel, over the same period. Either single particle (collisionless) or fluid (collision-dominated) approaches can be followed using Newton's laws of motion and Maxwell's equations of electromagnetism. The laws of conservation

of mass, momentum, energy, electric charge and magnetic flux may be applied, steady–state solutions derived and constitutive relations used (see [1]). A plethora of waves (basically electrostatic, electromagnetic or magnetohydrodynamic in nature) may propagate, and the appropriate dispersion relations derived. The solution to $D(\omega, \mathbf{k}) = 0$ gives $\omega(\mathbf{k})$, and determines the normal modes of the plasma, the phase velocity of the wave $v_\phi = \omega/k$, and the group velocity $v_g = \partial\omega/\partial k$. Here ω — angular wave frequency, k — wavenumber, Boltzmann's constant When the roots of the dispersion relation are complex, instabilities occur, leading to wave growth. For this, a source of free–energy — such as a beam or current, that is a non-Maxwellian velocity distribution function — is required [2]. Initially, the growth is linear, but often nonlinearities develop rapidly, with charged particles being trapped in the potential well of the wave (wave–particle interactions); the distribution function is modified. Turbulence, both microscopic and macroscopic, may arise when different modes interact, and lead to chaos. The results deduced in such ways have been applied to a wide variety of space plasma situations. Analytical studies, traditionally strong in eastern countries, are now giving way to numerical modelling using rapidly developing simulation techniques and powerful computers, especially in the west.

Recent progress in five areas:

(a) Energetic events on the Sun,

(b) Large scale features of the interplaense photosphere both observed directly and via scintillations of distant radio stars,

(c) The magnetosphere in general, and the aurora in particular,

(d) Wave-particle interactions, especially cyclotron resonance phenomena,

(e) The ionosphere, particularly when heated by powerful radio waves is discussed, and significant current challenges are mentioned.

2. ENERGETIC EVENTS ON THE SUN

Solar flares [3] occur in complex sunspot groups [4] after the eruption of a solar prominence when a sudden change (characteristic time scale $\tau \sim 10$ s) of the coronal magnetic field topology, termed reconnection, happens [5]. The energy density $B^2/2\mu_0$ (here B — magnetic flux density, μ_0 — permittivity of free space) of two oppositely directed magnetic fields, separated by strong electric currents, is converted into charged particle beams (with energy density Nmv^2) and heat (energy density NkT). Here N — plasma number density, m — particle mass, v — velocity, T — temperature. The temperature can reach $5 \cdot 10^7$ K [6]; X-rays [7] and gamma-rays [8] are emitted as bremsstrahlung radiation when energetic electrons move down into the dense photosphere.

Wave–particle interactions occur, and ions are accelerated stochastically on open field lines [7, 9].

Culhane [6] has presented a superposed X-ray image obtained by the Yohkoh satellite at 20.12 U.T. on 24 January 1992 on a simultaneous image from a ground–based coronagraph. The previously existing underlying prominence had disappeared, indicating that the earlier closed magnetic field structure was blown open by plasma, a so-called coronal mass ejection.

Harrison [10] has suggested that, some tens of minutes before a solar flare, a large magnetic arch structure (termed a precursor arch) brightens, and that this launches the coronal mass ejection (CME) — see Fig. 1. Later, a solar flare may occur at one foot of this arch structure. Thus, a solar flare does not cause a CME.

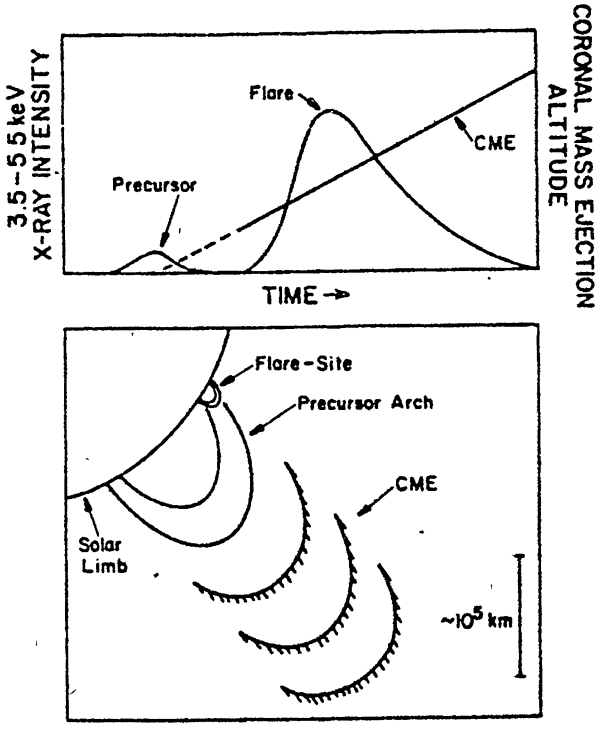

Fig. 1. Upper panel: time profile of soft X-rays before and during a solar flare, and corresponding altitude of the coronal mass ejection (CME). Lower panel: diagram showing the launching of a CME from a precursor arch, a magnetic field loop tied to the photosphere (from [10]).

A consideration of magnetic field turbulence in convection cells of the photosphere led Milovanov and Zelenyi [11] to present a fractal model for the solar wind.

Low density regions in the solar corona on open magnetic field lines, which do not emit X-rays, are termed coronal holes. Analysing thirteen years of data

of solar cycle 21 and part of 22, McIntosh et al. [12] have shown that the area of southern coronal holes exhibits a 19.5 month periodicity, whereas that for northern coronal holes does not. Since coronal holes, high speed solar wind streams and geomagnetic activity are strongly interrelated [13], this result could lead to better predictions of geomagnetic activity [14, 15].

There is much complex plasma physics involved in the redistribution of energy (on time scales ranging from fractions of a minute to decades) in the solar photosphere, chromosphere and corona. Such processes need to be better understood before good predictions of solar activity, and hence of features in the interplanetary medium which enhance geomagnetic activity [15], will become possible.

3. INTERPLANETARY MEDIUM

Observations of the scintillations of spacecraft radio transmissions (phase, or Doppler, scintillations) or of the intensity scintillations of distant radio stars give information on the spatial structures in the solar wind moving outwards from the Sun. Within 0.2 AU, Woo and Gazis [16] find that the average solar wind speed is slow, but with high variability related to CMEs. Near 0.5 AU, they report narrow regions of enhanced scintillation at 2.3 GHz associated with compressed plasma at the leading edges of recurrent high speed solar wind streams.

Bame et al. [17] have investigated high speed solar wind streams on the edge of the southern coronal hole at the Ulysses spacecraft. Energetic ions and electrons observed at Ulysses also showed a prominent 26 day (solar rotation) periodicity [18], evidence for a series of corotating interaction regions and their associated shocks.

Harrison [19] and Harrison et al. [20] considered 81.5 MHz radio star scintillations, identifying discrete structures, most probably related to transient density enhancements, and also periodic activity, related to interplanetary structures corotating with the Sun. They found weak correlations with geomagnetic activity.

Numerical simulations of such results have been presented by Tappin et al. [21] using a three–dimensional, time dependent magnetohydrodynamic (MHD) model. Both they and Akasofu and Lee [22] conclude that this is a promising tool for future investigations, given appropriate input conditions.

Radio emissions generated in the heliosphere away from the Sun also provide useful information on the structure of the interplanetary medium. Gurnett [23] has reviewed the generation of type III radio bursts, produced as electrostatic oscillations (Langmuir waves) by energetic electrons from solar flares which mode convert to electromagnetic radiation via nonlinear wave–wave interactions — see Fig. 2. On the other hand, type II radio bursts are produced by electrons accelerated at interplanetary shocks driven by CMEs [24] (see

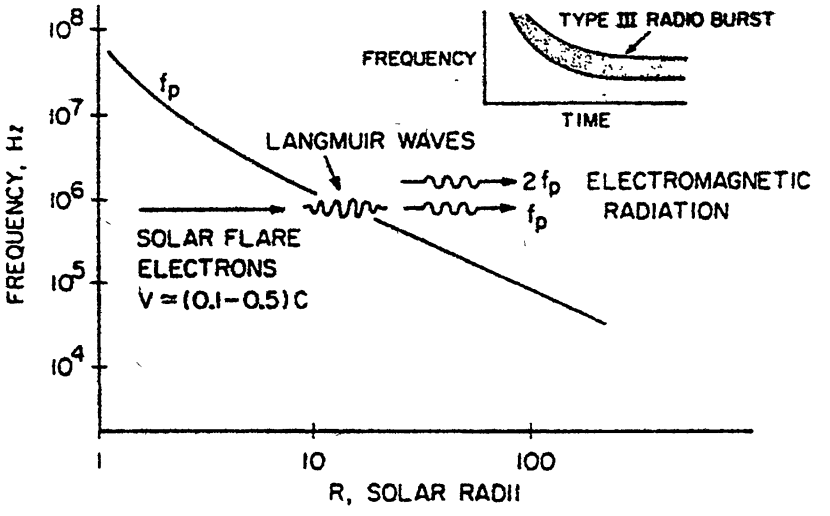

Fig. 2. The downward frequency drift of a type III radio burst is caused by the decreasing electron plasma frequency, f_p, encountered by the solar flare electrons as they stream outward from the Sun. Electromagnetic radiation is produced at f_p and $2f_p$ by mode conversion from Langmuir waves (from [23]).

Fig. 3). For both type III and type II radio bursts, radiation is observed at the electron plasma frequency and its second harmonic. Because the plasma frequency decreases with increasing radial distance away from the Sun, the frequency emitted decreases as time increases. Since the shock propagation speeds ($< 10^3$ km·s^{-1}) are much less than the solar flare electron speeds (> 104 km·s^{-1}), the frequency drift rates of type II radio bursts are much less than those of type III events.

The Langmuir waves associated with a type III burst observed one hour after a flare onset have a characteristic beat pattern. Gurnett et al. [25] believe this signal (up to 1.7 mV·m^{-1} only) to be due to the combination of a beam–driven Langmuir wave and the oppositely propagating Langmuir wave. Kellogg et al. [26] considered such events, having the characteristics of collapsed Langmuir waves, to result from a very nonlinear process predicted for a sufficiently strong Langmuir wave electric field by Zakharov [27]. Further investigations have been carried out by Li [28] and by Goldman and Newman [29].

The local plasma frequency at the spacecraft, for example Ulysses [30] may be deduced from solar wind plasma line radiation, generated on a long antenna by the random thermal motion of ambient electrons. Observations made by Ulysses at high heliographic latitudes are likely to produce new observations to challenge current theoretical ideas.

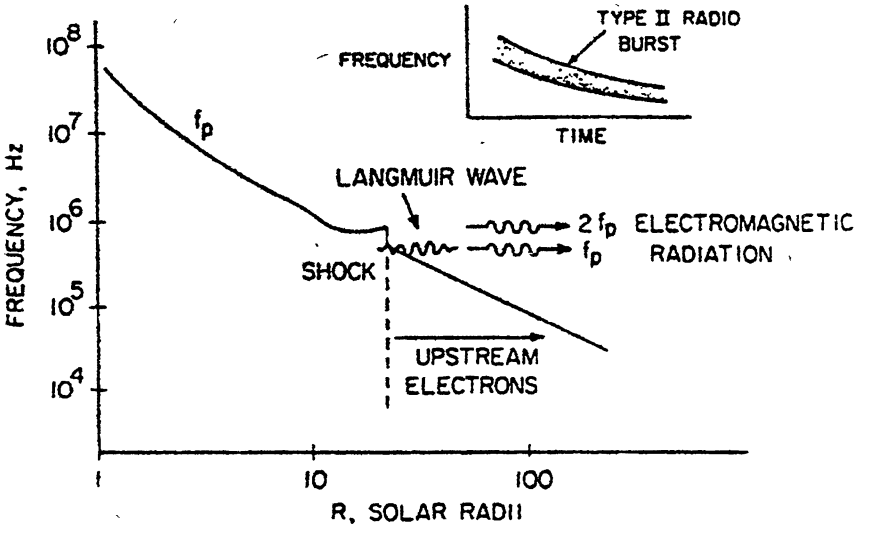

Fig. 3. The downward frequency drift of a type II radio burst is caused by the decreasing electron plasma frequency encountered by the interplanetary shock as it propagates outward from the Sun. Electrons accelerated at the shock are believed to produce Langmuir waves which mode convert to electromagnetic radiation at f_p and $2f_p$ (from [23]).

Natural radio and plasma waves are present throughout the heliosphere [30, 31]. Besides types III and II solar wind radio bursts, the planets are powerful sources. It is believed that the source of Jupiter's broadband kilometric radiation (bKOM) (free space wavelength $\sim 5 \cdot 10^3$ km) is the outer edge of Io's plasma torus. Radio emissions from auroral field lines of Jupiter and the Earth (auroral kilometric radiation, AKR) are also strong. They are considered to be produced by an electron cyclotron maser process, although the details are not fully understood.

Strong radio emissions are observed in the outer heliosphere at ~ 3 kHz. These are thought to be produced by a disturbance (an interplanetary shock wave) propagating from the Sun into the outer heliosphere and interacting with its boundary, the heliopause, at $> 10^2$ AU [23, 31]. It is likely to be some time before the Pioneer and Voyager spacecraft reach the heliopause in order to investigate it directly.

4. MAGNETOSPHERE

The interaction between the solar wind flowing away from the Sun and the Earth's magnetosphere is still not properly understood after more than thirty years of study [32, 33]. In this interaction, the physics of the magnetopause

is crucial; it is a thin boundary [34] separating two plasmas having different origins [35, 36].

The time varying reconnection of interplanetary and terrestrial magnetic field lines at the magnetopause can be thought of as causing a time varying electric field directed from dawn to dusk across the magnetosphere [37, 38]. Together with the electric field associated with the viscous interaction between the solar wind and the tail of the magnetosphere [39], this leads to large scale plasma motions within both the tail and body of the magnetosphere and in the two polar cap ionospheres [40, 41, 42]. The physical mechanisms responsible for redistributing energy stored in various forms in the magnetospheric plasma during geomagnetic storms — for example, to enhance the ring current — and also during auroral substorms are still a matter of debate [43, 44, 45]. The recently published book, edited by Ashour–Abdalla et al. [46], is helpful in this regard.

A promising research direction is the cause and effect study of the interaction between a large scale ($\sim$ 0.3 AU) magnetic field structure (termed a plasma cloud) and the magnetosphere [47]. Labelle et al. [48] have similarly studied smaller scale ($\sim 10^{-4}$ AU), impulsive solar wind discontinuities. The magnitude of the southward component of the interplanetary field is often found to be important in such interactions, possibly indicating transient reconnection near the subsolar magnetopause [49]. On the other hand, Woch and Lundin [50] report that the injection of magnetosheath plasma via transient boundary layer processes has the highest probability when the interplanetary magnetic field is confined to the ecliptic plane. Fairfield [51] and Roelof and Sibeck [52] have reported variations of the size and shape of the magnetosphere over the solar cycle.

The development of numerical models of magnetic reconnection is an expanding field [53, 54, 55]. Atkinson [56] has presented a novel mechanism whereby reconnection at X lines can cause discrete auroral arcs. As computer codes become more sophisticated, further significant results are to be expected from using this powerful technique.

The roles played by wave–particle interactions at the magnetopause have been reviewed by Thorne and Tsurutani [57]. The modified two stream instability, the lower hybrid drift instability, a velocity shear instability or an electromagnetic ion cyclotron wave may be important.

Winckler et al. [58] and Winckler [59] have presented the elegant results of active rocket–borne experiments injecting electron beams into the magnetosphere. A downward looking television camera in space viewed the glow generated by ionisation of the neutral atmosphere, near 100 km attitude, due to a 36 keV, 0.18 A pulsed electron beam injected upwards at a pitch angle of 130°. The helical Larmor orbit of the electrons is clearly evident — see Fig. 4. Electron echoes from the other hemisphere at $L \sim 7$ (L — McIlwain's parameter) were detected, from which the lengths of inflated field lines have been

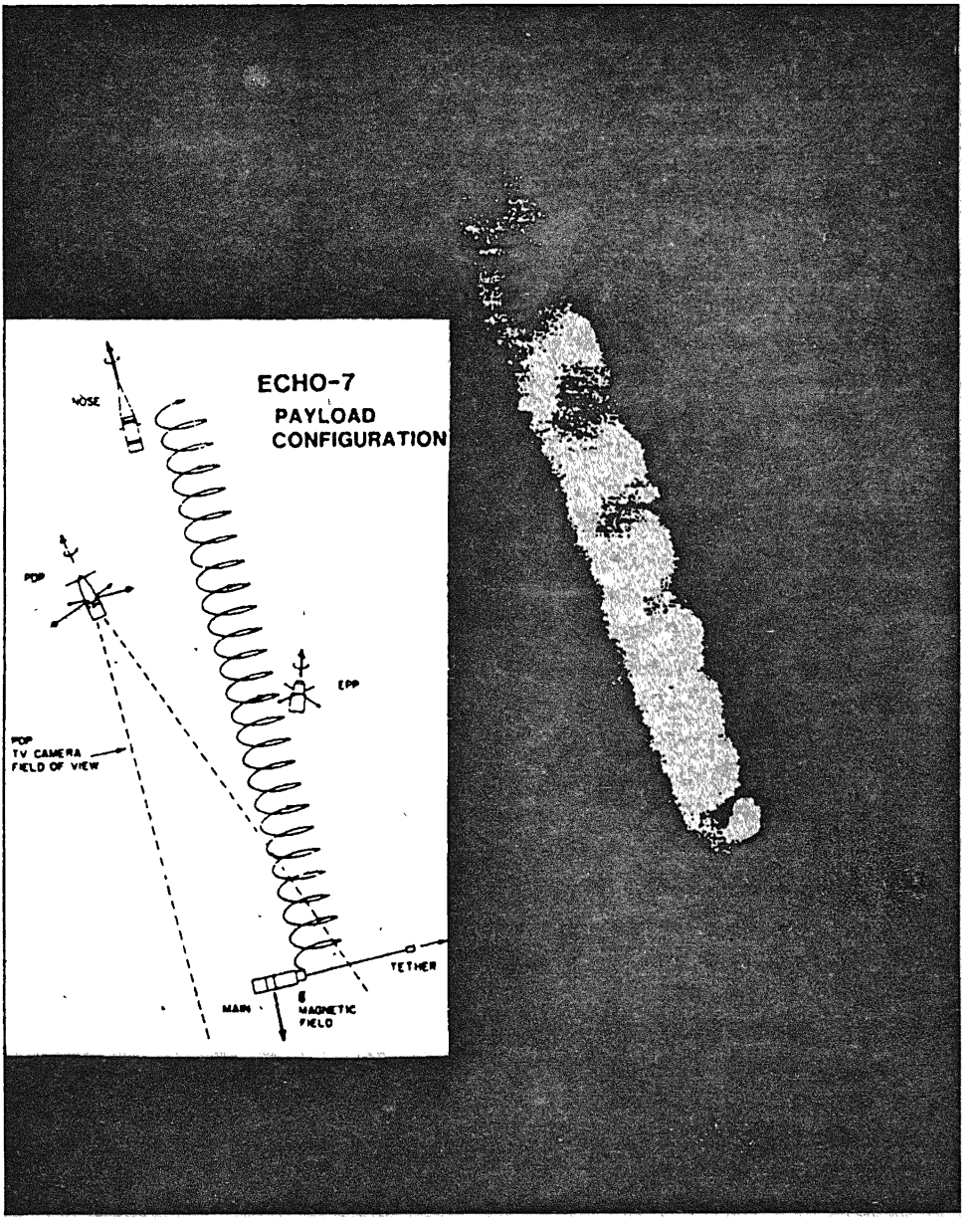

Fig. 4. Image from a television camera looking down to the 100 km altitude of a rocket–borne electron gun, injecting pulses of 36 keV electrons, whose cyclotron orbits are clearly evident (from [58]).

derived. Pitch angle diffusion, beam–plasma interaction phenomena, cross-L drifts, fluctuating electric fields in the magnetosphere and field–aligned potential drops have also been estimated. There is considerable potential for further similar and technically challenging experiments, especially at lower L-values.

Extensive plasma observations of auroral features, with good spatial and temporal resolution, are now being made by the Freja satellite at altitudes between 600 km and 1800 km in the topside ionosphere [60, 61]. Global views of the auroral oval are obtained from the Dynamics Explorer satellite, at higher altitudes [62, 63].

Rockets are also excellent observational platforms for investigating auroral phenomena. Garbe et al. [64] report that ions observed within a downcoming of $\sim$ 10 keV auroral electrons near local midnight were heated — below the rocket — to $\sim$ 3 eV transversely to the geomagnetic field. Moving adiabatically up to the rocket, they have a cone–shaped velocity distribution and are therefore termed ion conics — see Fig. 5. They are a source of ions which, when further accelerated, contribute to the magnetospheric ring current.

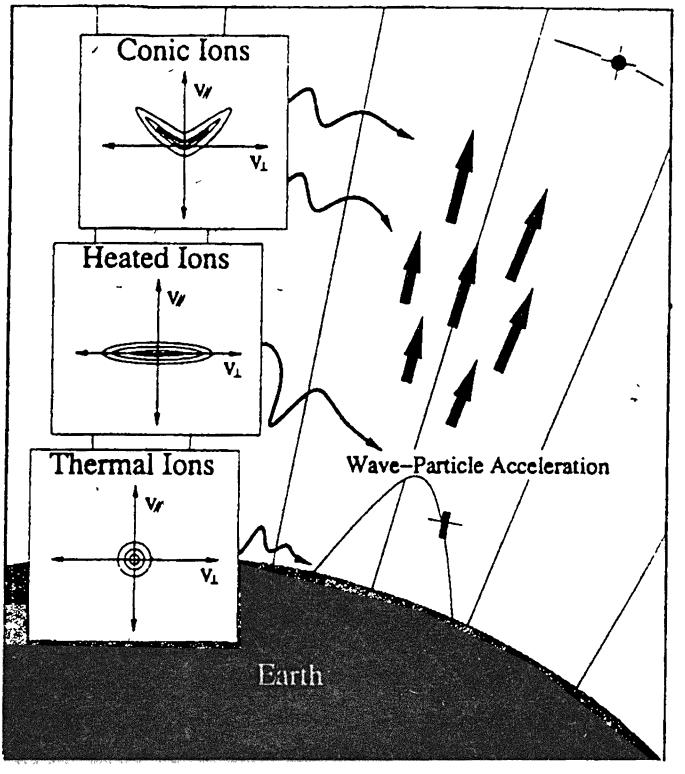

Fig. 5. Diagram indicating rocket and satellite studies of the transverse heating of ionospheric ions (by wave–particle interactions) and their adiabatic, upwards motion so that their velocity distribution function becomes a conic (from [65]).

Oxygen ion electrostatic cyclotron waves ($\sim$ few mV·m^{-1}) and cool ($\sim$ 0.1 eV) ions moving downwards were observed in the same region. The amplitude and coherency of these waves appear to be inadequate to produce the transverse heating. Also observed are waves ($\sim$ 100 mV·m^{-1}) near and above the lower hybrid resonance frequency in association with auroral hiss (see also [65, 66]). Arnoldy et al. [67] and Kintner et al. [68] believe that these intense lower hybrid waves, which occur in thin filamentary (along the geomagnetic field) regions of depleted plasma density [69], cause the transverse acceleration of ions. Bursts of these waves (solitary wave structures) occur about once per second, during bursts of field–aligned auroral electrons. The mechanism involved is considered to be due to the self–focusing of nonlinear lower hybrid waves and their collapse [70]. Similar observations need to be made on the dayside, to investigate cusp phenomena [71].

The results discussed in the previous paragraph could be taken to confirm earlier ideas put forward by Bingham et al. [72] that auroral electrons are stochastically accelerated by electrostatic lower hybrid waves rather than by an electrostatic potential difference. After all, observations of **every** auroral phenomenon indicate a dynamic, time varying situation, rather than a static condition. It has to be remembered that it is over twenty years since Hall and Bryant [73] introduced the idea that the electric field accelerating auroral electrons was fluctuating on time scales of milliseconds or less. The source of free energy for the waves could be earthward streaming ions in the boundary plasma sheet [72].

This fundamental field is surely ripe for further experimental, theoretical and numerical simulation studies.

5. WAVE–PARTICLE INTERACTIONS

One topic of the previous section, concerning auroral acceleration processes, has — perforce — dealt with the physics of wave–particle interactions. Attention is now focussed on phenomena at lower L-values.

Unstructured in the frequency–time domain, plasmaspheric ($L \sim 4$) hiss has been reviewed by Hayakawa and Sazhin [74]. It is believed to be generated by the electron cyclotron instability, with an anisotropic velocity distribution operating quasilinearly near the equatorial plane (see also [75]).

Also in the very low frequency (VLF, 3$\div$30 kHz) band, chorus (composed of discrete, rising frequency tones) is observed just outside the plasmapause [76]. Sazhin and Hayakawa [77] again invoked the electron cyclotron instability, with the nonlinear deformation of the hot electron distribution function, producing almost monochromatic wavelets. Recently Trakhtengerts et al. [78] proposed a step–like deformation of the electron distribution function at the boundary between electrons which are gyroresonant with hiss and those which are not,

leading to the generation of quasi monochromatic wavelets at the upper frequency of a hiss band. This step is the analogue, in velocity space, of a shock in physical space.

Omura et al. [79] reviewed VLF triggered emissions, considering the nonlinear gyroresonant current which causes nonlinear wave growth and a nonlinear frequency shift (see also [80]). They pointed out unresolved problems which may best be tackled by numerical modelling.

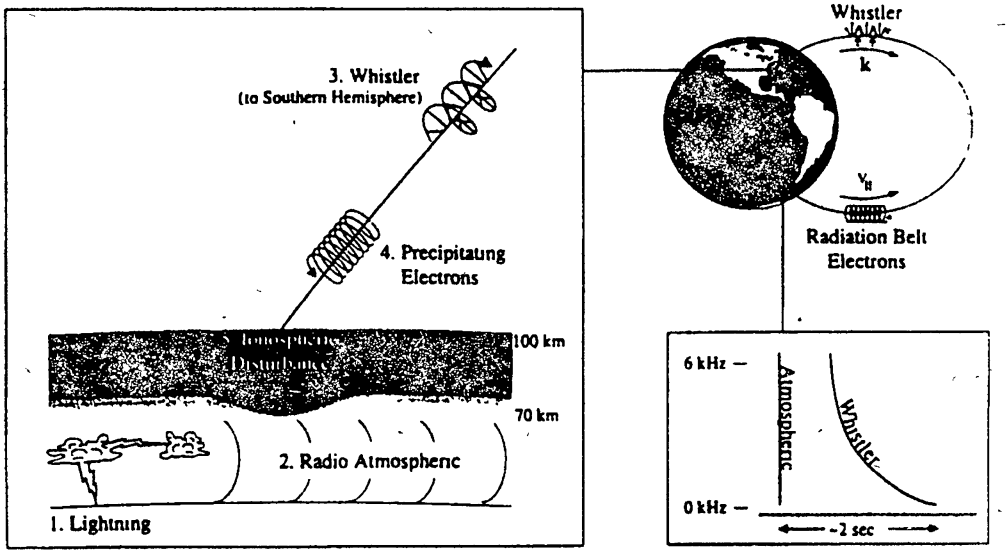

Fig. 6. Diagram illustrating electron precipitation produced by ducted whistlers.

Rycroft [81] has reviewed the salient features of the interactions between lightning-generated whistler mode waves and energetic electrons trapped in the magnetosphere. Via the electron cyclotron resonance mechanism, these lead to the precipitation of electrons into the upper atmosphere and hence to amplitude and/or phase variations of VLF radio signals propagating in the Earth–ionosphere waveguide — see Fig. 6. This diagram illustrates electron precipitation produced by ducted whistlers. A lightning discharge in the northern hemisphere (1) launches a radio atmospheric, or "sferic" (2), which propagates in the Earth–ionosphere waveguide. Enhancements of the plasma above the ionosphere, aligned with the geomagnetic field and known as "ducts", can trap a portion of the sferic energy and cause it to propagate along a field line to the opposite hemisphere as a whistler (3). During its journey the circularly polarised whistler can interact with gyrating energetic radiation belt electrons, scattering them in pitch angle so that some escape from their geomagnetic trap (4). Upon striking the ionosphere, the precipitating electrons cause significant secondary ionisation (5). Meanwhile, the whistler emerges from its duct and can be observed, along with the subionospherically propa-

gating causative sferic, with broadband VLF radio equipment in the southern hemisphere (from [82]). Taranenko et al. [83] have estimated the magnitude of similar transient effects on VLF signals due to the direct heating and ionisation of the lower ionosphere by strong electromagnetic fields from nearby lightning. The relative importance of these two processes will be discussed at the URSI (1996) General Assembly, as will the heating of the nighttime lower ionosphere by signals from VLF transmitters [84].

Nonlinear wave–wave interactions in the ionosphere between signals from a ground–based VLF transmitter (at Siple station, Antarctica) and a naturally occurring emission ~ 2.4 kHz have been reported by Ohnami et al. [85]. Trakhtengerts and Hayakawa [86] discussed the importance of the wave intensities for such interactions, and for the creation of sidebands. Nonlinear processes occurring in planetary magnetospheres have been generally reviewed by Gurnett [87].

Xu and Yeh [88] and Yeh and Xu [89] have studied the propagation of a VLF wavepacket in a dispersive and anisotropic medium. This causes the polarisation of the wavepacket to vary (from circular) as it propagates. This effect should be considered when modelling wave–particle interactions.

Numerical modelling of wave–particle and wave–wave interactions is proceeding apace. For example, Serizawa and Dum [90] have analysed finite beam–driven instabilities, while Nishikawa et al. [91] reported on a three–dimensional electromagnetic particle code to study electron beam–driven whistler waves. The latter's simulations were useful in relation to an experiment carried out aboard Spacelab 2.

6. IONOSPHERE

The ionosphere and thermosphere together constitute a weakly ionised plasma, with strong coupling between the ions and neutral molecules. The ions and neutrals respond differently to energy inputs in situ, from above and from below. Many phenomena in the polar and high latitude ionospheres are strongly controlled by magnetospheric processes. Ground–based experiments at high latitudes act as a "window" on space and complement rocket and satellite studies.

Rishbeth and van Eyken [92] discussed the first ten years of European incoherent scatter radar (EISCAT) operations in Northern Scandinavia, whereas Cowley et al. [93] presented the case for the extension of research to higher latitudes, using the Svalbard radar. Highlights of EISCAT results are as follows: sporadic-E layers [94], E-region electron densities, temperatures and $\mathbf{E} \wedge \mathbf{B}$ drifts [95], F-region plasma velocities in and near auroral arcs [96] and electron temperatures via photoelectron–enhanced plasma lines [97]. Hultqvist [98] mentions EISCAT observations in his review of upward flowing ionospheric ions.

The principles of coherent radar backscatter from irregularities created by plasma instabilities in the E-region have been reviewed by Schlegel [99], with emphasis being placed on the spectrum of the echoes observed under different auroral conditions. Kofman and St. Maurice [100] have discussed non-Maxwellian velocity distributions which lead to asymmetrically distorted spectra observed by EISCAT. For example, strong electric fields transverse to the geomagnetic field can accelerate ions to supersonic speeds, thereby creating asymmetric spectra. Applications of pure plasma physics theoretical results to ionospheric conditions lead to progress.

Heating the auroral ionosphere using powerful radio transmitters not only produces new observational results but also calls for new theories. Turunen et al. [101], Cannon [102] and Cannon et al. [103] reported the serendipitous observation of the generation of extremely low frequency (ELF, 3 Hz ÷ 3 kHz) radio signals via the nonlinear demodulation of low frequency (LF, 30 ÷ 300 kHz) or medium frequency (MF, 300 kHz ÷ 3 MHz) transmissions by the auroral electrojet. Similar, but controlled, experiments have been performed by Vas'kov et al. [104]. Also using the Sura heating facility near Nishny Novgorod, Blagoveshchenskaya et al. [105] reported the field–aligned scattering of diagnostic HF radio waves. The first direct investigation of electrojet temperature modifications by HF radio waves was reported by Robinson et al. [106] — see Fig. 7. They confirmed a recent theoretical model [107] in which the combined effects of radio frequency (RF) heating and of natural plasma turbulence associated with the Farley–Buneman instability had been considered.

Noble and Gordon [108] presented some results of the first two frequency, high power heating experiment using obliquely incident HF heater waves. HF sidebands were observed. Sergeev et al. [109] have reported stimulated electromagnetic emissions (SEE) at high harmonics of the electron cyclotron frequency produced by the Sura facility. When the heater is turned off, the emissions decay with a characteristic time scale of plasma wave damping. Ermakova and Trakhtengerts [110] have discussed beams of superthermal electrons in field–aligned electron density depletions which are associated with these experiments. Artificial plasma density irregularities created in such experiments have been reported by Boiko and Erukhimov [111]. Rietveld et al. [112] have reviewed the ionospheric heating experiments carried out at Tromsø. All these active experiments enable the field of ionospheric plasma physics to develop considerably.

Electron density depletions and whistler mode noise enhancements close to auroral arcs were reported by James [113] and James et al. [114]. For this sounding rocket experiment with an insulated conducting tether, these were considered to be sheath wave phenomena created by suprathermal particles which close the current due to auroral precipitation.

Another type of active experiment involves the injection of > 1 kg of

neutral molecules (such as barium or lithium) which are readily photoionised by solar ultraviolet radiation. On the combined release and radiation effects satellite (CRRES), studies of critical velocity ionisation [115], the geometry of the geomagnetic field observed via ion tracers, auroral excitation and ion–ion coupling were attempted [116]. Oraevsky et al. [117], Namazov et al. [118] and Milinevsky et al. [119] have discussed various observations made in Cuba following CRRES barium releases.

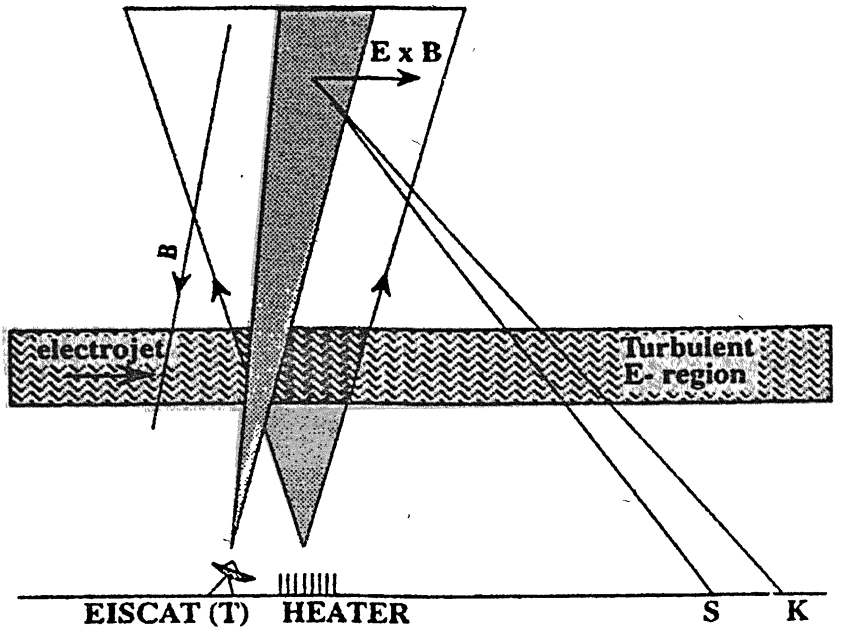

Fig. 7. Diagram showing the arrangement for EISCAT studies at Tromsø(T), Sodankyla (S) and Kiruna (K) of the ionospheric E-region heated by a powerful, colocated radio transmitter operating at 4.5 MHz (from [106]).

Geomagnetic storms perturb the ionosphere on a global scale. Some observational results for the great storm of 13 and 14 March 1989 and mechanisms have been reviewed by Rycroft [120]. Kurth [121] has commented upon this particular storm, and presented observations from Greenspan et al. [122] showing electron densities reduced by an order of magnitude from 20°N to 20°S magnetic latitude. These are believed to be due to electric fields, of magnetospheric origin, raising the equatorial ionospheric plasma, which then drifts polewards. Yeh et al. [123] have analysed the longitudinal dependence of the depleted F2 regions. Buonsanto et al. [124] and Foster et al. [125] have reported detailed observations of the ionosphere over eastern North America during geomagnetic disturbances one year later. Studies of magnetic storm phenomena in the ionosphere not only provide insight into the physical mechanisms at work but also are of practical benefit.

7. RELEVANCE OF SOLAR–TERRESTRIAL PHYSICS PHENOMENA TO HUMANITY

Nowadays, humanity routinely uses high technology services whose performance can be upset by unusual solar–terrestrial events, such as magnetic storms. These include:

- the disruption of electric power systems at mid to high latitudes, caused by changing ionospheric currents inducing e.m.f.s. and producing transient currents which burn out transformers,
- the induction of e.m.f.s. producing currents in long conductors, for example those used for cable communications or oil/water pipelines,
- the disruption of aeromagnetic surveys by time varying ionospheric currents perturbing the geomagnetic field,
- the disruption of ground–based and satellite radio communications, and of satellite navigation systems, by the disturbed ionosphere,
- the upset or even failure of chips, instruments or entire satellites in geostationary orbit, due to energetic charged particle and/or plasma effects,
- the destabilisation and decay of polar orbiting satellites by geomagnetic field changes and by thermospheric density changes, and
- radiation dangers to the crew and passengers of high–flying aircraft, and to astronauts, due to enhanced fluxes of energetic charged particles.

Improving knowledge of, and eventually predicting, disturbances in the near–Earth environment is a challenging and worthwhile task.

8. CONCLUDING REMARKS

Some recently obtained results, and some promising areas for future research, in the field of solar–terrestrial physics have been discussed in this broad review. Experimental, theoretical and modelling studies — carried out interactively — will surely lead to further progress.

REFERENCES

1. Chen F.F. Introduction to plasma physics. — Plenum Press, 1974. 329 pp.
2. Gary S.P. Theory of space plasma microinstabilities. — Cambridge University Press, 1993. 181 pp.
3. Foukal P.V. Solar astrophysics. — John Wiley & Sons, 1990. 475 pp.

4. Zirin H., Wang H. // Nature, 1993. V. 363. P. 426.
5. Priest E. R. — In: Solar system plasmas in space and time. /Eds. by J. L. Burch and J. H. Waite, Jr. — AGU, 1994. P. 1.
6. Culhane L. // Nature, 1993. V. 362. P. 496.
7. Reames D. V. // The Astrophysical Journal Supplement Series, 1990. V. 73. P. 235.
8. Rieger E. // The Astrophysical Journal Supplement Series, 1994. V. 90. P. 645.
9. Reames D. V., Richardson I. G., and Wenzel K. P. // The Astrophysical Journal, 1992. V. 387. P. 715.
10. Harrison R. A. // Astronomy and Astrophysics, 1986. V. 162. P. 283.
11. Milovanov A. V. and Zelenyi L. M. — In: Solar system plasmas in space and time. /Eds. by J. L. Burch and J. H. Waite, Jr. — AGU, 1994. P. 43.
12. McIntosh P. S., Thompson R. J., and Willock E. C. // Nature, 1992. V. 360. P. 322.
13. Sheeley N. R., Jr. and Harvey J. W. // Solar Physics, 1981. V. 70. P. 237.
14. Legrand J. P. and Simon P. A. // Annales Geophysicae, 1989. V. 7. P. 565.
15. Tsurutani B. T., Goldstein B. E., Smith E. J., Gonzalez W. D., Tang F., Akasofu S. I., Anderson R. R. // Planetary and Space Science, 1990. V. 38. P. 109.
16. Woo R. and Gazis P. // Nature, 1993. V. 366. P. 543.
17. Bame S. J., Goldstein B. E., Gosling J. T., Harvey J. W., McComas D. J., Neugebauer M., and Phillips J. L. // Geophysical Research Letters, 1993. V. 20. P. 2323.
18. Simnett G. M., Sayle K., Roelof E. C., and Tappin S. J. // Geophysical Research Letters, 1994. V. 21. P. 1561.
19. Harrison R. A. The Cambridge IPS array: RAL science report. — IPS-MRAO/RAL/NOAA/BAS, 1991.
20. Harrison R. A., Hapgood M. A., Moore V., and Lucek E. A. // Annales Geophysicae, 1992. V. 10. P. 519.
21. Tappin S. J., Dryer M., Han S. M., Wu S. T. // Planetary and Space Science, 1988. V. 36. P. 1155.
22. Akasofu S. I. and Lee L. H. // Planetary and Space Science, 1989. V. 37. P. 73.
23. Gurnett D. A. // Space Science Reviews, 1995. V. 72. P. 243.
24. Cane H. V., Sheeley N. R., Jr., Howard R. A. // Journal of Geophysical Research., 1987. V. 92. P. 9869.
25. Gurnett D. A., Hospodarsky G. B., Kurth W. S., Williams D. J., and Bolton S. J. // Journal of Geophysical Research, 1993. V. 98. P. 5631.
26. Kellogg P. J., Goetz K., Howard R. L., and Monson S. J. // Geophysical Research Letters, 1992. V. 19. P. 1303.

27. Zakharov V.E. // Zhurnal Eksperimentalnoi i teoretitcheskoi Fisiki, 1972. V.62. P.1745.
28. Li L.H. // Physics of Fluids B., 1993. V.5. P.1760.
29. Goldman M.V. and Newman D.L. — In: Solar system plasmas in space and time. /Eds. by J.L.Burch and J.H.Waite, Jr. — AGU, 1994. P.33.
30. Stone R.G., Bougeret J.L., Caldwell J., Canu P., de Conchy Y., Cornilleau-Wehrlin N., Desh M.D., Fainberg J., Goetz K., Goldstein M.L., Harvey C.C., Hoang S., Howard R., Kaiser M.L., Kellogg P.J., Klein B., Knoll R., Lecacheux A., Lengyel-Frey D., MacDowall R.J., Manning R., Meetre C.A., Meyer A., Mongue N., Monson S., Nicol G., Reiner M.J., Steinberg J.L., Torres E., de Villedary C., Wouters F., and Zarka P. // Astronomy & Astrophysics Supplement Series, 1992. V.92. P.291.
31. Gurnett D.A. — In: The astronomy and astrophysics encyclopedia. /Ed. by S.Maran. — Van Nostrand Reinhold, 1992. P.535.
32. Dungey J.W. // Physical Review Letters, 1961. V.6. P.47.
33. Dungey J.W. // Journal of Geophysical Research, 1994. V.99. P.19,189.
34. Alfven H. Cosmic Plasma. — D. Reidel Publishing Company, 1981. 164 pp.
35. Lundin R. // Space Science Reviews, 1988. V.48. P.263.
36. Hultqvist B. Magnetospheric Physics. /Eds. by B.Hultqvist and C.G.Falthammar. — 1990. P.21.
37. Rycroft M.J. // Memoirs of National Institute of Polar Research, Special Issue, 1987. V.48. P.196.
38. Cowley S. // Physics World, 1995. V.8. P.46.
39. Axford W.I. and Hines C.O. // Canadian Journal of Physics, 1961. V.39. P.1433.
40. Carlson H.C. // Journal of Geomagnetism and Geoelectricity, 1990. V.42. P.697.
41. Lockwood M., Denig W.F., Farmer A.D., Davda V.N., Cowley S.W.H., and Luhr H. // Nature, 1993. V.361. P.424.
42. Freeman M.P., Farrugia C.J., Burlaga L.F., Hairston M.R., Greenspan M.E., Ruohoniemi J.M., and Lepping R.P. // Journal of Geophysical Research, 1993. V.98. P.7633.
43. Lui A.T.Y. // Physics of Fluids B., 1992. V.4. P.2257.
44. Baker D.N., Pulkkinen T.I., McPherron R.L., and ClauerC.R. — In: Solar system plasmas in space and time. /Eds. by J.L.Burch and J.H.Waite, Jr. — AGU, 1994. P.101.
45. Winglee R.M., Menietti J.D., Peterson W.K., Burch J.L., Waite J.H., Jr. — In: Solar system plasmas in space and time. /Eds. by J.L.Burch and J.H.Waite, Jr. — AGU, 1994. P.171.

46. Ashour-Abdalla M., Chang T., and Dusenburg P., eds. Space plasmas: coupling between small and medium scale processes. — AGU, 1995. 390 pp.
47. Lepping R.P., Burlaga L.F., Tsurutani B.T., Ogilvie K.W., Lazarus A.J., Evans D.S., and Klein L.W. // Journal of Geophysical Research, 1991. V.96. P.9425.
48. Labelle J., Kistler L.M., Treumann R.A., Baumjohann W., Sibeck D.G., Baker D.N., and Belian R.D. // Planetary and Space Science, 1990. V.38. P.841.
49. Newell P.T. and Sibeck D.G. // Geophysical Research Letters, 1993. V.20. P.2829.
50. Woch J., Lundin R. // Journal of Geophysical Research, 1992. V.97. P.1431.
51. Fairfield D.H. // Journal of Geomagnetism and Geoelectricity, 1991. V.43, Suppl. P.117.
52. Roelof E.C. and Sibeck D.G. // Journal of Geophysical Research, 1993. V.98. P.21,421.
53. Sato T., Walker R.J., and Ashour-Abdalla M. // Journal of Geophysical Research, 1984. V.89. P.9761.
54. Lee L.C. and Fu Z.F. // Journal of Geophysical Research, 1986. V.91. P.13,373.
55. Scholer M. // Geophysical and Astrophysical Fluid Dynamics, 1991. V.62. P.51.
56. Atkinson G. // Journal of Geophysical Research, 1992. V.97. P.1337.
57. Thorne R.M. and TsurutaniB.T. — In: Physics of Space Plasma. SPI Conference Proceedings and Reprint Series. /Eds. by T.Chang, G.B.Crew and J.R.Jasperse. 1991.
58. Winckler J.R., Malcolm P.R., Arnoldy R.L., Burke W.J., Erickson K.N., Ernstmeyer J., Franz R.C., Hallinan T.J., Kellogg P.J., Monson S.J., Lynch K.A., Murphy G., and Nemzek R.J. // EOS, 1989. V.70. P.657.
59. Winckler J.R. // Reviews of Modern Physics, 1992. V.64. P.859.
60. Lundin R. and Haerendel G. // EOS, 1993. V.74. P.321.
61. Lundin R., Eliasson L., Norberg O., Marklund G., Zanetti L.R., Whalen B.A., Holback B., Murphree J.S., Haerendel G., Boehm M., and Paschmann G. — In: Solar system plasmas in space and time. /Eds. by J.L.Burch and J.H.Waite, Jr. — AGU, 1994. P.247.
62. Frank L.A., Craven J.D., and Rairden R.L. // Advances in Space Research, 1985. V.5. P.53.
63. Williams D.J., Roelof E.C., and Mitchell D.G. // Reviews of Geophysics, 1992. V.30. P.183.
64. Garbe G.P., Arnoldy R.L., Moore T.E., Kintner P.M., and Vago J.L. // Journal of Geophysical Research, 1992. V.97. P.1257.

65. Vago J.L., Kintner P.M., Chesney S.W., Arnoldy R.L., Lynch K.A., Moore T.E., and Pollock C.J. // Journal of Geophysical Research, 1992. V.97. P.16,935.
66. Sazhin S.S., Bullough K., Hayakawa M. // Planetary and Space Science, 1993. V.41. P.153.
67. Arnoldy R.L., Lynch K.A., Kintner P.M., Vago J., Chesney S., Moore T.E., and Pollock C.J. // Geophysical Research Letters. V.19. P.413.
68. Kintner P.M., Vago J., Chesney S., Arnoldy R.L., Lynch K.A., Pollock C.J., and Moore T.E. // Physical Review Letters, 1992. V.68. P.2448.
69. Lundin R. and Hultqvist B. // Journal of Geophysical Research, 1989. V.94. P.6665.
70. Sotnikov V.I., Shapiro V.D., and Shevchenko V.I. // Soviet Journal of Plasma Physics. English Translation, 1978. V.4. P.252.
71. Winglee R.M., Menietti J.D., Peterson W.K., Burch J.L., and Waite J.H., Jr. — In: Solar system plasmas in space and time. /Eds. by J.L.Burch and J.H.Waite, Jr. — AGU, 1994. P.171.
72. Bingham R., Bryant D.A., and Hall D.S. // Geophysical Research Letters, 1984. V.11. P.327.
73. Hall D.S. and Bryant D.A. // Nature, 1974. V.251, P.402.
74. Hayakawa M. and Sazhin S.S. // Planetary and Space Science, 1992. V.40. P.1325.
75. Cornilleau-Wehrlin N., Solomon J., Korth A., and Kremser G. // Journal of Geophysical Research, 1993. V.98. P.21,471.
76. Anderson R.R. — In: Dusty and dirty plasmas, noise, and chaos in space and in the laboratory. /Ed. by H.Kikuchi. — Plenum Press, 1994. P.73.
77. Sazhin S.S. and Hayakawa M. // Planetary and Space Science, 1992. V.40. P.681.
78. Trakhtengerts V.Y., Rycroft M.J., and Demekhov A.G. // Journal of Geophysical Research, 1995. In press.
79. Omura Y., Nunn D., Matsumoto H., and Rycroft M.J. // Journal of Atmospheric and Terrestrial Physics, 1991. V.53. P.351.
80. Shklyar D.R., Nunn D., Smith A.J., and Sazhin S.S. // Journal of Geophysical Research, 1992. V.97. P.19,389.
81. Rycroft M.J. — In: Review of Radio Science. /Ed. by W.Ross Stone. — Oxford University Press, 1993. P.631.
82. Burgess W.C. and Inan U.S. // Journal of Geophysical Research, 1993. V.98. P.15,643.
83. Taranenko Y.N., Inan U.S., and Bell T.F. // Geophysical Research Letters, 1993. V.20. P.1539.

84. Rodriguez J.V., Inan U.S., and Bell T.F. // Journal of Geophysical Research, 1994. V.99. P.23,329.
85. Ohnami S., Hayakawa M., Bell T.F., and Ondoh T. // Geophysical Research Letters, 1993. V.20. P.739.
86. Trakhtengerts V.Y. and Hayakawa M. // Journal of Geophysical Research, 1993. V.98. P.19,205.
87. Gurnett D.A. // University of Iowa, 1992. №92–11.
88. Xu J.S. and Yeh K.C. // Journal of Geophysical Research, 1990. V.95. P.10,481.
89. Yeh K.C., Xu J.S., and Dong B. // Journal of Electromagnetic Waves and Applications, 1991. V.5. P.221.
90. Serizawa Y. and Dum C.T. // Physics of Fluids B., 1992. V.4. P.2389.
91. Nishikawa K.I., Buneman O., and Neubert T. // Advances in Space Research, 1995. V.15. P.(12)17.
92. Rishbeth H. and Van Eyken A.P. // Journal of Atmospheric and Terrestrial Physics, 1993. V.55. P.525.
93. Cowley S.W.H., Van Eyken A.P., Thomas C.P., Williams P.J.S., and Willis D.M. // Journal of Atmospheric and Terrestrial Physics, 1990. V.52. P.645.
94. Lanchester B.S., Rishbeth H., Nygren T., Jalonen L., and Turunen T. // Journal of Atmospheric and Terrestrial Physics, 1989. V.51. P.179.
95. Maurice J.P.St., Kofman W., and Kluzek E. // Advances in Space Research, 1990. V.10. P.(6)225.
96. Haerendel G., Buchert S., La Hoz C., Raaf B., and Rieger E. // Journal of Geophysical Research, 1993. V.98. P.6087.
97. Kirkwood S. and Bjorna N. // Geophysical Research Letters, 1992. V.19. P.661.
98. Hultqvist B. // Journal of Atmospheric and Terrestrial Physics, 1991. V.53. P.3.
99. Schlegel K. // Journal of Atmospheric and Terrestrial Physics, 1996. In press.
100. Kofman W. and Maurice J.P.St. // Journal of Atmospheric and Terrestrial Physics, 1996. In press.
101. Turunen T., Cannon P.S., and Rycroft M.J. // Nature, 1980. V.286. P.375.
102. Cannon P.S. // Journal of Atmospheric and Terrestrial Physics, 1982. V.44. P.819.
103. Cannon P.S., Turunen T., and Rycroft M.J. // Journal of Atmospheric and Terrestrial Physics, 1982. V.44. P.831.
104. Vas'kov V.V., Bud'ko N.I., Kapustina O.V., Mikhailov Yu.M., Ryabova N.A., Komrakov G.P., Maresov A.N., and Gdalevich G.L. // Advances in Space Research, 1995. V.15. P.(12)49.

105. Blagoveshchenskaya N.F., Andreev A.D., and Kornienko V.A. // Advances in Space Research, 1995. V.15. P.(12)45.
106. Robinson T.R., Honary F., Stocker A., and Jones T.B. // Advances in Space Research, 1995. V.15. P.(12)41.
107. Robinson T.R. // Annales Geophysicae, 1994. V.12. P.316.
108. Noble S.T. and Gordon W.E. // Radio Science, 1993. V.28. P.351.
109. Sergeev E.N., Frolov V.L., Grach S.M., Shvarts M.M. // Advances in Space Research, 1995. V.15. P.(12)63.
110. Ermakova E.N. and TrakhtengertsV.Yu. // Advances in Space Research, 1995. V.15. P.(12)67.
111. Boiko G.N. and Erukhimov L.M. // Advances in Space Research, 1995. V.15. P.(12)71.
112. Rietveld M.T., Kohl H., Kopka H., and Stubbe P. // Journal of Atmospheric and Terrestrial Physics, 1993. V.55. P.577.
113. James H.G. // Journal of Geophysical Research, 1993. V.98. P.19,099.
114. James H.G., Balmain K.G., Bantin C.C., and Hulbert G.W. // Radio Science, 1995. V.30. P.57.
115. Alfven H. On the origin of the solar system. — Clarendon Press, 1954.
116. Reasoner D.L. // Journal of Spacecraft and Rockets, 1992. V.29. P.580.
117. Oraevsky V.N., Ruzhin Yu.Ya., Volokitin A.S., and Gorgutsa R.V. // Advances in Space Research, 1995. V.15. P.(12)99.
118. Namazov S., Nikolaishvili S., Romanovsky Y., and Ivanov V. // Advances in Space Research, 1995. V.15. P.(12)123.
119. Milinevsky G.P., Alpatov V.V., Gurvich A.V., Evtushevsky A.M., Peres J., and Romanovsky Yu.A. // Advances in Space Research, 1995. V.15. P.(12)131.
120. Rycroft M.J. // Journal of Geomagnetism and Geoelectricity, 1991. V.43, Suppl. P.845.
121. Kurth W.S. // Nature, 1991. V.353. P.705.
122. Greenspan M.E., Rasmussen C.E., Burke W.J., and Abdu M.A. // Journal of Geophysical Research, 1991. V.96. P.13,931.
123. Yeh K.C., Lin K.H., and Conkright R.O. // Canadian Journal of Physics, 1992. V.70. P.532.
124. Buonsanto M.J., Foster J.C., and Sipler D.P. // Journal of Geophysical Research, 1992. V.97. P.1225.
125. Foster J.C., Buonsanto M.J., Mendillo M., Nottingham D., Rich F.J., and Denig W. // Journal of Geophysical Research, 1994. V.99. P.11,429.

International Space University,
France

Поступила в редакцию
19 декабря 1995 г.

УДК 524.35.6

ЭФФЕКТ МЕЙССНЕРА В СВЕРХПРОВОДЯЩИХ ЯДРАХ НЕЙТРОННЫХ ЗВЕЗД

В. В. Кочаровский, Вл. В. Кочаровский, В. А. Кукушкин

Рассматривается влияние сверхпроводимости протонной плазмы в ядре нейтронной звезды (пульсара) на эволюцию ее магнитного поля. Согласно последовательно проведенным оценкам утверждается, что выталкивание поля из ядра звезды вследствие эффекта Мейсснера для *пре*-сверхпроводника второго рода является неэффективным для магнитных полей $B_0 \lesssim 10^{14}$ Гс. Поэтому такое поле без учета других механизмов выталкивания (например, связанных с плавучестью абрикосовских вихрей или их пиннингом к вихрям Онсагера–Фейнмана в сверхтекучей нейтронной жидкости вращающейся звезды) должно быть "вмороженным" в ядро на время $\gtrsim 10^{10}$ лет, т.е. на все время жизни звезды.

1. ВВЕДЕНИЕ

Согласно современным представлениям (см., например, [1,2]), нейтронные звезды (проявляющие себя как пульсары) являются вращающимися шарами с массой порядка солнечной и радиусом $R \sim 10$ км. Они состоят из твердой коры и жидкого ядра. Кора, имеющая толщину $\Delta R \sim 1$ км, образована, главным образом, ядрами ^{56}Fe, упакованными в кристаллическую решетку, и газом свободных электронов. В ядре звезды плотность достигает величины, характерной для атомных ядер, и вещество состоит, в основном, из *пре*-фазы, являющейся смесью нейтронов, протонов и электронов. Концентрации протонов и электронов равны и составляют несколько процентов от концентрации нейтронов.

Благодаря высокой плотности вещества в ядре звезды, межпротонное расстояние достаточно мало для проявления сильного протон–протонного взаимодействия, носящего притягивательный характер. В результате возможно образование $^1S_0$ куперовских протонных пар и переход ядра звезды в сверхпроводящее состояние [3–5]. Оценка критической температуры перехода, T_c, дает согласно [6] величину порядка $2 \cdot 10^9$ К, что превышает типичные внутренние температуры нейтронных звезд T в возрасте больше нескольких десятков лет [7,8]. Следовательно, ядра подавляющего большинства нейтронных звезд должны находиться в сверхпроводящем состоянии.

Согласно данным [2,9], протонный сверхпроводник в ядре звезды относится ко второму роду с лондоновской глубиной $\delta \simeq 10^{-11}\sqrt{T_c/(T_c - T)}$ см

и длиной когерентности $\xi \simeq 10^{-12}\sqrt{T_c/(T_c - T)}$ см. Для его описания используем теорию сверхпроводимости БКШ [10].

2. СТРУКТУРА МАГНИТНОГО ПОЛЯ НЕЙТРОННОЙ ЗВЕЗДЫ СО СВЕРХПРОВОДЯЩИМ ЯДРОМ

Будем рассматривать простейшую модель структуры магнитного поля нейтронной звезды, рождающейся с однородным внутренним полем $B_0 \lesssim 10^{14}$ Гс и с соответствующим дипольным полем снаружи. Очень быстро, примерно за 10 лет [7,8], ее внутренняя температура становится равной критической температуре T_c. За это время токи в ядре [11] и коре [12] нейтронной звезды не успевают затухнуть, а следовательно, ее магнитное поле практически не успевает измениться. При дальнейшем остывании жидкое ядро звезды переходит в сверхпроводящее состояние. Вследствие наличия магнитного поля B_0 указанный переход происходит при температуре T, слегка меньшей критической температуры T_c. Поле в коре и вне звезды никак не затрагивается сверхпроводящим фазовым переходом, а магнитное поле в ядре, как хорошо известно из исследований земных (твердотельных) сверхпроводников второго рода [10], разбивается на прямолинейные абрикосовские вихри (рис. 1), начинающиеся и заканчивающиеся на поверхности ядра (рис. 2). Каждый вихрь представляет собой очень тонкую (радиус порядка δ) трубку магнитных силовых линий $\mathbf{B}$ и содержит один квант магнитного потока $\phi = 2 \cdot 10^{-7}$ Гс·см^2. Магнитное поле вихря создается циркулирующим в нем кольцевым сверхпроводящим током $\mathbf{j}_s$. (Следует отметить, что в настоящее время вопрос о динамике и физических явлениях на движущемся фронте фазового перехода между сверхпроводящим и несверхпроводящим *пре*-состоянием остается открытым.)

По аналогии с земными сверхпроводниками второго рода примем для определенности, что в перпендикулярной их направлению плоскости вихри образуют треугольную решетку с межвихревым расстоянием $d = \sqrt{2}/3^{1/4}\sqrt{n}$. Здесь n — число вихрей, пронизывающих единичную площадку, перпендикулярную их направлению. (Заметим, впрочем, что сделанные ниже качественные выводы об эволюции магнитного поля нейтронной звезды практически не зависят от вида решетки абрикосовских вихрей.)

Макроскопическое магнитное поле $\bar{\mathbf{B}}$ в ядре представляется результатом усреднения создаваемого вихрями микроскопического поля $\mathbf{B}$ по пространственным масштабам, много большим радиусов вихрей и расстояний между ними. Поле $\bar{\mathbf{B}}$ направлено вдоль вихрей, и его величина равна $\bar{B} = \phi n$. В начальный момент времени $\bar{B} = B_0 \equiv \phi n_0$.

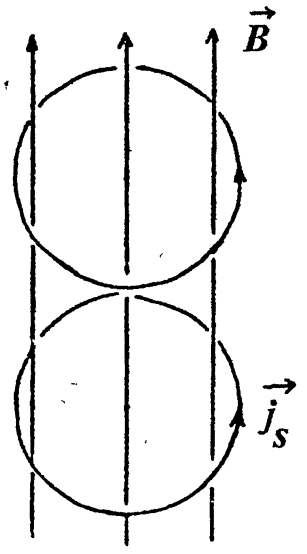

Рис. 1. Абрикосовский вихрь.

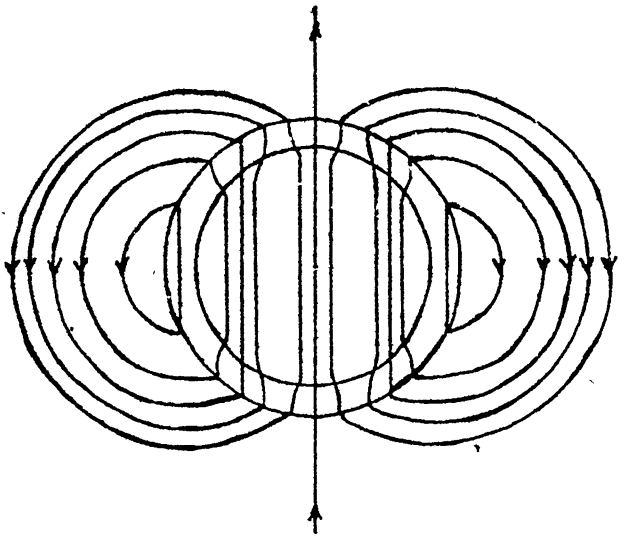

Рис. 2. Магнитное поле нейтронной звезды в момент перехода ее ядра в сверхпроводящее состояние.

3. ДИНАМИКА АБРИКОСОВСКОГО ВИХРЯ В СВЕРХПРОВОДЯЩЕМ ЯДРЕ НЕЙТРОННОЙ ЗВЕЗДЫ

Вследствие отталкивания друг от друга вихри, оставаясь прямолинейными, начинают двигаться поперек магнитного поля и выходить из ядра звезды в ее кору, где время затухания магнитного поля за счет омических потерь может быть достаточно мало́, вплоть до времени порядка миллиона лет [12]. Это приводит к уменьшению плотности вихрей n, т.е. к выталкиванию магнитного поля $\vec{B}$ из сверхпроводника, известному как эффект Мейсснера [10]. Для оценки минимального времени выталкивания поля $\tau_{\min}$ перейдем к цилиндрической геометрии, т.е. заменим сверхпроводящее сферическое ядро звезды бесконечным цилиндром радиуса $R - \Delta R \simeq R$. Абрикосовские вихри направлены вдоль оси цилиндра и, оставаясь прямолинейными, движутся со скоростью $\mathbf{v} \perp \mathbf{B}$ (рис. 3).

Благодаря отталкиванию от окружающих соседей на единицу длины каждого вихря действует сила $-g(n)\vec{\nabla}n$, отличная от нуля только в случае неоднородного распределения вихрей n. Функция $g(n)$ легко вычисляется в предельных случаях $\xi \ll d \ll \delta$ и $d \gg \delta \gg \xi$ с использованием полученного в лондоновском приближении выражения для силы отталкивания двух отдельных вихрей [10]. В первом случае суммирование по окружающим данный вихрь соседям можно заменить интегрированием и учесть

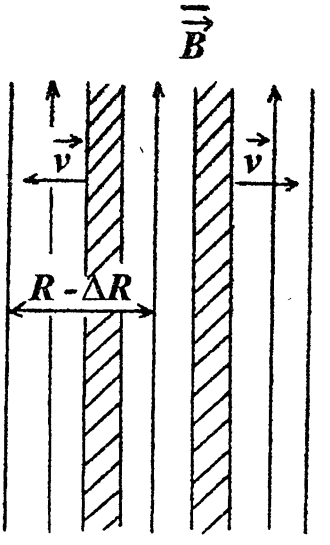

Рис. 3. Расталкивание и динамика абрикосовских вихрей (заштрихованы) в цилиндрической модели ядра радиуса $R - \Delta R \simeq R$.

в подынтегральном выражении малость изменения n на расстояниях порядка δ:

$$g(n) \simeq \frac{\phi^2}{4\pi}, \quad : \xi \ll d \ll \delta. \tag{1}$$

Во втором случае экспоненциальная слабость силы отталкивания вихрей позволяет для вычисления функции $g(n)$ учитывать отталкивание данного вихря лишь от ближайших шести соседей в решетке:

$$g(n) \simeq \sqrt{\frac{3}{2}} \frac{\phi^2}{16\pi^{3/2}} \left(\frac{\sqrt{2}}{3^{1/4}\sqrt{n}\,\delta} \right)^{7/2} \exp\left(-\frac{\sqrt{2}}{3^{1/4}\sqrt{n\delta}} \right), \quad d \gg \delta \gg \xi. \tag{2}$$

Сила $-g(n)\vec{\nabla} n$ уравновешивается действующими на единицу длины вихря силой вязкого трения $-\eta \mathbf{v}$ и перпендикулярной $\mathbf{v}$ силой Магнуса [13], возникающими вследствие рассеяния электронов магнитным полем движущегося вихря. В цилиндрической геометрии сила Магнуса приводит к уменьшению радиальной и появлению азимутальной составляющей у скорости $\mathbf{v}$, т.е. к увеличению времени выталкивания поля из сверхпроводника. Для оценки минимального времени выталкивания поля $\tau_{\min}$ она поэтому учитываться не будет. Коэффициент вязкости оценивается исходя из полученного в [14,15] времени релаксации средней относительной скорости свободных электронов и абрикосовских вихрей: $\eta \sim 10^7$ дин·с/см^2. Можно показать, что аналогичное значение для η (по порядку величины) дает классическое рассмотрение рассеяния электронов магнитным полем движущегося вихря.

В результате получаем основное уравнение динамики вихря:

$$-g(n)\vec{\nabla}n - \eta\mathbf{v} = 0. \tag{3}$$

Оно вместе с уравнением непрерывности

$$\frac{\partial n}{\partial t} + \operatorname{div}(n\mathbf{v}) = 0 \tag{4}$$

образует замкнутую систему уравнений для неизвестных функций $\mathbf{v}$, n.

4. "ВМОРАЖИВАНИЕ" МАГНИТНОГО ПОЛЯ В СВЕРХПРОВОДЯЩЕЕ ЯДРО НЕЙТРОННОЙ ЗВЕЗДЫ

Выражая $\mathbf{v}$ из (3) и подставляя в (4), получаем для плотности вихрей n нелинейное уравнение диффузии с переменным коэффициентом диффузии $ng(n)/\eta$:

$$\frac{\partial n}{\partial t} - \operatorname{div}\left(\frac{ng(n)\vec{\nabla}n}{\eta}\right) = 0. \tag{5}$$

Коэффициент диффузии $ng(n)/\eta$ уменьшается с уменьшением n. Поэтому для оценки минимального значения $\tau_{\min}$ времени выталкивания поля можно заменить в (5) переменный коэффициент диффузии на его максимальное значение $n_0 g(n_0)/\eta$, достигаемое в начальный момент времени. Получающееся таким образом линейное уравнение диффузии приводит к следующей оценке:

$$\tau_{\min} \sim R^2\eta/n_0 g(n_0). \tag{6}$$

Согласно [16] эта оценка не зависит (по порядку величины) от конкретного вида граничного условия для n на границе сверхпроводящего цилиндра.

Для магнитных полей $B_0 \lesssim 10^{14}$ Гс случай (1) реализуется лишь при $T_c - T \ll T_c$. В этом случае из оценки (6) для $B_0 = 10^{12}$, 10^{13}, 10^{14} Гс получаем соответственно $\tau_{\min} \sim 2\cdot 10^7$, $2\cdot 10^6$, $2\cdot 10^5$ лет. Однако значительно быстрее [7,8] внутренняя температура звезды T станет значительно ниже критической температуры T_c, так что функция $g(n)$ будет определяться выражением (2). Тогда из (6) для тех же значений начального магнитного поля получаем соответственно $\tau_{\min} \sim 10^{23}$, $3\cdot 10^{11}$, 10^{10} лет.

Формула (6) позволяет оценить также максимальную толщину $\Delta r_{\max}$ области на внешней границе сверхпроводящего цилиндра, из которой магнитное поле вытесняется за данное время τ:

$$\Delta r_{\max} \sim \sqrt{\tau n_0 g(n_0)/\eta}. \tag{7}$$

Так, для времени $\tau = 10^9$ лет при указанных выше значениях магнитного поля оценка (7) дает соответственно $\Delta r_{\max} \sim 1\cdot 10^{-1}$, $6\cdot 10^4$, $3\cdot 10^5$ см.

Магнитное поле $B_0 \lesssim 10^{14}$ Гс, следовательно, "вмораживается" в ядро звезды и остается в нем практически постоянным в течение всей ее жизни. В результате у старой нейтронной звезды существует постоянный дипольный магнитный момент, сравнимый с его исходной величиной. Небольшое затухание магнитного момента в начале ее жизни связано с омической диссипацией токов в тонкой несверхпроводящей коре звезды.

5. ЗАКЛЮЧЕНИЕ

Вывод о "вмороженности" магнитного поля в сверхпроводящее ядро нейтронной звезды был сделан еще в работе [17]. Однако в ней фактически рассматривался только сверхпроводник первого рода, а "вмороженность" поля в него объяснялась высокой проводимостью σ его несверхпроводящего состояния. В настоящей заметке нам пришлось вновь обратиться к проблеме "вмороженности", поскольку, согласно современным представлениям, ядро нейтронной звезды является сверхпроводником второго рода. Поле в виде вихрей "вмораживается" в него вследствие экспоненциальной слабости силы их взаимного отталкивания (см. раздел 4), а не вследствие высокой проводимости σ. Использование последней для вычисления действующей на движущийся вихрь силы вязкого трения в условиях сверхпроводящего ядра нейтронной звезды вообще неправомерно. Это связано с тем, что омическая диссипация в движущемся вихре происходит только в его очень тонкой сердцевине (радиус порядка ξ), где вещество находится в нормальном несверхпроводящем состоянии. В то же время радиус сердцевины ξ для всех рассматриваемых температур T значительно меньше длины свободного пробега электронов [11], обуславливающих высокую проводимость несверхпроводящего состояния σ. Поэтому использование обычной формулы $j_n^2 \pi \xi^2 / \sigma$ для скорости омической диссипации несверхпроводящих токов $\mathbf{j}_n$ в сердцевине движущегося вихря при вычислении действующей на вихрь силы вязкого трения теряет смысл. Вместе с тем, представленные в данной заметке корректные оценки не меняют общего качественного вывода о "вмороженности" поля.

Вывод о "вмороженности" поля в сверхпроводящее ядро нейтронной звезды был сделан в разделе 4 в результате рассмотрения только одного механизма выталкивания поля, аналогичного эффекту Мейсснера в обычных твердотельных сверхпроводниках второго рода. Однако магнитное поле может выталкиваться из сверхпроводящего ядра нейтронной звезды вследствие иных причин, в принципе отсутствующих в земных свехпроводниках второго рода, но способных ускорить выталкивание магнитного поля из ядра нейтронной звезды. Эти причины могут быть связаны, например, со всплыванием абрикосовских вихрей в жидком ядре нейтронной звезды [18] или с их пиннингом к вихрям Онсагера–Фейнмана, возникающим в сверхтекучей нейтронной жидкости ядра вращающейся звезды

[19,20]. Поэтому только более детальное исследование этих и других возможных механизмов выталкивания магнитного поля из сверхпроводящего ядра нейтронной звезды может показать обоснованность вывода о "вмороженности" магнитного поля в сверхпроводящее ядро, сделанного на основе анализа лишь одного эффекта Мейсснера. Иными словами, проведенного выше исследования еще не достаточно для того, чтобы считать дипольный магнитный момент звезды постоянным на временах порядка времени ее жизни, поскольку магнитный момент может затухать значительно быстрее из-за вытеснения магнитного поля в несверхпроводящую кору вследствие иных причин, отличных от эффекта Мейсснера.

В заключение авторы выражают благодарность В. В. Курину, Ю. В. Петухову, Д. А. Рындыку и В. Ю. Трахтенгерцу за обсуждение проблем динамики абрикосовских вихрей и эволюции магнитного поля нейтронных звезд.

ЛИТЕРАТУРА

1. Манчестер Р., Тейлор Дж. Пульсары. — М.: Мир, 1980. С. 190.
2. Седракян Д. М., Шахабасян К. М. // УФН. 1991. Т. 161. N 7. С. 3.
3. Мигдал А. Б. // ЖЭТФ. 1959. Т. 37. N 1. С. 249.
4. Гинзбург В. Л., Киржниц Д. А. // ЖЭТФ. 1964. Т. 47. N 5. С. 2006.
5. Wolf R. A. // Astrophys. J. 1966. V. 145. N 3. P. 834.
6. Amundsen L., Ostgaard E. // Nucl. Phys. Ser. A. V. 437. P. 487.
7. Richardson M. B. et. al. // Astrophys. J. 1982. V. 255. N 2. Part 1. P. 624
8. Lattimer J. M. et. al. // Astrophys. J. 1994. V. 425. N 2. Part 1. P. 802.
9. Harrison E. // MNRAS. 1991. V. 248. N 3. P. 419.
10. Лифшиц Е. М., Питаевский Л. П. Статистическая физика, ч. 2. — М.: Наука, 1978. С. 185.
11. Baym G., Pethick C., Pines D. // Nature. 1969. V. 224. P. 674.
12. Урпин В. А., Муслимов А. Г. // Астрономический журнал. 1994. Т. 71. N 2. С. 257.
13. Хюбенер Р. П. Структуры магнитных потоков в сверхпроводниках. — М.: Машиностроение, 1984. С. 107.
14. Sauls J. A., Stein D. L., Sérene J. W. // Phys. Rev. D. 1982. V. 25. Third series. N 4. P. 967.
15. Седракян Д. М., Шахабасян К. М., Мовсисян А. Г. // Астрофизика. 1985. Т. 22. Вып. 1. С. 137.
16. Тихонов А. Н., Самарский А. А. Уравнения математической физики. — М.: Наука, 1966. С. 177, 447.
17. Baym G., Pethick C., Pines D. // Nature. 1969. V. 224. P. 673.
18. Wendell C. E. // Astrophys. J. 1988. V. 333. N 2. Part 2. P. 95.
19. Седракян Д. М., Седракян А. Д. // ЖЭТФ. 1991. Т. 100. N 2(8). С. 353.
20. Srinivasan G. et. al. // Current Science. 1990. V. 59. N 1. P. 31.

Институт прикладной физики
РАН, г.Н. Новгород

Поступила в редакцию
4 октября 1995 г.

MEISSNER EFFECT IN SUPERCONDUCTING CORES OF NEUTRON STARS

V. V. Kocharovsky, Vl. V. Kocharovsky, V. A. Kukushkin

The evolution of magnetic field under the influence of proton plasma superconductivity in the core of a neutron star (pulsar) is considered. It is shown that for the magnetic fields $B_0 \lesssim 10^{14}$ G the Meissner effect in a *npe*-superconductor of the second type cannot expulse the field from a star core. This means that without taking into account other expulsion mechanisms (such as floating of the Abrikosov vortexes and their pinning to the Onsager-Feynman vortexes in a superfluid interior of a rotating star) the magnetic field $B_0 \lesssim 10^{14}$ G should be frozen in a core for a time $\gtrsim 10^{10}$ year, i.e., during whole life of a neutron star.

DYNAMICS OF THE FLUTE-INSTABILITY IN ACCRETION DISKS OF AGN

G. Z. Machabeli, G. I. Melikidze, V. S. Paverman

A new model for the accretion flows onto black holes is suggested. The model provides the high-frequency radiation from AGNs. The possibility of plasma retention by the magnetic field is discussed. It is shown that due to development of the flute instability the region where the magnetic and kinetic pressures are equal to each other can be located farther from the central object than the last stable Kepplerian orbit.

1. INTRODUCTION

The standard model for the most powerful active galactic nuclei (AGN) comprises a central massive black hole of mass $M = 10^8 - 10^9\, M_\odot$ (where $M_\odot$ is the mass of the Sun) surrounded by an accretion disk. The inner dimension of the disk equals the radius of the last stable Kepplerian orbit. This radius turns out to be $3\, r_g$, where r_g is a gravitational radius. The magnetic field is assumed to be freezed in the plasma of the disk and its tension (B) changes as $B \propto 1/r$.

Observations show that from the compact central object (size of which is of the order of 3 pc) the narrow jets flow out. The length of jets is 10^5 times longer than the size of the central object. Existence of the magnetic field with $B \propto 1/r$ corresponds to the observations and may be due to currents flowing along a jet. This current creates the toroidal component of the magnetic field.

The maximum velocity of the ions is about $v \propto c(r_g/r) \propto c/3$. Corresponding maximum Lorentz-factor of electrons, which they can gain due to collisions with ions cannot be more than $\gamma \propto 10^3$. In order to explain the high-frequency (x and γ-rays) radiation from AGNs it is necessary to assume presence of a strong ($B \propto 10^7$ G) magnetic field in the region of emission. If this field had poloidal structure (it means the field changes as $1/r$), at the distance of 3 pc from the central object its tension would be much higher than observed value [1]. So it is necessary to assume that at the distance of few parcecs field has the poloidal structure while near the centre the field has toroidal structure and changes as $1/r^3$. In this case the equilibrium between the magnetic and kinetic pressures can be obtained at the large distances. As it was shown in the papers [2, 3] poloidal magnetic field can suspend the accreting plasma even in vicinity of the central black hole.

In the standard model of the AGN the mechanism of the inverse Compton scattering is used for the explanation of the high-frequency radiation. But

for transformation of the low–frequency waves into high frequency waves it is necessary that the high–energy particles above of the emission region exist. But acceleration of the particles up to very high velocities seems to be an insoluble problem.

Therefore we propose an alternative model for the AGN.

2. MODEL FOR AGN

At the distance of few parsecs from the central object we can assume that the field changes as $B \propto 1/r^3$. Using this assumption and the virial theorem ($r^3B^2/8\pi \leq GM^2/r$) (G is the gravitational constant) we obtain that the maximum possible magnetic field is $B \approx 10^5$ G (for $M \approx 10^9 M_\odot$) at the distance 10^{17} cm [1, 4].

If the density changes as $\rho \propto (1/r)^{3/2}$ and the magnetic field as $B \propto (1/r)^2$ when the plasma falls onto central massive object the condition of equilibrium $B^2/8\pi \sim \rho u^2/2$ will be fulfilled at some distance from the central object. Not only can the induced magnetic field exist in this region but also a filed generated by a ring current. This current creates the poloidal magnetic field. The current flows along an inner side of the disk. It is well known that such current generates a dipole magnetic field decreasing as $B \propto 1/r^3$. So, it is clear that at the large distance from the compact object the magnetic field is determined by the current of the jet, while at the accretion disk (at the distance about few parsecs) contribution of the ring current may be predominant. The strength of the magnetic field at the distance few parsecs from the central object can be estimated as 0.1 G. This estimation is in a good agreement with the observations of the radioemission the jets from the distance 10^5 pc. According to it $B \sim 10^{-6}$ G (if $B \propto 1/r$). The magnetic field of the ring current is described as

$$\nabla \times \vec{B} = \frac{4\pi}{c}\vec{j}_g \simeq \frac{4\pi\rho_*}{B^2}[\vec{g} \times \vec{B}], \qquad (1)$$

This current supports the poloidal magnetic field, which supports the falling plasma. Of course this equilibrium is unstable. So the name 'disk' for such configuration is quite conditional and we can speak only about the region where the condition of equilibrium is fulfilled. Inflow of plasma in this region depends on accretion rate, but outflow depends on the growth rate of instabilities of the inner edge of the disk. The most powerful hydrodynamic instability in this case is the Raleigh–Taylor instability. This instability in the plasma usually is called as the flute–instability [5]. The magnetic field plays the role of a light liquid and a plasma is a heavy liquid.

Bellow we will show that rate of plasma outflow from the disk due to the flute–Instability is proportional to ρ — plasma density. So near the central object the rate of outflow may be more than inflow. Consequently if at the

beginning the disk were formed near the black hole the magnetic field lines would move out of the centre due to the outflow of plasma until the balance between the inflow and outflow rates would establish. This condition will determine the region of equality of the kinetic and magnetic pressures.

3. THE FLUTE–INSTABILITY

From the orbit theory it is well known that a guiding centre drift arises from the centrifugal force (in the particle frame) felt by the particles as they move along the curved magnetic field lines. If $V_{\|i}^2$ is the average square of the component of random velocity along the magnetic field lines, the average centrifugal force is $m_i V_{\|i}^2 \mathbf{R_c}/R_c^2$, where R_c is the radius of curvature. This force causes protons and electrons to drift in the opposite directions. The resulting space charge produces an electric field which causes the particles to drift in the direction of the centrifugal force. This is analogous to the Raleigh–Taylor instability with $V_{\|i}^2/R_c$ playing the role of gravitational acceleration $\vec{g}$. If $\vec{g}$ is directed opposite to the direction of the increasing particle density, the plasma is unstable against the flute or Raleigh–Taylor instability leading to increased magnetic field curvature. In the presence of a straight magnetic field, the acceleration due to gravity of the central object can replace the centrifugal acceleration. In the AGN magnetosphere the two effects are of the same order. The flute instability is an aperiodic instability with a growth rate γ_{fl} given by

$$\gamma_{\text{fl}} \simeq \left(\frac{kV_{\|i}^2}{R_c}\right)^{1/2} \equiv (kg)^{1/2} \tag{2}$$

under the conditions:

$$(kr_i)^2 < \frac{4a}{R_c} \qquad \text{and} \qquad m_i n_o V(r)^2 \geq \frac{B_o^2}{4\pi}, \tag{3}$$

where a is the transverse dimension of the flux tube, r_i is the ion Larmor radius and $k \simeq a^{-1}$ is the wave vector. Here, we assume $|V_{\|i}^2/R_c| \simeq |g|$.

Now we can estimate rate of plasma outflow due the flute–instability

$$\dot{M}_{\text{fl}} = \rho l a^2 \gamma_{\text{fl}} N \tag{4}$$

where N is the number of filaments falling simultaneously along the inner edge of the disk and l is the linear dimension of the flux tube. From the condition (3) we can estimate a $a \simeq (r_i^2 R_c/4)^{1/3}$. Then

$$\dot{M}_{\text{fl}} \simeq \rho \propto r^{-3/2} \tag{5}$$

Consequently the nearer is the region of equality of magnetic and kinetic pressures the higher is plasma outflow rate from the disk. Therefore comparing

$\dot{M}_B$ with the constant accretion rate of plasma from the surrounding medium towards the disk $\dot{M}$ we can find the distance where the equilibrium of pressures will be established.

As the instability develops, the plasma particles rush towards the black hole, carrying along the magnetic field lines, narrowing the region through which the magnetic flux tubes fall. From flux conservation, one concludes that the magnetic field intensity and the particle density increase as $(10^{17}/r)^2$, where $r \leq 10^{17}$ cm is the distance from the central object. Each falling tube has a volume of $a^2 l$, where l, the linear dimension of the flux tube is of the order of the radius of curvature of the magnetic field R_c. The l/a number of tubes falling simultaneously from region above the first tube form a filament. The total power content of the filaments is

$$L = \frac{n_o m_i V(r)^2 a l}{2\tau_B} \frac{l}{a} N \tag{6}$$

and $\tau_B = 1/\gamma_B$ and the corresponding accretion rate is determined from:

$$\dot{M} = \frac{L}{c^2} \frac{r}{r_g}. \tag{7}$$

4. CONCLUSION

So we find the place of the flute–instability development, which does not necessarily coincide with the last stable Kepplerian orbit. This place can be located farther from the central object. Farther we suppose the following scenario of development of physical processes which leads to the generation of high–frequency radiation:

(1) the flute instability takes the accreted plasma flux tube closer to the central object in order to feel a higher gravitational potential;

(2) the electrostatic ion–cyclotron instability is excited due to temperature anisotropy of the ions and hence it tries to isotropize the ion velocity distribution function through quasi–linear diffusion;

(3) the Coulomb collisions between electrons and protons in this rather high density plasma tube try to equilibrate the electron and ion temperatures, dominantly increasing the electron energy in a direction parallel to the magnetic field;

(4) the fire–hose instability which is excited under the circumstances $\left(P_{\|} - P_{\perp}\right)/\rho V_A^2 > 1$, transfers the parallel electron energy to perpendicular electron energy; here $P_{\|}$ and $P_{\perp}$ are the particle pressures along and perpendicular to the magnetic field, V_A is the Alfven speed and ρ is the mass density, and

(5) the last but not least — this perpendicular electron energy is radiated into X-rays through synchrotron processes.

In the next papers we are going to discuss each of these processes in detail.

REFERENCES

1. Begelman M.C., Blandford R.D., and Rees M.J. // Rev. mod. Phys., 1984. V.56. P.255.
2. Znajek R.L. // Nature, 1976. V.262. P.270.
3. Blandford R.D. and Znajek R.L. // M.N.R.A.S., 1977. V.179. P.433.
4. Sturrock P.A. // Nature, 1965. V.205. P.861.
5. Mikhailovskii A.B. Theory of Plasma Instabilities. — Moscow: Atomizdat, 1975.

Abastumani Astrophysical
Observatory, Institute of Physics,
Georgian Academy of Sciences

Поступила в редакцию
13 ноября 1995 г.

CENTRIFUGAL ACCELERATION SURPRISES

G. Z. Machabeli, I. S. Nanobashvili, A. D. Rogava

A *gedanken experiment* of a bead motion along the rotating pipe with the relativistic velocities is discussed. It is shown, that when $v_0 > \frac{c}{\sqrt{2}}$, the centrifugal acceleration changes its sign and the braking is beginning. It is pointeed out, that while investigating the pulsar magnetospheres, we must take into account the effect of rotating relativistic stream braking.

1. INTRODUCTION

In connection with several astrophysical problems, e.g. the investigation of pulsar magnetospheres, the question of investigation of a relativistic plasma stream ejection from the rotating source (a star) along the magnetic field lines is arising. It is very important for such rotating relativistic streams to discuss the centrifugal acceleration problem. We will discuss it in section 2. In section 3 we will discuss the same problem in the case, when the rotating energy of the source is limited.

It is most convenient in our case to discuss the problem in two frames: in noninertial rotating frame (NRF), which rotates together with the radius (plasma moves along the radius), or in the laboratory inertial frame (LIF).

From generally covariant equatin of motion, one can find, that in NRF it has the following form (here we will write the equation in three–dimentional form):

$$\frac{d\vec{p}}{dt} = e\left(\vec{E} + \frac{1}{c}[\vec{v}\vec{B}]\right) + \vec{F}_c. \tag{1.1}$$

Here m, e, $\vec{v}$ and $\vec{p}$ are the particle mass, charge, three–velocity and momentum respectively, $\vec{E}$ and $\vec{B}$ are the electric and magnetic fields. $\vec{F}_c = \gamma m\omega^2\vec{r}$ (here γ m and $\vec{r}$ are the particle Lorentz–factor, mass and radius–vector respectively and ω is the angular velocity of the star) is the centrifugal force. All quantities are defined in NRF. In LIF the equation of motion has the following form:

$$\frac{d\vec{p}}{dt} = e\left(\vec{E} + \frac{1}{c}[\vec{v}\vec{B}]\right). \tag{1.2}$$

Here all quantities are same, but they are defined in LIF.

As we can see, in equation (1.2) the centrifugal force does not exist. This is the seeming contradiction and it can be easily removed if we note, that the magnetic field is nonuniform in LIF (the field is unifrom in NRF). Than

we must mark out the uniform part from the magnetic field (this procedure is well known, for e.g. see the problem of Alfven in [1] and the relativistic generalization of this problem in [2]) and after this in the equation of motion (1.2) we will have not only the Lorentz force but also the centrifugal force evidently. We must also mention, that the freezing-in condition $(\vec{E} + \frac{1}{c}[\vec{v}\vec{B}] = 0)$ can be used in LIF only for the uniform part of the field,but this condition is fulfilled generally in NRF (see in detail [3]).

2. CENTRIFUGAL ACCELERATION

Recently, in [4], it was described a simple *gedanken experiment*, revealing the strange dynamics of rotational motion in special relativity. The experimental layout consisted of a straight, long and narrow pipe rotating around an axle normal to its symmetry axis and a small bead which could move inside the pipe without friction. The pipe rotated with constant angular velocity $\omega = \text{const}$ and was assumed to be massles and absolutely rigid. At $t = 0$ the bead was just above the pivot ($r_0 = 0$) and had an initial velocity v_0. The problem was considered in the noninertial rotating frame (NRF) of reference of the pipe. Let us consider the motion of the bead in the LIF, where the spacetime is just Minkowskian. Owing to the polar symmetry of the experimental set-up it is convenient for the forthcoming purposes to write the spatial part of the metric in polar ($g_{\varphi\varphi} = r^2$, $g_{rr} = 1$) coordinates:

$$ds^2 \equiv -d\tau^2 = -dt^2 + r^2 d\varphi^2 + dr^2, \tag{2.1}$$

where τ is the proper time of the bead. We use units in which $c = 1$.

The motion of the bead in LIF is characterised by the three–velocity $\vec{v}$ with the nonzero physical components: $v \equiv v_{\hat{r}} = dr/dt$ and $u \equiv v_{\hat{\varphi}} = r\omega$. Note that $v_{\hat{\varphi}}$ and $v_{\hat{r}}$ are connected with their contravariant and covariant components as $v_{\hat{\varphi}} = rv^{\varphi} = v_{\varphi}/r$ and $v_{\hat{r}} = v^r = v_r$.

The equation of the bead motion in LIF may be written simply as:

$$\frac{d\vec{p}}{dt} = \vec{f}, \tag{2.2}$$

where $\vec{p} \equiv m_0 \gamma \vec{v}$ is a three–momentum of the bead, m_0 is its rest mass, and γ — its Lorentz factor as measured in LIF:

$$\gamma = \left(1 - \omega^2 r^2 - v^2\right)^{-1/2}, \tag{2.3}$$

while $\vec{f}$ is a *real* three–force acting on the bead (pipe reaction force). This force has only one, azimuthal, nonzero component: $f_{\varphi} \neq 0$. It means that the orthogonal radial component of the bead three–acceleration $(d\vec{p}/dt)_r$, specified

by the left hand side of (2.2), is equal to zero. Note that $(d\vec{p}/dt)_i = dp_i/dt + v^k p_{i;k} \neq dp_i/dt$ since the spatial part of the metric (2.1) is curved. In particular, radial component of the equation of the bead motion leads to

$$\frac{d}{dt}(mv) - m\omega^2 r = 0, \tag{2.4}$$

where $m(t) \equiv m_0\gamma$ is the relativistic (inertial) mass of the bead, which varies with time and measures the beads' *variable resistance* to acceleration. Note that $m(t)$ depends not only on the radial velocity of the bead $v(t)$, but also on its radial coordinate $r(t)$. Taking into account (2.3) we find

$$\frac{dm}{dt} = mv\gamma^2\left(\omega^2 r + \frac{dv}{dt}\right), \tag{2.5}$$

and (2.4) yields:

$$\frac{d^2r}{dt^2} = \frac{\omega^2 r}{1-\omega^2 r^2}\left(1 - \omega^2 r^2 - 2v^2\right). \tag{2.6}$$

This is exactly the same equation, which we get in [4] for the radial acceleration of the bead as measured in NRF. This equation may also be written in the following surprisingly elegant form:

$$\frac{d^2r}{dt^2} = \frac{(1-\gamma^2 v^2)}{(1+\gamma^2 v^2)}\omega^2 r. \tag{2.7}$$

This equation distinctly represents peculiarities of the bead motion: when the motion is nonrelativistic ($\gamma v \ll 1$) it reduces to the usual classic equation for centrifugal acceleration: $d^2r/dt^2 = \omega^2 r$, in the ultrarelativistic limit ($v_0 \to 1$) the sign of the right hand side is just the opposite: $d^2r/dt^2 = -\omega^2 r$. When $\gamma_0 v_0 = 1$ ($v_0 = \sqrt{2}/2$) the sign reversal occurs from the very beginning of the motion.

One more interesting point, which also slipped off our attention in [4], is that if we introduce new variables: $\phi \equiv 2\arccos(\omega r)$, $\lambda \equiv \omega t$, and $\Omega^2 \equiv 1 - v_0^2$, we can reduce (2.6) to the following, remarkably simple equation:

$$\frac{d^2\phi}{d\lambda^2} + \Omega^2 \sin\phi = 0. \tag{2.8}$$

This is well-known *pendulum equation*, describing nonlinear oscillations of a free mathematical pendulum. The easiest way for getting (2.8) is to write the equation for the radial velocity of the bead [4]:

$$\frac{dr}{dt} = \sqrt{(1-\omega^2 r^2)\left[1 - (1-v_0^2)(1-\omega^2 r^2)\right]},$$

to rewrite it in above introduced notations as $d\phi/d\lambda = -2\sqrt{1 - \Omega^2 \sin^2(\phi/2)}$, and to take one more derivative by λ. The striking resemblance of our solutions

with mathematical pendulum motion, noticed already in [4], becomes, now, more clear and appreciable. If we introduce the concept of an *analogous pendulum*, governed by (2.8), then our initial conditions ($r_0 = 0$, $(dr/dt)_{t=0} = v_0$) for this pendulum are replaced by $\phi_0 = \pi$ and $(d\phi/d\lambda)_{\lambda=0} = -2v_0$. This pendulum rotates in the vertical plane, performing periodic motion with the effective frequency Ω. The time interval, needed by the bead to reach $\omega r = 1$ "light cylinder" point [4] corresponds, now, to the time needed by the analogous pendulum to reach its stable equilibrium ($\phi = 0$) point.

The LIF treatment has one more advantage: it allows to find out the pipe reaction force $f \equiv f_{\hat{\varphi}}$, which acts on the bead and forces it to corotate with the rigidly rotating pipe. This force is explicitly expressed by the azimuthal component of Eq. (2.3). The result is:

$$f = m_0\omega\left(r\frac{d\gamma}{dt} + 2\gamma v\right) = \frac{2m\omega v}{1-\omega^2 r^2}. \tag{2.9}$$

3. THE CASE OF THE LIMITED ROTATING ENERGY

From now on, we assume that the total energy of the whole rotating system (rotator+pipe+bead) is fixed and constant. In other words, the system is assumed to be conservative. In particular, let the rotator be a solid sphere with a mass M, radius R, and a moment of inertia $I = (2/5)MR^2$. The pipe is still assumed to be massless. The rest mass of the bead is m_0, and at $t = 0$ it is located at $r_0 = R$ (at the rotator surface) and has an initial velocity v_0. We take ω_0 as low as to ensure $\omega_0 R \ll c$ condition. Since the rotation angular velocity will be a decreasing function of time, it guarantees the nonrelativistic rotation of the rotator. On the contrary, we do not put any constraints on v_0 — it may be arbitrarily high. The rotator has, thus, initially an energy $E_{01} = (I/2)\omega_0^2$, and an angular momentum $L_{01} = I\omega_0$, while an initial energy of the bead is $E_{02} = m_0c^2\gamma_0$, and its angular momentum is $L_{02} = m_0R^2\omega_0\gamma_0$. By γ_0 is denoted a Lorentz factor of the bead: $\gamma_0 \equiv (1-(\omega_0 R/c)^2-(v_0/c)^2)^{-1/2}$. An absolute rigidness of the pipe — another quite artificial assumption — ensures a rigid rotation of the system: at each moment of time the rotator, the pipe as the whole and the bead have the same angular velocity $\omega(t)$.

Certainly, the total energy and the total angular momentum of the system are conserved quantities $E(t) \equiv E_1(t) + E_2(t) = E_0$ and $L(t) \equiv L_1(t) + L_2(t) = L_0$. So, we have the following equations:

$$\frac{I}{2}\omega^2 + m_0c^2\gamma = E_0, \tag{3.1}$$

$$I\omega + m_0r^2\omega\gamma = L_0, \tag{3.2}$$

where $\gamma(t)\equiv(1-(\omega r/c)^2-(v/c)^2)^{-1/2}$, $v(t)\equiv dr/dt$ is a radial velocity of the bead, and $r(t)$ is a radial coordinate of the bead as a function of time. The latter function may be expressed explicitly as a function of $\omega(t)$ by combining (3.1) and (3.2)

$$r = c\sqrt{\frac{2(L_0 - I\omega)}{\omega(2E_0 - I\omega^2)}}, \tag{3.3}$$

and the Lorentz factor $\gamma(t)$ may also be expressed through $\omega(t)$ in the following way:

$$\gamma = \frac{2E_0 - I\omega^2}{2m_0c^2}. \tag{3.4}$$

Using the definition of the Lorentz factor and (3.3) we can also write an explicit equation for $v(t)$:

$$v = c\frac{\sqrt{(2E_0 - I\omega^2)(2E_0 - 2L_0\omega + I\omega^2) - 4m_0^2c^4}}{2E_0 - I\omega^2}. \tag{3.5}$$

Now, it remains to find an equation for $\omega(t)$ by itself. For this purpose, one may take a derivative of (3.3), expess dr/dt through $d\omega/dt$, and take into account (3.5). By this procedure we get for $\omega(t)$ the following, rather complicated, first order differential equation:

$$\frac{d\omega}{dt} = \frac{\sqrt{2\omega^3(L_0 - I\omega)(2E_0 - I\omega^2)}}{3IL_0\omega^2 - 2I^2\omega^3 - 2E_0L_0} \cdot \frac{\sqrt{[(2E_0 - I\omega^2)(2E_0 - 2L_0\omega + I\omega^2) - 4m_0^2c^4]}}{3IL_0\omega^2 - 2I^2\omega^3 - 2E_0L_0}, \tag{3.6}$$

Let us introduce the following dimensionless notations: $\lambda\equiv\omega_0 t$, $\Omega(t)\equiv\omega/\omega_0$, $\varepsilon\equiv m_0/M$, $x_0\equiv\omega_0 R/c = R/R_{LC}$, $x(t)\equiv\omega_0 r/c = r/R_{LC}$, $V(t)\equiv v(t)/c$, $a\equiv E_{02}/E_{01}$, $b\equiv L_{02}/L_{01}$. In these notations above derived equations may be rewritten in the following dimensionless form:

$$\frac{d\Omega}{dt} = \frac{\sqrt{2\Omega^3(1-\Omega+b)(1-\Omega^2+a)}}{3(1+b)\Omega^2 - 2\Omega^3 - (1+a)(1+b)} \cdot \frac{\sqrt{[(1-\Omega^2+a)((1-\Omega)^2+a-2\Omega) - a^2/\gamma_0^2]}}{3(1+b)\Omega^2 - 2\Omega^3 - (1+a)(1+b)}. \tag{3.7}$$

$$x = \sqrt{\frac{2(1-\Omega+b)}{\Omega(1-\Omega^2+a)}}, \tag{3.8}$$

$$\gamma = \gamma_0\left[1 + \frac{1-\Omega^2}{a}\right], \tag{3.9}$$

$$V = \frac{\sqrt{(1-\Omega^2+a)[(1-\Omega)^2+a-2b\Omega]-a^2/\gamma_0{}^2}}{1-\Omega^2+a}. \qquad (3.10)$$

For the ratio of the bead and rotator energies we get:

$$E_2/E_1 = \frac{1-\Omega^2+a}{\Omega^2}. \qquad (3.11)$$

The derived system of equations may be solved numerically. However, it seems useful to write the radial component of an equation of the bead motion. In above introduced dimensionless notations it reduces to the following form:

$$\frac{d^2x}{d\lambda^2} = x\Omega^2\frac{1-\Omega^2x^2-2(dx/d\lambda)^2}{1-\Omega^2x^2} - \frac{x^2\Omega}{1-\Omega^2x^2}\left(\frac{d\Omega}{d\lambda}\right)\left(\frac{dx}{d\lambda}\right). \qquad (3.12)$$

When $\omega = \text{const}$ (steady rotation) the second term on the right hand side vanishes and (3.12) reduces to the one derived in [4] for the radial acceleration. So, it should be expected that when $d\Omega/d\lambda$ is small, the solutions of the present problem should match smoothly with the corresponding solutions from [4].

The solutions of the (3.7)–(3.10) system depend on three parameters: a, b, and γ_0. In physical terms, they depend on the ratio of the bead and the rotator masses ε, on the "rotation rate" x_0, which measures the ratio of the initial rotational linear velocity at the surface of the rotator to the speed of light, and the initial Lorentz factor of the bead γ_0. Note that x_0 is the ratio of the rotator radius to the radius of its "light cylinder" R_{LC}. Note also that $b = ax_0{}^2/2$.

The solutions of the equations show, that as the distance increases, the particle radial velocity behaves as in the previous case, i.e. when $v_0 > \frac{c}{\sqrt{2}}$ the particle braking is beginning, but near the light cylinder the particle is accelerated. At the same time the particle azimuthal velocity increases before the light cylinder, but after the light cylinder, it decreases. This means, that before the light cylinder the radial component of energy is transformed into the azimuthal one. Then (in the case of rigid pipe) the particle energy increases and the rotation of the source is slowing down.

4. CONCLUSION

We have discussed a *gedanken experiment* and of course the obtained results are far from reality, except the effect of particle braking along the radius (i.e. the magnetic field line), when $v_0 > \frac{c}{\sqrt{2}}$. This effect must be taken into account during the formulation of the hydrodynamical equatios and also in the investigation of pulsar winds and pulsar magnetosphere formation process.

5. AKNOWLEDGEMENTS

G. Z. Machabeli's investigation was suppotred, in part, by INTAS No 1010 ct 930015.

REFERENCES

1. Landau L. D. and Lifshitz E. M. Theory of the field. — M.: Nauka, 1988 (in Russian).
2. Sivukhin D. V. The drift theory of charge particle moving in the electromagnetic field. — In: Voprosy Teorii Plazmy /Ed. Leontovich M. A. — M.: Atomizdat, 1963. V. 1 (in Russian).
3. Nanobashvili I. S. Some problems of the description of a relativistic plasma stream, which corotates with the pulsar magnetosphere. // Czech. J. Phys. (to be published).
4. Machabeli G. Z. and Rogava A. D. // Phys. Rev. A, 1994. V. 50. P. 98.

Abastumani Astrophysical
Observatory, Tbilisi State
University, Republic of Georgia

Поступила в редакцию
13 ноября 1995 г.

УДК 523.165

STUDY OF THE RELATIONSHIP BETWEEN CORONAL MASS EJECTIONS AND ENERGETIC ELECTRONS IN INTERPLANETARY SPACE

E. I. Daibog, S. W. Kahler, V. G. Stolpovskii

We consider time characteristics of energetic electron events in interplanetary space after solar flares associated with coronal mass ejections (CME). Analysis of electron intensity–time profiles shows that independently of flare duration times to electron event maximum from flare onset and from electron event onset increase with increasing of CME velocity. Possible interpretation of this effect is electron acceleration by CME associated shock wave.

1. INTRODUCTION

An important problem of solar energetic particle (SEP) events is whether SEPs are accelerated in impulsive phase of a flare or by coronal and interplanetary shocks associated with CMEs (Coronal Mass Ejection). As a whole particle acceleration by shocks is widespread phenomenon in the heliosphere and many astrophysical objects [1]. Some time ago it has been recognized that shocks are of fundamental importance for SEP events [2, 3].

As for observations of shock accelerated particles there are clear evidencies and identifications of shock particle enhancements at energies of hundreds keV–MeVs for protons and up to tens keV for electrons [4]. Situation with energetic electrons ($E > 0.1$ MeV) is not so transparent. Energetic electrons can easily escape from the shock front and their motion has another time as well as length scales. Moreover they can go away and greatly outstrip a shock front.

The majority of observations both at low and high energies concerns proton events. Direct detailed measurements of energetic electron component of SEPs are less numerous and its relation to shocks is known much worse than in a proton case. The main ideas on accelerated electron dynamics in a source and solar atmosphere were obtained using solar X– and radioemission observations and are extremely model–dependent. Their application to electron events in interplanetary space gives ambiguous results. So better understanding of an interrelation between energetic electron fluxes and shocks may be achieved when results of direct electron measurements and data of X– and radioemission observations are considered together. But such investigations are not numerous.

There are both pro and contra arguments for shock subrelativistic and relativistic electron acceleration. Observations of energetic electron events lasting for many hours following large flares [5], electron events without hard X–ray association [6] and other arguments [7] can be supports of the point of view, that energetic electrons were accelerated in long duration process and a shock source is a possible explanation for these events. However up to now the contribution to interplanetary electron fluxes from acceleration in coronal or interplanetary shocks is poorly understood.

In [7] we studied a probaibility of shock acceleration of > 70 keV electrons. If these electrons in SEP events can arise from either flares or shocks, then we should expect that the electron escape efficiency should be different for flares with and without CME. We estimated an escape efficiency comparing maximum electron flux with hard X–emission fluence and found that it is some higher (by factor of 2) in the case of flares associated with CME. It may be considered that the shock electron population is comparable to that of impulsive component. But statistics was not rich enough and only well–connected events were taken into account. So the conclusion must be cleared up.

In the present paper we examine the association and timing of flares and CMEs for a sample of 24 SEP events observed by ISEE 3 from 1980 through 1985. We examine the intensity–time pofiles of electron enhancements to see if there is any distinction in profile shape in the cases of flares with and without CMEs. In [8] we have considered > 0.3 MeV electron intensity–time profiles in SEP events according to Helios data from 1979 through 1982. It was assumed that if an acceleration occurs during an extended period of shock propagation in corona then time interval for which SEP intensity rises to the maximum will be longer in comparison with acceleration in impulsive phase of a flare. We established that on the average rise time of electron enhancements related to flares with CMEs is really some longer. But statistics was not high. We shall compare relations between flare, CME and electron enhancement parameters obtained for a sample of ISEE 3 events with those ones from Helios and Phobos 2 observations [8, 9]. In a number of cases the same SEP events were observed by Helios, ISEE 3 and Venera.

2. DATA SOURCE AND PROCESSING METHODS

Data considered includes an information on SEP events, flares and CMEs. Energetic particle fluxes were measured onboard ISEE 3 which was in the inner Lagrangian point between Sun and the Earth. Electrons with energy between 0.22 and 2.0 MeV and 4–19 MeV were measured in the GSFC medium–energy cosmic ray experiment. Time resolution of electron measurements was high enough and we used 15 min averaged data in our investigation in according to [10].

Standard information about H_α–flares and bursts of flare in hard X– and radioemission was taken from Solar–Geophysical Data and from Internet network. In the case of electromagnetic bursts we used not only table data but also intensity–time plots. An informatiom on corresponding hard X–bursts was provided by HXRBS observations on SMM [11].

During the periods considered CMEs were observed by the Solwind coronagraph on P78–1 at distance from 2.5 $R_\odot$ to 10 $R_\odot$ and coronagraph/polarimeter on SMM. Data of Solwind observations were prepared by N. R. Sheeley [12]. In the case of SMM observations we have a revised and expanded catalogue [13] which permits us to obtain time, velocity, position angle and other parameters of CMEs associated with selected SEP events.

Selection of electron events was made on the basis of energetic electron intensity–time variations. Sharp intensity rise, followed by more or less gradual decay of electron flux was considered as SEP event. Those enhancements having duration more than 3 hours and amplitude exeeeding the background by 3σ were taken into account. According to 3σ condition we could distinguish electron enhancements with the amplitude of > 0.2 MeV electron flux greater than 0.05 particle/cm^2 sec sr.

The particle source identifications for the majority of SEP events considered have been published previously. We began, however, by making flare/CME associations without reference to these previous studies. We used standard method of identification of parent flare [14]. The associations derived were essentially the same as those arrived in earlier studies. But our event list contains a number of smaller events which were not included in previous lists.

The observer's magnetic footpoint was determined by the method described in [15], taking into account the real solar wind velocity. For recalculating times of electron intensity maximum from one angular distance between magnetic footpoint and flare site to another one it's necessary to employ some model notions. We used ideas of simple diffusion model and took into account a difference of angular distances. Here we used formalism of coronal propagation [16] which is supposed to be independent of the physical content of phenomena considered. So we used approximation formulae for coronal propagation of > 0.5 McV electrons from [17] and recalculated them to 0.2 MeV. A fit to the data was performed by assuming that the constant delay within certain angular distance $\varphi_0 = 26$ (Fast Propagation Region) is due to interplanetary propagation and that time to maximum tm increases linearly beyond φ_0. Then may be aproximated by the next formula

$$t_m(1\ \mathrm{AU}, \varphi) = 78 + 4.1(\varphi - 26)\ ,\ \mathrm{min} \qquad (1)$$

where the first and the second terms describe interplanetary to $r = 1$ AU and coronal propagation, respectively.

We suppose that there must be some correlation between rise time of SEP event and a velocity of coronal shock. Let us suppose for simplicity that CME

velocity is changing with constant acceleration and CME driven shock can accelerate electrons if shock velocity is higher than some V_{lim}. Let the CME speed rises till the value V_0. Then the time during which electrons should be shock accelerated increases with increasing Vo and a distance that shock travels during this time also increases with increasing V_0. In a case of constant CME and shock speed distance at which shock can accelerate particles, would be traveled by the shock in a time decreasing with increase of V_0. As a mattter of fact it is necessary to take into account damping of shock and decreasing of ambient plasma density but as a whole the character of V_0 vs t dependence would be the same: $t(V_0)$ — decreasing function, if $V = V_0 = \text{const}$, and $t(V_0)$ — increasing function, if CME acceleration or deceleration takes place.

So as we know about acceleration — deceleration of the shock, we are waiting as a result of our investigation that rise time of SEP event is increasing function of CME traveling speed, because the injection continues for longer times with faster CMEs, and a size of injection region increases faster than linearly with CME speed. Preliminary investigation [8] showed that there is a tendency of increasing rise time vs CME speed.

If the cone containing CME intersects with limb plane then measured CME velocity is the real one. If not, we obtain the "real" CME velocity by recalculation of the nearest to the sky plane forming of the CME cone. Recalculated V_{CME} is

$$V_{\text{calc}} = V_{\text{CME}} \Big/ \cos(\xi - \alpha/2) , \tag{2}$$

where ξ is an angle between radial flare extension and the sky plane,

$$\xi = \arccos\left[\cos^2\theta \cdot \sin^2 B + \sin^2\theta\right]^{1/2} . \tag{3}$$

Angle α in (2) is a real dimension of CME cone,

$$\alpha = 2\text{arctg}\left[\text{tg}(D/2) \cdot \cos\xi\right] , \tag{4}$$

angle D is dimension of CME cone in the sky plane.

4. RESULTS AND DISCUSSION

ISEE data list includes 24 events obtained at 1 AU and is shown in the table.

Here "1" is event number; "2"— event date; "3" — flare location; "4" — CME initial position angle and width (in parenthesies); "5" — CME velocity, km/s; "6" — CME velocity, calculated according to (2), km/s; "7" — angular distance φ; FPR means that observation point is projected to fast propagation region; "8" — time to maximum of electron event corrected accoding to (1), hrs; "9" — electron event rise time, hrs; time, hrs; "10" — soft X-rays duration (L — long, > 1 hour, S — short, < 1 hour).

1	2	3	4	5	6	7	8	9	10
1	040480	N27W34	N07W(140)	840	840	FPR	3.0	2.1	L
2	070680	N13W70	no			FPR	1.2	1.0	S
3	070680	N14W70	no			FPR	0.8	0.6	S
4	230381	N10W54	N30W(40)	400	420	FPR	1.7	1.0	S
5	250381	N09W87	N25W(70)	900	900	W50	2.5	2.0	S
6	300381	N13W72	N10W(180)	1300	1300	FPR	2.0	1.0	L
7	040481	S44W87	S45W(35)	900	900	W40	3.6	2.5	S
8	280481	N16W90	N05W(30)	1000	1000	W48	3.2	3.0	L
9	071181	S10W39	no			FPR	1.3	0.8	S
10	141181	N16W49	N05W(110)	585	615	FPR	4.6	4.5	L
11	051281	N20W40	N45W(60)	840	905	FPR	6.5	5.5	L
12	020182	N19W88	N10W(40)	650	650	W45	2.0	1.0	S
13	080282	S13W88	N05W(10)	1310	1310	FPR	1.3	1.1	S
14	090282	S14W90	N05W(30)	1600	1600	W33	1.5	1.6	S
15	070382	N19W53	N10W(60)	1140	1240	FPR	2.9	2.4	L
16	190782	N21W45	N45W(40)	630	700	FPR	1.8	1.5	S
17	080882	S09W65	S10W(10)	600	640	FPR	3.0	2.0	S
18	130882	N11W59	S30W(20)	300	330	FPR	0.8	0.6	S
19	140882	N11W63	no			FPR	1.0	0.7	S
20	221182	S08W34				FPR	1.6	1.3	S
21	221182	S11W36	S10W(60)	740	805	FPR	3.1	2.7	L
22	071282	S19W86	S10W(20)	1250	1250	FPR	3.4	2.5	L
23	050183	>W90	no			FPR	1.7	1.0	S
24	150583	S10W80	S25W(50)	1110	1110	FPR	2.5	1.0	S

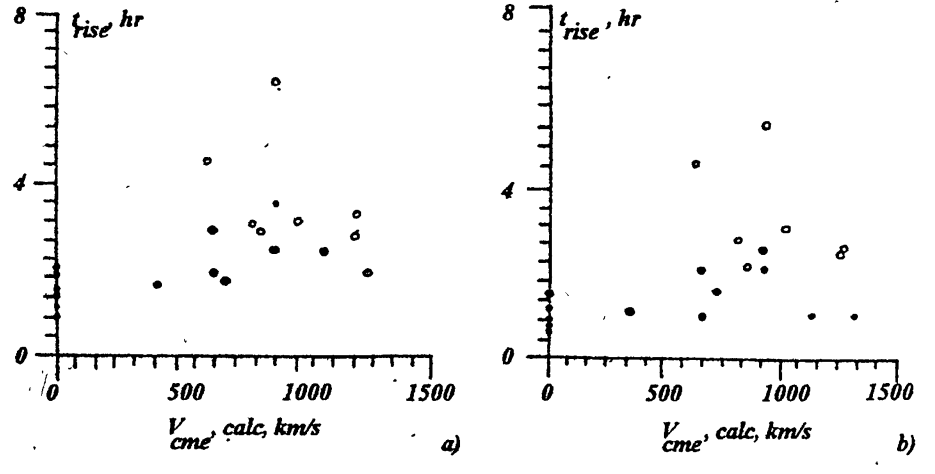

Рис. 1.

In Fig. 1 we present time to maximum (a) and rise time (b) vs calculated Vcme. Events $\mathcal{N}\mathcal{N}$ 13, 14 and 18 of the table were excluded from the figure as the corresponding flares were in opposite hemispheres with observed CMEs. Two points with highest values of t_m and $t_{\rm rise}$ concern $\mathcal{N}\mathcal{N}$ 10 and 11 events. We compared these values with t_m and $t_{\rm rise}$ obtained by Helios and Venera observations [6, 7]. In the case of Nov. 14, 1981 event Venera was near the Earth and values t_m and $t_{\rm rise}$ were 4.2 hrs and 4.0 hrs, respectively. For Dec. 5, 1981 event Helios and Venera were located at $r = 0.95$ AU and $r = 0.44$ AU, respectively. Venera's magnetic footpoint was in FPR, angular distance for Helios was E95. Normalized values t_m were 7.0 and 8.1 hrs for Venera and Helios, respectively. Thus high values of t_m and $t_{\rm rise}$ obtained in three different points are practically the same. It seems that these events are related to disturbances which could be caused by filament dissapearance. For Dec. 5, 1981 it was proved in [18]. It confirms that energetic electrons can be accelerated by CME driven shock.

We see from Fig. 1 that t_m and $t_{\rm rise}$ are slowly increasing with increasing $V_{\rm CME}$ and that all values of t_m and $t_{\rm rise}$ are less for non-CME associated flares than for CME-associated ones. Open circles are for L, dark points — for S events. As there is no difference between L and S events in Fig. 1 one may conclude that t_m and $t_{\rm rise}$ are caused rather by time extended shock acceleration than by flare duration.

Работа поддержана грантом РФФИ $\mathcal{N}$ 94–02–04453 и контрактом SPC–94–4071 с EOARD.

REFERENCES

1. Johnson F. C., Elisson D. C. // Space Sci. Rev. 1991. V. 58. P. 259.
2. Evenson P. A., Meyer P., Yanagita S. // J. Geophys. Res. 1982. V. 87. P. 625.
3. Cane H. V., Reams D. V., Von Rosenving T. // J. Geophys. Res. 1988. V. 93. P. 9555.
4. Krimigis S. M. // Space Sci. Rev. 1992. V. 59. P. 83.
5. Lin R. P. // Solar Phys. 1985. V. 100. P. 537.
6. Daibog E. I., Kurt V. G., Logachev Yu. I., Stolpovskii V. G. // Kosm. Issled. 1989. V. 27. P. 113.
7. Kahler S. W., Daibog E. I., Kurt V. G., Stolpovskii V. G. // Ap. J. 1994. V. 422. P. 394.
8. Kahler S. W., Stolpovskii V. G., Daibog E. I. // IAU Colloq. 1994. P. 479.
9. Stolpovskii V. G., Erdos G. et al. // Proc. 24th Int. Cosm. Ray Conf. 1995. V. 4. P. 301.
10. Richardson I. // private communication.

11. Dennis B.R. et al. // NASA TM–4332, 1991.
12. Sheeley N.R., Jr. // private communication.
13. Burkepile J.T., St. Cyr O.C. // NCAR/TN–369+STR, 1993.
14. van Hollebecke M.A.I. et al // Solar Phys. 1975. V. 41. P. 189.
15. Notle J.T., Roelof E.C. // Solar Phys. 1973. V. 33. P. 241.
16. Lin R.P., Mewaldt R.A., van Hollebeke M.A.L. // Ap. J. 1982. V. 253. P. 949.
17. Kahler S.W. et al. // Ap. J. 1986. V. 502. P. 504.

Nuclear Physics Institute
Moscow State University, Russia
Geophysics Directorate Phillips
Laboratory Hanscom, USA

Поступила в редакцию
5 декабря 1995 г.

УДК 523.987.4

О ДИНАМИКЕ ПЛАЗМЫ В СОЛНЕЧНЫХ МАГНИТНЫХ ТРУБКАХ

М. Л. Ходаченко

На основе известного автомодельного решения системы МГД уравнений, описывающего течения плазмы с однородной деформацией, построена динамическая модель солнечной магнитной трубки. При построении данной модели использовалась развернутая форма уравнения энергии, учитывающего джоулев нагрев, радиационное охлаждение, эффекты, связанные с теплопроводностью и вязкостью. Были исследованы различные динамические режимы эволюции магнитной петли. Большой интерес представляют процесс быстрой, носящей вспышечный характер, компрессии и нагрева плазмы в трубке, процесс компрессии плазмы, сопровождаемой ее охлаждением, соответствующий формированию протуберанца в трубке, а также различные осцилляторные режимы и процессы декомпрессии плазмы, сопровождаемые как ее охдаждением, так и нагревом. Проведено аналитическое и численное исследование предлагаемой модели.

1. ВВЕДЕНИЕ

В настоящее время достигнут значительный прогресс в деле изучения на основе МГД уравнений разнообразных стационарных ($d/dt = 0$) задач, которые образовали собой крупный раздел в МГД теории Солнца, именуемый солнечной магнитогидростатикой. В рамках магнитогидростатики построены и исследованы модели равновесия различных солнечных плазменно–магнитных структур, таких как протуберанцы [1–10] и всевозможные магнитные силовые трубки [11–15], получены критерии их устойчивости [8, 16–22].

Вместе с тем, наземные и космические наблюдения последних лет показывают, что солнечная плазма находится в непрерывном движении. Имеется большое разнообразие течений плазмы (эвершедовские, спикульные, корональные дожди, сифонные потоки, конвективное движение в фотосфере), не принимавшихся во внимание при построении стационарных моделей. Кроме того, как протуберанцы, так и магнитные петли не существуют бесконечно во времени, все они формируются в результате определенных процессов, развиваются в течение некоторого конечного времени жизни, по истечении которого исчезают, разрушаясь или трансформируясь в другие объекты. Например, нагрев плазмы протуберанца может сделать его невидимым в традиционном диапазоне длин волн H_α, что выглядит как исчезновение протуберанца (disparition brusque — внезапное

исчезновение). Известны также случаи активизации спокойных протуберанцев и их превращения в эруптивные, характеризующиеся мощными выбросами вещества, приводящими к разрушению волокна. С другой стороны, увеличение плотности плазмы в магнитной петле, сопровождаемое ростом потерь на излучение, создает условия для формирования плотного холодного петельного протуберанца. Наконец, согласно наблюдениям, и протуберанцы, и магнитные петли являются "активными участниками" такого значительного и существенно не стационарного события как солнечные вспышки, оказывающего влияние на многие процессы не только на Солнце, но и в межпланетном пространстве и на Земле.

Все эти обстоятельства обуславливают повышенное внимание к нестационарным процессам в солнечной физике, диктуют необходимость их более детального изучения и построения динамических моделей известных объектов.

Однако аналитическое решение системы нестационарных МГД уравнений в общем случае является затруднительным, поэтому среди исследователей Солнца большой популярностью пользуются различные численные модели МГД процессов [9, 23–28]. Но как всякие численные модели они бывают порой весьма сложны и лишены простой математической наглядности. В связи с этим, особый интерес представляет рассмотрение и применение к солнечным задачам различных нестационарных автомодельных решений. Такой подход сужает класс изучаемых процессов, накладывает на них определенную специфику, но, вместе с тем, он позволяет получить их более простое аналитическое описание.

В данной работе мы рассматриваем динамическую модель солнечной силовой магнитной трубки, построенную на базе известного автомодельного решения [29, 30] МГД уравнений, описывающего течения плазмы с однородной деформацией, в которых связь между эйлеровыми x_i и лагранжевыми x_i^0 координатами имеет вид [31]:

$$x_i = M_{ij}(t)x_j^0 + m_i(t), \tag{1}$$

где $M_{ij}(t)$ тензор деформации, задающий изменение во времени и поворот осей эллипсоида, определяющего лагранжеву поверхность, движущуюся вместе с плазмой. Предлагаемая модель позволяет описать ряд характерных для эволюции солнечных магнитных трубок процессов, включая быстрый, носящий вспышечный характер, нагрев трубки, ее пульсации, а также охлаждение трубки и формирование в ней протуберанца.

Для МГД течений с однородной деформацией характерны линейные зависимости скорости плазмы и напряженности магнитного поля от координат:

$$V_i(\mathbf{x},t) = w_{ij}(t)x_j + u_i(t), \tag{2}$$

$$B_i(\mathbf{x},t) = A_{ij}(t)x_j + b_i(t), \qquad A_{kk}(t) = 0. \tag{3}$$

Плотность плазмы при этом зависит только от времени $\rho(t)$, а давление представляется полиномом второй степени от координат:

$$p(\mathbf{x},t) = \frac{1}{2}P_{ij}(t)x_i x_j + P_k(t)x_k + P_0(t), \qquad P_{ij}(t) = P_{ji}(t). \tag{4}$$

Здесь необходимо отметить, что подобного вида автомодельные решения уже рассматривались в ряде работ применительно к процессам, происходящим в солнечной атмосфере. Так в работах С. И. Сыроватского [29, 32] и С. В. Буланова [33] исследовалось поведение токовых слоев и магнитный коллапс с точки зрения физических процессов, происходящих в солнечных вспышках. У Дж.-И. Сакая совместно с различными соавторами имеется целый цикл работ, посвященных изучению динамики области слияния двух магнитных петель [34–38], а также работы, посвященные вопросам формирования и эволюции протуберанцев [39, 40]. Авторам этой статьи совместно с В. В. Зайцевым динамическая модель протуберанца [40] была обобщена на случай частичноионизированной плазмы [41, 42]. Основной идеализацией названных выше моделей является то, что в большинстве из них [35, 38–42] предполагается адиабатичность рассматриваемых процессов, а в других [34, 36, 37] используется чрезвычайно упрощенный вид уравнения энергии, учитывающего лишь слагаемое, связанное с Джоулевым нагревом.

Кроме того, в указанных работах Дж.-И. Сакая исследуется только область слияния двух токовых трубок, тогда как мы рассматриваем здесь динамические процессы, происходящие в отдельной магнитной петле. В предлагаемой нами в данной статье неадиабатической модели солнечной магнитной трубки рассматривается более полная форма уравнения энергии, в котором наряду с Джоулевым нагревом учитываются существенно превосходящие его в хромосфере и короне по величине потери энергии, связанные с излучением, а также вклад теплопроводности и нагрев, обусловленный вязкостной диссипацией. Еще одно отличие рассматриваемой здесь модели от ранее существовавших состоит в том, что в ней учитывается связанная с пространственной неоднородностью температуры пространственная неоднородность проводимости плазмы $\sigma(\mathbf{x}) \propto T^{3/2}(\mathbf{x})$.

Заметим, что рассматривая среди прочих режим пульсаций трубки, мы, по существу, исследуем возбуждение в ней "сосисочной" моды быстрых магнитозвуковых колебаний, в которых пространственный масштаб возбуждаемой волны, λ, полагается много большим длины рассматриваемого фрагмента трубки L. Численное моделирование быстрых магнитозвуковых волн в корональной плазме и, в частности, исследование пульсирующих режимов, обусловленных "сосисочной" модой, как в линейном, так и нелинейном случаях проводилось Б. Робертсом и К. Муравским в работах [43] (линейные пульсации) и [44] (нелинейные пульсации). В этих работах корональная магнитная трубка моделировалась плазменным

слоем с плавным изменением плотности плазмы на границах слоя, и решалась система МГД уравнений в приближении малого β.

Общая структура статьи следующая: в разделе 2 получены уравнения, описывающие динамику автомодельных решений системы МГД уравнений для модели солнечной магнитной трубки, в разделе 3 осуществляется аналитическое исследование и численное решение этих уравнений, рассматриваются возможные динамические режимы эволюции магнитной трубки, в заключении приводится графическая интерпретация возможных динамических режимов и обсуждаются вопросы, связанные с реализацией полученных решений в условиях Солнца.

2. ОСНОВНЫЕ УРАВНЕНИЯ, ОПИСЫВАЮЩИЕ ДИНАМИЧЕСКУЮ МОДЕЛЬ СОЛНЕЧНОЙ МАГНИТНОЙ ТРУБКИ

Предлагаемая в данной работе модель описывает класс достаточно тонких магнитных петель с током, для которых характерный масштаб R, являющийся радиусом их поперечного сечения, оказывается меньше других масштабов, L и R^*, характеризующих продольный и поперечный размеры всей магнитной структуры, включающей в себя и токовую магнитную трубку.

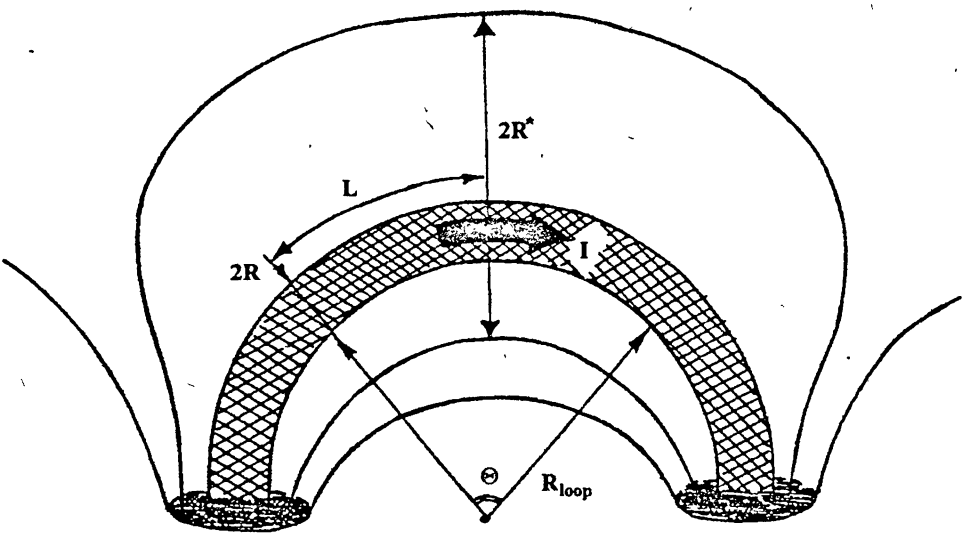

Рис. 1. Образующая петлю тонкая магнитная трубка с током, находящаяся внутри магнитной структуры с характерными поперечным, R^*, и продольным, L, масштабами.

Проводимый ниже анализ справедлив для низких петель в целом, если их высота оказывается меньше атмосферной шкалы высот Λ, а также для

описания процессов, имеющих место в верхней части магнитной петли произвольных размеров, если радиус кривизны R_{loop} и угловой размер Θ исследуемого участка токовой трубки (см. рис. 1) удовлетворяют требованию:

$$\left\{2R,\ R_{\text{loop}}\left(1-\cos\left(\frac{\Theta}{2}\right)\right)\right\} \ll \Lambda\,. \tag{5}$$

Условие (5) позволяет пренебречь в уравнении движения плазмы слагаемым, обусловленным гравитацией ($\rho\mathbf{g}$). Кроме того, мы будем полагать диаметр поперечного сечения трубки, $2R$, много меньшим по сравнению с ее радиусом кривизны, R_{loop}, что позволяет нам пренебрегать изогнутостью трубки и проводить рассмотрение как в случае прямого цилиндра. При этом плазму в трубке считаем полностью ионизированной. Соответствующая такой задаче система МГД уравнений имеет следующий вид:

$$\frac{\partial\rho}{\partial t} + \operatorname{div}(\rho\mathbf{V}) = 0\,, \tag{6}$$

$$\rho\left[\frac{\partial\mathbf{V}}{\partial t} + (\mathbf{V}\cdot\nabla)\mathbf{V}\right] = -\nabla p + \frac{1}{c}[\mathbf{j}\times\mathbf{B}] + \mathbf{F}_v\,, \tag{7}$$

$$\frac{\partial\mathbf{B}}{\partial t} = \operatorname{rot}[\mathbf{V}\times\mathbf{B}] + \frac{c^2}{4\pi\sigma}\Delta\mathbf{B} - \frac{1}{ne}\operatorname{rot}[\mathbf{j}\times\mathbf{B}] - \frac{c^2}{4\pi}\left[\nabla\left(\frac{1}{\sigma}\right)\times\operatorname{rot}\mathbf{B}\right], \tag{8}$$

$$\frac{\partial p}{\partial t} + (\mathbf{V}\cdot\nabla)p + \gamma p\,\operatorname{div}\mathbf{V} = -(\gamma-1)\mathbf{L}\,, \tag{9}$$

$$p = 2nk_BT\,. \tag{10}$$

Здесь ρ, $\mathbf{V}$, p, T, $\mathbf{B}$ являются соответственно плотностью, скоростью, давлением, температурой плазмы и магнитным полем, $\gamma = c_p/c_v$ — постоянная адиабаты. Через $\mathbf{F}_v$ в уравнении (7) обозначена сила вязкости

$$\mathbf{F}_v = \rho\nu\left(\Delta\mathbf{V} + \frac{1}{3}\nabla(\operatorname{div}\mathbf{V})\right), \tag{11}$$

где ν — коэффициент кинематической вязкости. Для полностью ионизированной водородной плазмы, основываясь на [45], будем использовать приближенное выражение:

$$\rho\nu \approx 2{,}21\cdot 10^{-16}T^{5/2}\ [\text{г}\cdot\text{см}^{-1}\cdot\text{с}^{-1}]\,. \tag{12}$$

Появление последнего слагаемого в правой части уравнения (8) связано с учетом возможной пространственной неоднородности проводимости σ.

В уравнении энергии (9) L обозначает сумму различных источников и потерь энергии:

$$\mathrm{L} = q_r - \frac{d}{ds}\left(\kappa_0 T^{5/2}\,\frac{dT}{ds}\right) - \frac{j^2}{\sigma} - H\,. \tag{13}$$

Здесь q_r — потери энергии за счет излучения, которые мы аппроксимируем зависимостью:

$$q_r = \chi\rho^2 T^{\alpha}\,, \tag{14}$$

где α и χ — константы. Для изменений температуры плазмы в диапазоне $2\cdot 10^4\ \mathrm{K} < T < 2\cdot 10^7\ \mathrm{K}$ эти константы имеют следующие приближенные значения: $\alpha \approx -1/2$, $\chi \approx 2.5\cdot 10^{28}$ [46]. Второе слагаемое в (13) связано с теплопроводностью. При этом мы считали магнитное поле достаточно большим и пренебрегали потоком тепла поперек поля ($\kappa_\perp \ll \kappa_\parallel = \kappa_0 T^{5/2}$, $\kappa_0 \approx 10^{-6}$), а также полагали неизменной вдоль исследуемого фрагмента магнитной петли площадь его поперечного сечения. Через s обозначено расстояние, измеряемое вдоль силовой линии магнитного поля. Третье слагаемое в (13) обусловлено джоулевым нагревом, а последнее представляет собой сумму всех других источников нагрева, среди которых мы будем здесь учитывать нагрев, связанный с вязкостной диссипацией

$$H_v = \rho\nu\left[\frac{1}{2}e_{ij}e_{ij} - \frac{2}{3}(\mathrm{div}\mathbf{V})^2\right], \tag{15}$$

где $e_{ij} = \dfrac{\partial V_i}{\partial x_j} + \dfrac{\partial V_j}{\partial x_i}$.

Работая в цилиндрической системе координат с осью z, направленной вдоль оси магнитной трубки, будем рассматривать автомодельное решение системы уравнений (6)–(10), описывающее течение плазмы с однородной деформацией, характеризуемое следующими зависимостями физических величин от времени и координат:

$$V_r(\mathbf{x},t) = \frac{\dot a}{a}\,r, \qquad V_\varphi(\mathbf{x},t) = 0, \qquad V_z(\mathbf{x},t) = \frac{\dot b}{b}\,z\,, \tag{16}$$

$$B_r(\mathbf{x},t) = 0, \qquad B_\varphi(\mathbf{x},t) = B_{\varphi 0}(t)\frac{r}{R^*}, \qquad B_z(\mathbf{x},t) = B_{z0}(t)\,, \tag{17}$$

$$\rho(\mathbf{x},t) = \rho(t)\,, \tag{18}$$

$$p(\mathbf{x},t) = p_0(t) - p_1(t)\left(\frac{r}{R}\right)^2 - p_2(t)\left(\frac{z}{L}\right)^2. \tag{19}$$

где R и L — характерные поперечный и продольный пространственные масштабы токовой трубки, R^* — внешний поперечный масштаб исследуемой магнитной конфигурации, а $a(t)$ и $b(t)$ — безразмерные функции времени, характеризующие степень сжатия плазмы в трубке, являющиеся компонентами тензора деформации $M_{xx}(t) = M_{yy}(t) = a(t)$, $M_{zz}(t) = b(t)$, тогда как другие компоненты этого тензора в нашем рассмотрении полагаются равными нулю. Без ограничения общности для функций $a(t)$ и $b(t)$ можно задать следующие начальные условия [29]: $a(0) = b(0) = 1$.

Здесь необходимо отметить, что данные автомодельные решения адекватно описывают поведение исследуемой физической системы лишь при выполнении определенных специфических граничных условий, которые были получены и исследованы в [47, 48]. Эти условия соответствуют изменению потенциала внешних токов, создающих цилиндрическое магнитное поле (17), по вполне определенному закону и предполагают наличие внешних по отношению к исследуемому фиксированному объему плазмы сил. Однако, при исследовании реальных плазменно–магнитных конфигураций можно выделить два случая, когда влиянием граничных условий можно пренебречь, полагая их произвольными, и описывать с помощью (16)–(19) реальные течения плазмы [36, 40–42]:

- при рассмотрении процессов в плазме на временных интервалах t, не превосходящих характерное время $\tau \approx \min\{L_i\}/V^*$ [36, 40, 48], за которое информация о граничных условиях распространяется внутрь исследованной плазменно–магнитной конфигурации. Здесь L_i — внешние пространственные масштабы, а V^* — скорость распространения наибыстрейшей моды, несущей информацию о граничных условиях [49].
- при описании динамики достаточно компактных и плотных плазменных образований (например токовых трубок на Солнце или протуберанцев [41, 42]), находящихся внутри более крупных магнитных конфигураций. При этом, наличие на границе рассматриваемой области скачка концентрации n и температуры T плазмы обуславливает появление поверхностного импеданса, снижающего влияние внешних по отношению к исследуемому объему плазмы полей. Требование балланса давлений при условии непрерывности магнитного поля на границе такого плазменного образования определяет связь между значениями температуры (T_1) и концентрации плазмы (n_1) внутри и вне (T_2, n_2) его: $T_1 n_1 = T_2 n_2$.

В обоих указанных случаях мы имеем дело не с граничной, а с начальной задачей и используем предположение о безграничности среды, помня, однако, что при этом наше рассмотрение не выходит за рамки области, ограниченной масштабом $R < \min L_i$. Кроме того, как указывалось в [29], обсуждаемое автомодельное решение можно рассматривать

при определенных условиях как общую локальную аппроксимацию неоднородного течения плазмы в неоднородном магнитном поле в случае пространственно неоднородной температуры плазмы. Или, иными словами, как главный член общего разложения решения, соответствующего развившемуся течению плазмы в окрестности оси токовой трубки, когда имеет место сходимость разложения этого решения по степеням малого параметра (r/R^*). В этом случае граничная задача теряет смысл и вытекающие из нее ограничения на внешний потенциал исчезают.

Учитывая (10) и (18), мы можем записать на основе (19) аналогичное выражение для температуры плазмы:

$$T(\mathbf{x},t) = T_0(t) - T_1(t)\left(\frac{r}{R}\right)^2 - T_2(t)\left(\frac{z}{L}\right)^2, \tag{20}$$

где

$$T_k(t) = \frac{p_k(t)m_i}{2k_B\rho(t)}, \qquad k = 0,\,1,\,2\,. \tag{21}$$

При этом в нашем дальнейшем рассмотрении мы будем полагать малыми по сравнению с единицей величины:

$$\frac{p_1}{p_0}\left(\frac{r}{R}\right)^2 = \frac{T_1}{T_0}\left(\frac{r}{R}\right)^2 \ll 1\,, \tag{22}$$

$$\frac{p_2}{p_0}\left(\frac{z}{L}\right)^2 = \frac{T_2}{T_0}\left(\frac{z}{L}\right)^2 \ll 1\,, \tag{23}$$

что позволяет использовать разложение в ряд, где будем ограничиваться слагаемыми первого порядка по этим величинам:

$$T^\alpha(\mathbf{x},t) \approx T_0^\alpha(t)\left[1 - \alpha\,\frac{T_1}{T_0}\left(\frac{r}{R}\right)^2 - \alpha\,\frac{T_2}{T_0}\left(\frac{z}{L}\right)^2\right]. \tag{24}$$

Такой подход означает, что рассматриваемое нами решение МГД уравнений имеет асимптотический характер.

Подставляя (16) в уравнение непрерывности (6) и учитывая (18), для плотности плазмы находим:

$$\rho(t) = \frac{\rho_0}{a^2 b}\,, \tag{25}$$

где ρ_0 — постоянная величина, определяемая начальными условиями.

Используя выражения (16), (17) и (18), а также разложение в ряд (24), из уравнения (8), проектируя его на оси, получаем:

$$\frac{\dot{B}_{\varphi 0}}{B_{\varphi 0}} = -\left(2\,\frac{\dot{a}}{a} + \frac{\dot{b}}{b}\right) + \frac{c^2}{4\pi\sigma_0}\,\frac{6}{R^2}\,\frac{T_1}{T_0}\,, \tag{26}$$

$$\frac{\dot{B}_{z0}}{B_{z0}} = -2\frac{\dot{a}}{a}. \tag{27}$$

В уравнении (26) $\sigma_0 = \sigma(T_0)$ — значение проводимости в точке $\{r{=}0, z{=}0\}$. Можно показать, что в условиях хромосферной и корональной плазмы при рассмотрении процессов с характерным временем, много меньшим 10^9 с, второе слагаемое в уравнении (26) оказывается мало по сравнению с первым и им можно пренебречь. Таким образом, на основании решений уравнений (26) и (27) для компонент магнитного поля, учитывая (17), получим следующие выражения:

$$B_\varphi(r,t) = \frac{B_{10}}{a^2 b}\frac{r}{R^*}, \tag{28}$$

$$B_z(t) = \frac{B_{20}}{a^2}, \tag{29}$$

где B_{10} и B_{20} — определяемые начальными условиями значения магнитного поля на внешней границе исследуемой магнитной конфигурации. Из уравнения движения плазмы (7), подставляя в него выражения для автомодельного решения (16)–(19) и учитывая зависимости (28), (29), после проектирования на оси получим уравнения, описывающие динамику безразмерных функций $a(t)$ и $b(t)$, которые, в свою очередь, определяют изменение магнитного поля (см. (28), (29)), скорости (16) и плотности (см.(25)) плазмы:

$$\ddot{a} = \frac{2}{\tau_M^2}\left(\beta\tilde{T}_1 a - \frac{1}{ab}\right), \tag{30}$$

$$\ddot{b} = \frac{2}{\tau_S^2}\tilde{T}_2 b. \tag{31}$$

В уравнениях (30) и (31) нами введены параметры $\tau_M^2 = R^2/V_A^2$, где $V_A^2 = \frac{B_{10}^2}{4\pi\rho_0}\left(\frac{R}{R^*}\right)^2$, $\tau_S^2 = L^2/C_S^2$, где $C_S^2 = \frac{p_0(t{=}0)}{\rho_0}$ и $\beta = \frac{4\pi p_0(t{=}0)}{B_{10}^2(R/R^*)^2}$, а также безразмерные температурные функции времени: $\tilde{T}_1(t) = T_1(t)/T_0(t{=}0)$ и $\tilde{T}_2(t) = T_2(t)/T_0(t{=}0)$.

Наконец, из уравнения энергии (9) с учетом (13), (14) и (15), подставляя в него (19) и (16), принимая во внимание соотношение (21) и используя для слагаемых, пропорциональных различным степеням $T(\mathbf{x},t)$, разложение в ряд (24), после группировки коэффициентов при $\left(\frac{r}{R}\right)^0$, $\left(\frac{z}{L}\right)^0$, $\left(\frac{r}{R}\right)^2$ и $\left(\frac{z}{L}\right)^2$, аналогичного проведенному при получении (30) и (31) нормирования температурных функций $T_0(t)$, $T_1(t)$ и $T_2(t)$ получим уравнения, определяющие изменение безразмерных функций

$\tilde{T}_0(t) = T_0(t)/T_0(t{=}0)$, $\tilde{T}_1(t) = T_1(t)/T_0(t{=}0)$ и $\tilde{T}_2(t) = T_2(t)/T_0(t{=}0)$:

$$\dot{\tilde{T}}_0 = (1-\gamma)\left\{-f_1\frac{\tilde{T}_0^{-3/2}}{a^2b} + f_2\frac{\tilde{T}_0^{\alpha}}{a^2b} + f_3\,a^2b\tilde{T}_2\tilde{T}_0^{5/2} - \right.$$

$$\left. - f_4\,a^2b\tilde{T}_0^{5/2}F(\dot{a},\dot{b},a,b)\right\} + (1-\gamma)\tilde{T}_0\left(2\frac{\dot{a}}{a}+\frac{\dot{b}}{b}\right), \qquad (32)$$

$$\dot{\tilde{T}}_1 = (\gamma-1)\frac{\tilde{T}_1}{\tilde{T}_0}\left\{-f_1\frac{3}{2}\frac{\tilde{T}_0^{-3/2}}{a^2b} - f_2\,\alpha\frac{\tilde{T}_0^{\alpha}}{a^2b} + f_4\frac{5}{2}a^2b\tilde{T}_0^{5/2}F(\dot{a},\dot{b},a,b)\right\} -$$

$$-(\gamma-1)f_3a^2b\tilde{T}_2\tilde{T}_0^{5/2}\left(\frac{\tilde{T}_1}{\tilde{T}_0}\frac{5}{2} - \frac{B_{10}R}{B_{20}R^*}b^{-2}\right) - \tilde{T}_1\left(2\gamma\frac{\dot{a}}{a} + (\gamma-1)\frac{\dot{b}}{b}\right), \qquad (33)$$

$$\dot{\tilde{T}}_2 = (\gamma-1)\frac{\tilde{T}_2}{\tilde{T}_0}\left\{-f_1\frac{3}{2}\frac{\tilde{T}_0^{-3/2}}{a^2b} - f_2\alpha\frac{\tilde{T}_0^{\alpha}}{a^2b} - 5f_3\,a^2b\tilde{T}_2\tilde{T}_0^{3/2}\left(\frac{\tilde{T}_0}{2}+\tilde{T}_2\right) + \right.$$

$$\left. + f_4\frac{5}{2}\,a^2b\tilde{T}_0^{5/2}F(\dot{a},\dot{b},a,b)\right\} - \tilde{T}_2\left(2(\gamma-1)\frac{\dot{a}}{a} + (\gamma+1)\frac{\dot{b}}{b}\right), \qquad (34)$$

в которых введена функция

$$F(\dot{a},\dot{b},a,b) = \frac{4}{3}\left\{\left(\frac{\dot{a}}{a}\right)^2 + \left(\frac{\dot{b}}{b}\right)^2\right\} - \frac{8}{3}\frac{\dot{a}\dot{b}}{ab}. \qquad (35)$$

Коэффициенты f_i, $i = 1, 2, 3, 4$, в (32)–(34) определяются начальными значениями магнитного поля, плотности и температуры плазмы, а также характерными продольным и поперечным пространственными масштабами R, R^* и L:

$$f_1 = 8{,}8\cdot10^4\,\frac{B_{10}^2(R/R^*)^2}{R^2\rho_0T_0^{5/2}(t{=}0)}, \qquad f_2 = 7{,}2\cdot10^{-9}\chi\rho_0T_0^{\alpha-1}(t{=}0),$$

$$f_3 = 1{,}45\cdot10^{-8}\,\frac{\kappa_0T_0^{5/2}(t{=}0)}{\rho_0L^2}, \qquad f_4 = 1{,}6\cdot10^{-24}\frac{T_0^{3/2}}{\rho_0}. \qquad (36)$$

Уравнения (30), (31), (32)–(34) представляют собой замкнутую систему дифференциальных уравнений, описывающую эволюцию во времени автомодельных решений (16)–(19).

Остановимся теперь более подробно на анализе этой системы уравнений и ее применении вместе с автомодельными решениями (16)–(19)

для описания некоторых процессов, происходящих в солнечных магнитных трубках. Здесь необходимо отметить, что характер поведения описываемой автомодельными решениями (16)–(19) совместно с дифференциальными уравнениями (30), (31), (32)–(34) динамической модели солнечной магнитной трубки в каждом конкретном случае определяется выбором начальных условий и значениями пространственных масштабов: $a(0) = b(0) = 1$, $\dot{a}(0)$, $\dot{b}(0)$, $T_k(0)$ $(k = 0, 1, 2)$, $\rho(0) = \rho_0$, $B_{\varphi 0}(0) = B_{10}$, $B_{z0}(0) = B_{20}$, R, R^*, L. Варьируя эти параметры, мы можем получить большое разнообразие различных решений. Вместе с тем, все эти решения могут быть объединены в три основных группы, соответствующие трем возможным динамическим режимам эволюции магнитной трубки: Это 1) режим компрессии плазмы, 2) режим квазипериодических осцилляций или пульсирующий режим и 3) режим декомпрессии.

Указанные режимы являются в конечном счете результатом конкуренции двух сил, определяющих движение плазмы в трубке: силы, связанной с градиентом плазменного давления, и силы Ампера, обусловленной наличием тока в магнитной петле, — или, иными словами, конкуренции между кинетическим и магнитным давлением. При этом, в режиме компрессии можно выделить два подкласса возможных решений: первый — это сжатие плазмы, сопровождаемое ее нагревом, что в солнечных условиях могло бы соответствовать развитию тепловой вспышки в петле, и второй — сжатие, сопровождаемое охлаждением плазмы, способным привести к конденсации протуберанца в вершине петли.

3. ДИНАМИЧЕСКИЕ РЕЖИМЫ ЭВОЛЮЦИИ МАГНИТНОЙ ТРУБКИ

3.1. Режим компрессии

Режим компрессии обеспечивается силой Лоренца, превосходящей по величине градиент плазменного давления, и действующей на движущиеся заряженные частицы плазмы, создающие в трубке продольный ток $j_z = \dfrac{c}{2\pi R^*} B_{\varphi 0}(t)$. Это явление представляет собой так называемый эффект самовоздействия линейного тока, и для того, чтобы исследовать его в чистом виде, рассмотрим более простой частный случай. Будем полагать температуру плазмы в трубке однородной по всем координатам: $T(\mathbf{x}, t) = T_0(t)$. В этом случае от исходной системы дифференциальных уравнений (30), (31), (32)–(34), описывающей эволюцию динамической модели солнечной магнитной трубки, останутся лишь уравнения (30) и (32), в которых $\tilde{T}_k(t) = 0$, $k = 1, 2$, и $b(t) = b(0) = 1$:

$$\ddot{a} = -\frac{2}{\tau_M^2}\frac{1}{a}, \tag{37}$$

$$\dot{\tilde{T}}_0 = (1-\gamma)\left\{-f_1\frac{\tilde{T}_0^{-3/2}}{a^2} + f_2\frac{\tilde{T}_0^{\alpha}}{a^2} - f_4\frac{4}{3}\tilde{T}_0^{5/2}(\dot{a})^2 + 2\tilde{T}_0\frac{\dot{a}}{a}\right\}. \qquad (38)$$

Из уравнения (37), полагая начальные условия $a(0) = 1$, $\dot{a}(0) = 0$, соответствующие случаю покоящейся в момент времени $t = 0$ плазмы, можно получить характеризующую процесс компрессии плазмы в трубке связь между значениями убывающей функции $a(t) \le 1$ и временем t:

$$t = \sqrt{\pi}\,\frac{\tau_M}{2}\,\mathrm{erf}\left(\sqrt{|\ln(a)|}\right), \qquad a \le 1. \qquad (39)$$

Уравнение (38) описывает изменение температуры плазмы с течением времени и в процессе уменьшения $a(t)$. При этом знак производной от безразмерной температуры по времени, $\dot{\tilde{T}}_0$, определяется знаком выражения, стоящего в правой части (38) в фигурных скобках. Поскольку $\gamma = 5/3$ для полностью ионизированной водородной плазмы, то имеет место рост ее температуры во времени, если выражение в фигурных скобках в (38) меньше нуля, и уменьшение температуры, если оно больше нуля.

Заметим, что в начальный момент времени, когда $a(0) = 1$, $\dot{a}(0) = 0$, $\tilde{T}_0(0) = 1$ при $\rho_0 = 2\cdot(10^{-14} \div 10^{-15})$ г·см$^{-3}$, $T_0(0) = 10^6$ К, $R \simeq$ $\simeq (10^7 \div 10^8)$ см, $R^* \simeq (10^8 \div 10^9)$ см и широком спектре значений 0 Гс $< B_{10} <$ 1000 Гс коэффициент f_1 в (38) оказывается много меньше f_2, а это значит, что $\dot{\tilde{T}}_0(0) < 0$. Таким образом, в первые моменты времени при осуществлении режима компрессии в трубке происходит понижение температуры плазмы. Однако по мере уменьшения $a(t)$ и увеличения модуля отрицательной величины $\dot{a}(t)$ знак выражения в фигурных скобках в (38) изменяется на противоположный. Происходит это, главным образом, благодаря последнему слагаемому в этом выражении, обусловленному неоднородностью потока плазмы. После этого дальнейшее сжатие плазмы в магнитной трубке сопровождается быстрым увеличением ее температуры, что в условиях Солнца могло бы выглядеть как развитие вспышечного процесса. На рис. 2 показаны соответствующие такому режиму временные зависимости плотности, температуры и максимального значения радиальной скорости плазмы, достигаемого на периферии трубки ($r = R$), полученные в результате численного решения системы уравнений (37), (38) с начальными условиями $a(0) = 1$, $\dot{a}(0) = 0$, $\tilde{T}_0(0) = 1$, для различных значений магнитного поля: $B_{10} = 30$ Гс, 100 Гс, 300 Гс, – и плотности плазмы: $\rho_0 = 2\cdot 10^{-14}$ г·см$^{-3}$ (рис. 2а), $\rho_0 = 2\cdot 10^{-15}$ г·см$^{-3}$ (рис. 2б), при параметрах модели $T_0(0) = 10^6$ К, $R = 3\cdot 10^7$ см, $R^* = 9\cdot 10^8$ см. Первоначальное охлаждение плазмы здесь оказывается весьма кратковременным и очень незначительным и поэтому

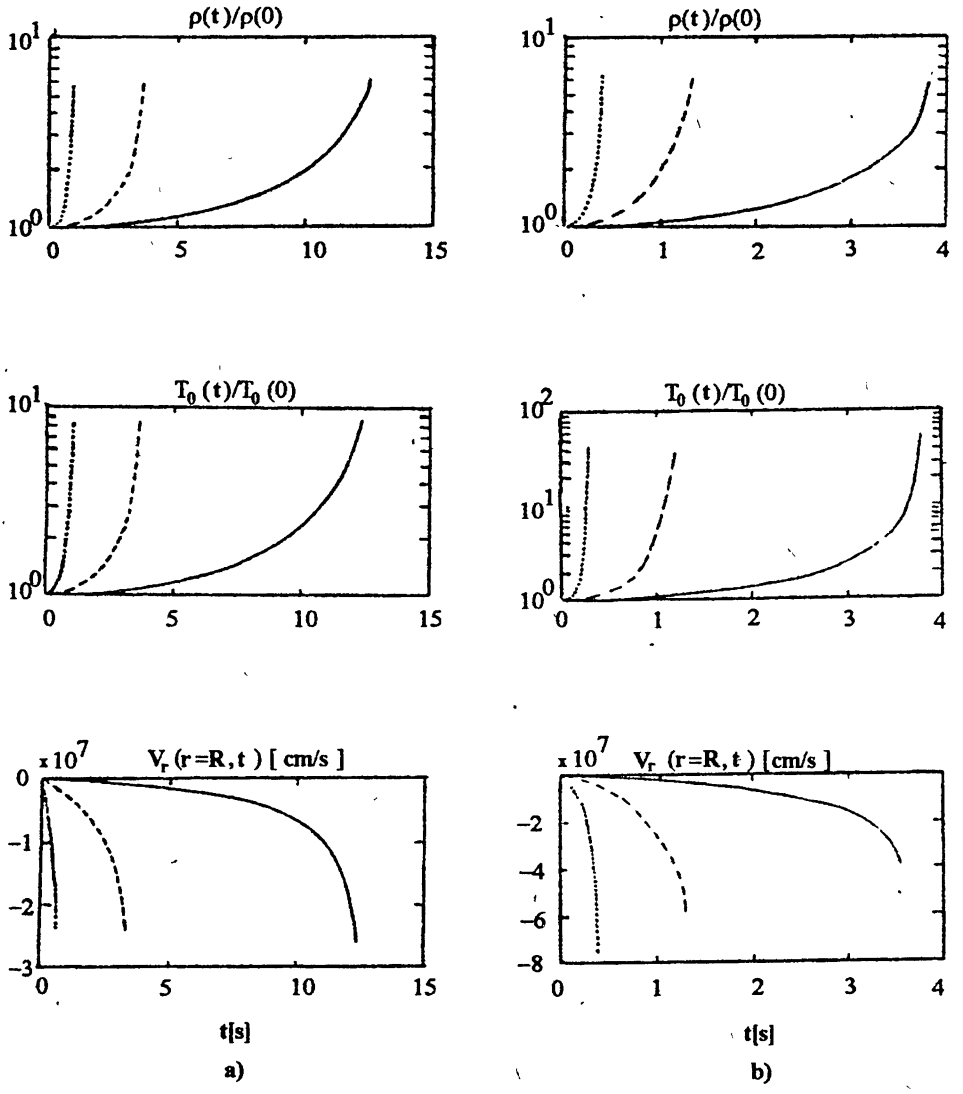

Рис. 2. Изменение во времени в условиях режима компрессии плотности $\rho(t)/\rho(0)$, температуры $T_0(t)/T_0(0)$ и радиальной компоненты скорости плазмы на периферии трубки $V_r(r{=}R,t)$ для различных начальных значений плотности плазмы: a) $\rho(0) = 2 \cdot 10^{-14}$ г·см$^{-3}$; b) $\rho(0) = 2 \cdot 10^{-15}$ г·см$^{-3}$ и магнитного поля $B_\varphi(r{=}R^*, t{=}0) = 30$ Гс (сплошная линия), 100 Гс (штриховая линия) и 300 Гс (пунктир) при начальной температуре $T_0(0) = 10^6$ К, $R = 3 \cdot 10^7$ см, $R^* = 9 \cdot 10^8$ см.

не заметно на графиках. С уменьшением ρ_0 и/или ростом B_{10} происходит сокращение времени компрессии и нагрева плазмы, так как при этом возрастает сила Лоренца, сжимающая плазму.

Подбирая параметры модели таким образом, чтобы уменьшить скорость убывания функции $a(t)$ и еще больше увеличить разницу между коэффициентами f_1 и f_2, f_4 и f_2 в (38), можно сделать первоначальное уменьшение температуры плазмы при ее сжатии более существенным и получить режим компрессии, в процессе которого происходит охлаждение трубки и конденсация в ней протуберанца. Этот случай продемонстрирован на рис. 3, где показаны зависимости от времени температуры и плотности плазмы в трубке, полученные в результате численного решения системы уравнений (37), (38) при начальных условиях $a(0) = 1$, $\dot{a}(0) = 0$, $\tilde{T}_0(0) = 1$ и параметрах модели $T_0(0) = 10^6$ К, $B_{10} = 10$ Гс, $R = 9 \cdot 10^7$ см, $R^* = 9 \cdot 10^9$ см для $\rho_0 = 2 \cdot 10^{-14}$, 10^{-14}, $2 \cdot 10^{-15}$ г·см$^{-3}$. В частности, при $\rho_0 = 2 \cdot 10^{-14}$ г·см$^{-3}$ имеет место значительное охлаждение плазмы (до значений $T_0 \simeq 10^4$ К, характерных для протуберанца) в процессе ее сжатия, достигаемое за время порядка нескольких минут; при $\rho_0 = 10^{-14}$ г·см$^{-3}$ это охлаждение существенно меньше ($\tilde{T}_{0\min} \approx 0{,}98$), а для $\rho_0 = 2 \cdot 10^{-15}$ г·см$^{-3}$ оно практически отсутствует.

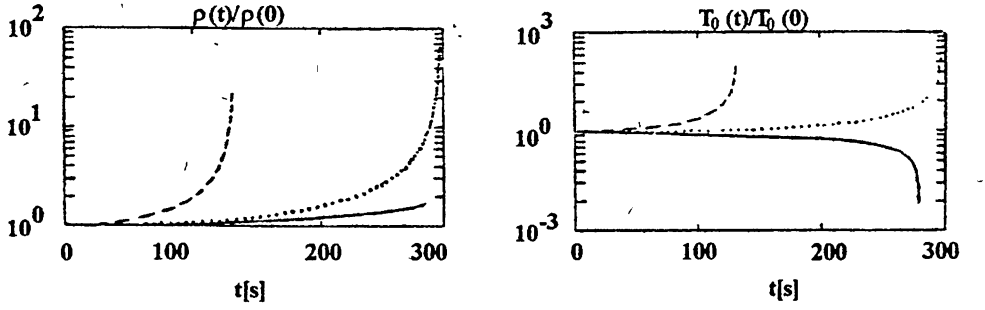

Рис. 3. Изменение во времени в условиях режима компрессии плотности $\rho(t)/\rho(0)$ и температуры $T_0(t)/T_0(0)$ плазмы для различных начальных значений плотности $\rho(0)$: $2 \cdot 10^{-14}$ г·см$^{-3}$ (сплошная линия), $2 \cdot 10^{-15}$ г·см$^{-3}$ (штриховая линия) и 10^{-14} г·см$^{-3}$ (пунктир) при начальных магнитном поле $B_\varphi(r{=}R^*, t{=}0) = 10$ Гс и температуре $T_0(0) = 10^6$ К, $R = 9 \cdot 10^7$ см, $R^* = 9 \cdot 10^9$ см. В случае $\rho(0) = 2 \cdot 10^{-14}$ г·см$^{-3}$ в трубке происходит конденсация протуберанца.

Из уравнения (38) можно получить условие, которому должны удовлетворять значения $a(t)$, $\dot{a}(t)$, $T_0(t)$ и параметры модели для того, чтобы обеспечить охлаждение плазмы в процессе эволюции модели во времени.

Это условие выглядит следующим образом:

$$X_1 < a\dot{a} < X_2, \tag{40}$$

где

$$X_{1,2} = \frac{\tilde{T}_0^{1/2} \mp \sqrt{\tilde{T}_0(1+\frac{4}{3}f_4f_2) - \frac{4}{3}f_4f_1}}{\frac{4}{3}f_4\tilde{T}_0^2}. \tag{41}$$

Выражение под квадратным корнем в (41) остается положительным, например, при $T_0(0) = 10^6$ К, $\rho_0 = 2 \cdot 10^{-14}$ г·см$^{-3}$, $B_{10} = 30$ Гс, $R = 3 \cdot 10^7$ см и $R^* = 9 \cdot 10^8$ см вплоть до значений $\tilde{T}_0(t) \simeq 10^{-14}$. Столь низкие значения температуры лежат далеко за пределами применимости нашей модели, и поэтому мы можем считать значения $X_{1,2}$ определенными повсюду. Условие (40) является универсальным критерием остывания трубки, справедливым также и в случае реализации других динамических режимов. Что касается режима компрессии, то для него $a\dot{a} < 0$, и из (40) следует более простое условие:

$$X_1 < a\dot{a}. \tag{42}$$

При этом X_1 остается меньше нуля для $\tilde{T}_0(t) \geq 10^{-15}$, что опять-таки с хорошим запасом обеспечивается на температурном интервале применимости рассматриваемой модели.

3.2. Режим осцилляций

В случае, когда в магнитной трубке имеет место неоднородность температуры в поперечном направлении, то есть $\tilde{T}_1(t) \neq 0$, в исследуемой динамической модели при определенных параметрах оказывается возможным осцилляторный режим, сопровождаемый колебаниями плотности, температуры и скорости движения плазмы, а также величины магнитного поля. Этот режим становится возможным, если значения градиентов кинетического и магнитного давлений оказываются сравнимы между собой. Для выявления некоторых закономерностей осцилляторного режима эволюции магнитной трубки мы будем исследовать случай, когда в ней отсутствуют продольные движения плазмы, то есть когда $b(t) = 1$, $\dot{b}(t) = 0$, что соответствует ситуации $\tilde{T}_2(t) = 0$.

Уравнение (30) можно рассматривать как уравнение движения материальной точки с единичной массой в потенциальном поле $U(a)$:

$$U(a) = \frac{2}{\tau_M^2}\Big(\ln(a) - \beta \int \tilde{T}_1(a)\, a\, da\Big). \tag{43}$$

При этом режим нелинейных колебаний значения функции $a(t)$, определяющей колебания магнитного поля, плотности, температуры и скорости плазмы в трубке, оказывается возможным, если функция потенциала

$U(a)$ имеет точку минимума. Соответствующее экстремуму $U(a)$ значение a^* функции $a(t)$ определяется уравнением:

$$\tilde{T}_1(a^*) = \frac{1}{(a^*)^2\beta}. \qquad (44)$$

Для того, чтобы a^* являлось минимумом функции $U(a)$, необходимо, чтобы $U''_{aa}(a^*) > 0$. Из этого условия вытекает требование к значению производной от безразмерной температурной функции $\tilde{T}_1(a)$ в точке a^*, при выполнении которого в трубке устанавливается режим осцилляций:

$$\tilde{T}_1'(a^*) < -\frac{2}{(a^*)^3\beta}. \qquad (45)$$

Таким образом, для того, чтобы в рассматриваемой модели был возможен режим нелинейных осцилляций, необходимо, чтобы в экстремальной точке a^* безразмерная температурная функция $\tilde{T}_1(a)$ убывала быстрее, чем $(1/\beta)a^{-2}$.

Заметим здесь, что, в принципе, безразмерная температурная функция $\tilde{T}_1(a)$ помимо неявной зависимости, через $a(t)$, может содержать еще и явную зависимость от времени. В этом случае значение $a^*(t)$ функции $a(t)$, соответствующее экстремуму $U(a)$, будет изменяться с течением времени. Это обстоятельство может привести к тому, что в определенный момент неравенство (45) перестанет выполняться и режим нелинейных осцилляций трубки сменится другим динамическим режимом. Именно эта ситуация реализуется в представленных на рис. 4 зависимостях от времени плотности безразмерных температурных функций и скорости плазмы в трубке, полученных в результате численного решения системы уравнений (30), (31), (32)–(34) в самом общем случае, с учётом возможности существования в магнитной трубке продольного течения плазмы ($V_z \neq 0$), при начальных условиях: $a(0) = b(0) = 1$, $\dot{a}(0) = \dot{b}(0) = 0$, $\tilde{T}_0(0) = 1$, $\tilde{T}_1(0) = \tilde{T}_2(0) = 10^{-2}$, — и соответствующих трубкам активной области параметрах модели: $T_0(0) = 10^6$ К, $\rho_0 = 2 \cdot 10^{-14}$ г·см$^{-3}$, $R = 3 \cdot 10^7$ см, $R^* = 1{,}5 \cdot 10^9$ см, $L = 10^9$ см, $B_{10} = 25$ Гс, 50 Гс, 75 Гс. При $B_{10} = 50$ Гс и 75 Гс в магнитной трубке осуществляется режим нелинейных осцилляций с постепенно нарастающим периодом, переходящий затем в режим монотонной декомпрессии. В случае $B_{10} = 25$ Гс преобладающий над силой Лоренца градиент плазменного давления обуславливает режим квазипериодической декомпрессии с быстро затухающими осцилляциями. Результаты численного решения этой же системы уравнений с аналогичными предыдущему случаю начальными условиями и при характерных для простых вспышечных петель параметрах модели: $T_0(0) = 10^7$ К, $\rho_0 = 2 \cdot 10^{-13}$ г·см$^{-3}$, $B_{10} = 300$ Гс, $R = 3 \cdot 10^7$ см, $R^* = 9 \cdot 10^8$ см, $L = 10^9$ см, — представлены на рис. 5. Здесь в трубке также происходят

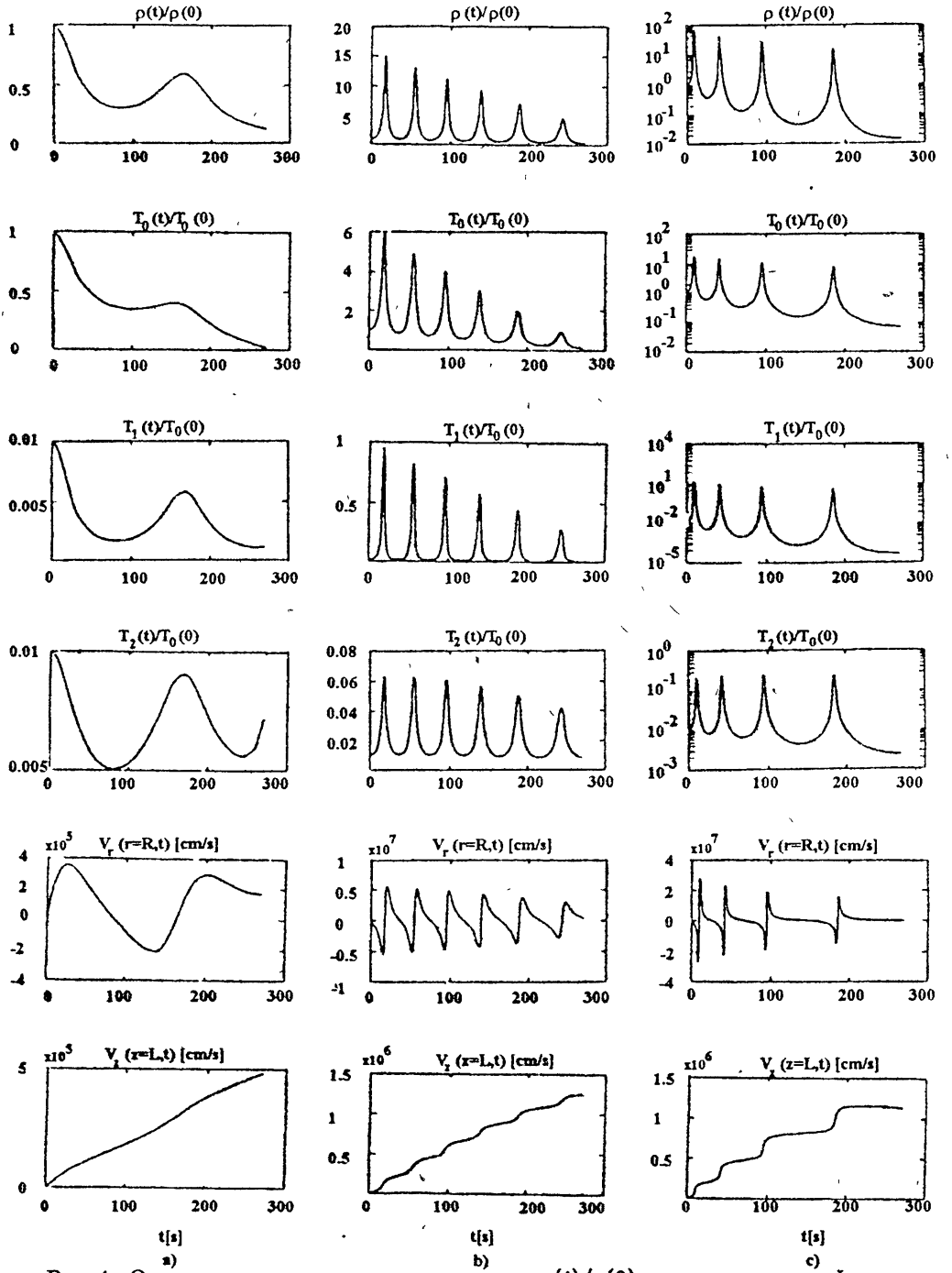

Рис. 4. Осцилляторная эволюция плотности $\rho(t)/\rho(0)$, температурных функций $\tilde{T}_0(t) = T_0(t)/T_0(0)$, $\tilde{T}_1(t) = T_1(t)/T_1(0)$, $\tilde{T}_2(t) = T_2(t)/T_2(0)$ и компонент скорости плазмы $V_r(r{=}R,t)$, $V_z(z{=}L,t)$ в трубках активной области для различных начальных значений магнитного поля $B_\varphi(r{=}R^*,t{=}0)$: а) 25 Гс, б) 50 Гс, в) 75 Гс — при $R = 3 \cdot 10^7$ см, $R^* = 1{,}5 \cdot 10^9$ см, $L = 10^9$ см, $\rho(0) = 2 \cdot 10^{-14}$ г·см$^{-3}$, $T_0(0) = 10^6$ К, $\tilde{T}_2(0) = \tilde{T}_1(0) = 10^{-2}$

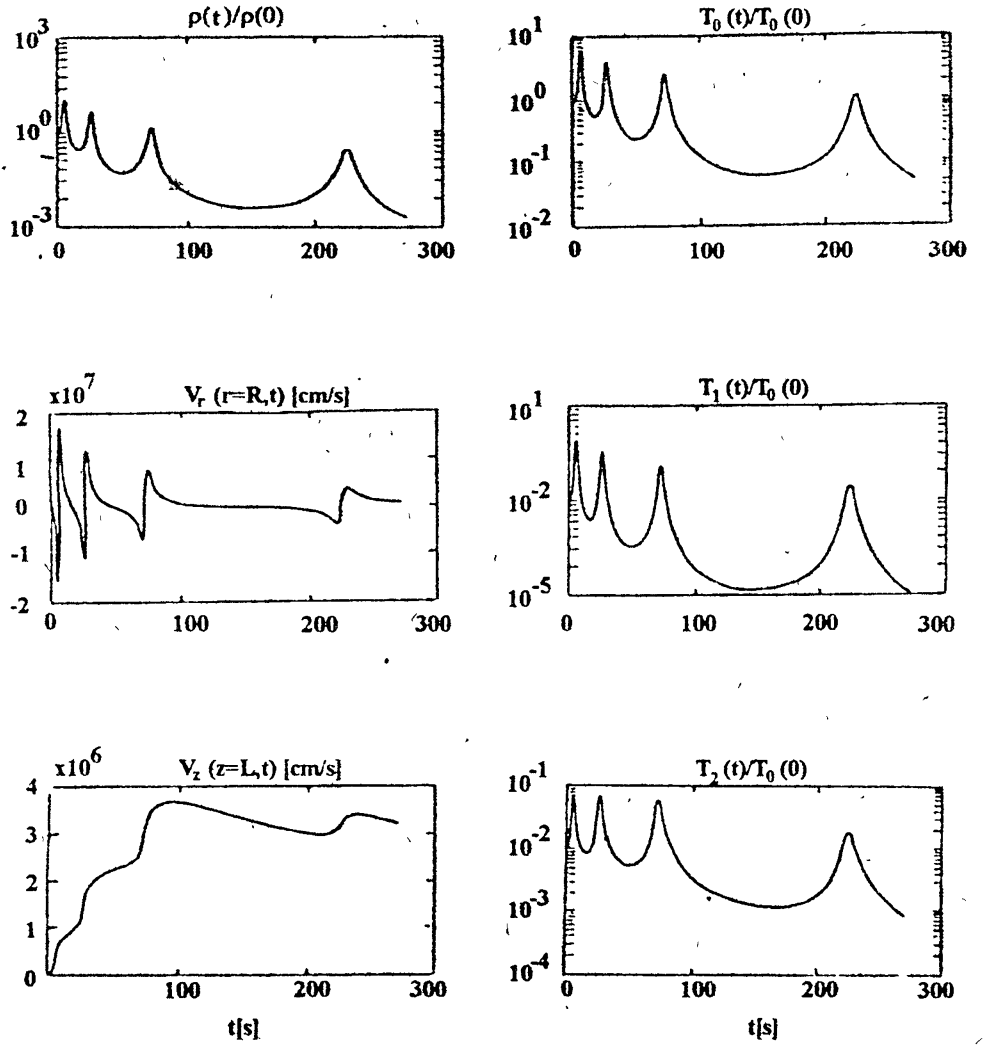

Рис. 5. Осцилляторное изменение во времени плотности $\rho(t)/\rho(0)$, температурных функций $\tilde{T}_0(t) = T_0(t)/T_0(0)$, $\tilde{T}_1(t) = T_1(t)/T_1(0)$, $\tilde{T}_2(t) = T_2(t)/T_2(0)$ и компонент скорости плазмы $V_r(r{=}R,t)$, $V_z(z{=}L,t)$ во вспышечной петле при начальных значениях плотности $\rho(0) = 2 \cdot 10^{-13}$ г·см$^{-3}$, магнитного поля $B_\varphi(r{=}R^*,t{=}0) = 300$ Гс, температуры плазмы на оси трубки $T_0(0) = 10^7$ К, и $R = 3 \cdot 10^7$ см, $R^* = 9 \cdot 10^8$ см, $L = 10^9$ см, $\tilde{T}_2(0) = \tilde{T}_1(0) = 10^{-2}$.

нелинейные осцилляции с постепенно увеличивающимся периодом, сменяющиеся затем монотонной декомпрессией.

В случае предположения об адиабатичности процессов в магнитной трубке, то есть когда $f_k = 0$, $k = 1, 2, 3, 4$ (аналогичная ситуация исследовалась в [33]) для рассматривавшегося выше частного случая, предполагающего отсутствие в трубке продольного течения плазмы ($\dot{b} = 0$, $b(t) = 1$, $T_2(t) = 0$), из уравнений (32), (33) можно получить выражения для безразмерных температурных функций:

$$\tilde{T}_0 = \frac{\tilde{T}_0(0)}{a^{2(\gamma-1)}}, \qquad \tilde{T}_1 = \frac{\tilde{T}_1(0)}{a^{2\gamma}}, \tag{46}$$

которые не содержат явной зависимости от времени t. Таким образом, определяемое уравнением (44), соответствующее экстремуму $U(a)$ значение a^* функции $a(t)$ не зависит от времени и остается постоянным в процессе эволюции рассматриваемой модели:

$$a^*_{\rm ad} = (\beta\,\tilde{T}_1(0))^{1/(2\gamma-2)} = \beta_1^{1/(2\gamma-2)}. \tag{47}$$

Здесь $\beta_1 = \dfrac{4\pi p_1(t=0)}{B_{10}^2\,(R/R^*)^2}$.

Определяемая выражением (47) величина $a^*_{\rm ad}$ соответствует состоянию равновесия адиабатической модели магнитной трубки. В зависимости от значения параметра $\gamma = c_p/c_v$ тип этого состояния равновесия на фазовой плоскости может быть "седло", при $\gamma < 1$, или "центр", при $\gamma > 1$. В последнем случае в системе оказываются возможны колебания скорости течения, плотности, температуры плазмы и величины магнитного поля. Линеаризуя (30) с учетом (46) в случае колебаний с достаточно малой амплитудой можно определить их период:

$$\mathcal{T}_{\rm ad} = \frac{2\pi\tau_M a^*_{\rm ad}}{\sqrt{\gamma-1}}. \tag{48}$$

В частности, для $R = 3\cdot10^7$ см, $R^* = 1{,}5\cdot10^9$ см, $T_0(0) = 10^6$ K, $\tilde{T}_1(0) = 10^{-2}$ и при различных ρ_0 и B_{10} определяемые формулой (48) значения периода адиабатических осцилляций приведены в табл. 1.

Здесь необходимо отметить некоторое отличие в зависимости от величины B_{10}, определяющей $\tau_M = R^*\sqrt{4\pi\rho_0}/B_{10}$, периода линейных адиабатических колебаний (48) и среднего периода нелинейных колебаний, полученного в результате численного решения уравнений неадиабатической модели. В частности, с ростом B_{10} для линейных адиабатических колебаний период уменьшается, а в случае неадиабатических колебаний, наоборот, имеет место увеличение среднего значения периода (см. рис. 4). Это обстоятельство может быть объяснено тем, что для неадиабатической модели, вследствие, определяемой уравнением (33), более сложной, по сравнению с адиабатическим случаем, зависимости температурной функции

$\tilde{T}_1(t, a(t))$ от времени и функции $a(t)$, происходит непрерывное изменение с течением времени формы эффективного потенциального рельефа (43) в сторону увеличения ширины и уменьшения глубины потенциальной ямы, сопровождаемое смещением самой точки минимума в область больших значений. Подобная динамика эффективного потенциального рельефа обуславливает постепенное увеличение временного интервала между следующими один за другим импульсами сжатия и нагрева плазмы в трубке. Вместе с тем, содержащаяся в (48) тенденция к уменьшению периода адиабатических колебаний с ростом B отражается в эффекте сокращения времени нарастания первого всплеска в случае неадиабатической модели (см. рис. 4), то есть в первые моменты ее эволюции, пока неадиабатичность еще не очень существенна.

Таблица 1

Значения периода осцилляций плотности, скорости, температуры плазмы и величины магнитного поля в линейном приближении для адиабатической модели с $R = 3 \cdot 10^7$ см, $R^* = 1{,}5 \cdot 10^9$ см, $T_0(0) = 10^6$ К, $\tilde{T}_1(0) = 10^{-2}$ при различных плотности ρ и магнитном поле $B_\varphi(r{=}R^*, t{=}0) = B_{10}$

ρ_0 [г·см$^{-3}$] / B_{10}[Гс]	$2 \cdot 10^{-15}$	10^{-14}	$2 \cdot 10^{-14}$
25	16,6 сек	126 сек	294 сек
50	2,97 сек	21,9 сек	52,3 сек
75	1,07 сек	7,98 сек	18,9 сек
100	0,16 сек	1,24 сек	2 сек

3.3. Режим декомпрессии

Еще одним возможным динамическим режимом рассматриваемой модели солнечной магнитной трубки является режим декомпрессии, во время которого происходит монотонное истечение плазмы из трубки, то есть $\dot{a}(t) > 0$. При этом, как и в случае режима компрессии, здесь можно выделить два типа эволюции системы: режим декомпрессии, сопровождаемый охлаждением, и режим декомпрессии, сопровождаемый нагревом плазмы. Последний оказывается возможным в случае достаточно высоких значений скорости истечения плазмы из магнитной трубки, когда становится существенным нагрев, обусловленный вязкостной диссипацией (15). В частности, для рассматривавшейся в п. 3.1 модели трубки с однородной

температурой ($\tilde{T}_1(t) = \tilde{T}_2(t) = 0$) из критерия (40) следует, что увеличение температуры плазмы в процессе истечения ее из трубки ($\dot{a} > 0$) происходит при

$$a\dot{a} > X_2, \tag{49}$$

где X_2 определяется выражением (41), тогда как для $a\dot{a} < X_2$ имеет место остывание плазмы. Заметим, что для адиабатической модели ($f_k = 0$, $k = 1, 2, 3, 4$) значение X_2 устремляется к бесконечности, и вытекание плазмы из трубки здесь всегда сопровождается понижением ее температуры.

4. ЗАКЛЮЧЕНИЕ

Выше нами была рассмотрена динамическая модель, описывающая эволюцию достаточно тонких и низкорасположенных магнитных петель в целом, а также динамику плазмы в верхней части более высоких магнитных петель.

Данная модель основана на автомодельных решениях системы МГД уравнений, описывающих течения плазмы с однородной деформацией. Рассматриваемые автомодельные решения адекватно описывают движение плазмы в магнитной трубке в двух случаях: 1) когда длительность рассматриваемых процессов не превышает характерный временной масштаб $\tau \approx \min\{R^*, L\}/V^*$, в течение которого информация о граничных условиях распространяется внутрь трубки [40, 48]; 2) когда имеет место скачек плотности на границе, более плотной и холодной по сравнению с окружающей корональной плазмой магнитной трубки. Этот скачек обуславливает появление своего рода поверхностного импеданса, снижающего влияние внешних полей, и позволяет описывать магнитное поле, плотность и давление плазмы внутри трубки с помощью выражений (16)–(19).

Согласно предлагаемой модели в образующей солнечную магнитную петлю токовой трубке в зависимости от параметров плазмы в ней и начальных условий могут реализоваться различные динамические режимы. В том числе оказываются возможными режим монотонного нарастания плотности плазмы за счет ее притока в трубку из внешних областей, сопровождаемого ее достаточно быстрым нагревом, что в условиях Солнца могло бы выглядеть как тепловая вспышка, либо режим роста плотности плазмы и ее охлаждения, что аналогично процессу образования в солнечной трубке протуберанца. Кроме того, при определенных условиях в магнитной трубке имеет место режим уменьшения плотности плазмы, вследствие ее истечения через боковую поверхность и торцы, которое также может сопровождаться как нагревом плазмы, так и ее охлаждением. Возможные продольные течения плазмы в рассматриваемой модели магнитной трубки могут служить аналогом различных спикульных течений и

серджей на Солнце. Особый интерес представляет возможность возбуждения в магнитной трубке колебаний скорости движения, температуры и плотности плазмы, которые могут быть зарегистрированы как серии квазипериодических импульсов в микроволновом и мягком рентгеновском излучении.

Для иллюстрации всех этих динамических режимов предлагаемой модели солнечной магнитной трубки и их взаимного соотношения удобно, помимо упоминавшейся уже выше аналогии с движением материальной точки в потенциальном поле, воспользоваться простой графической схемой. В частности, для случая, когда в трубке отсутствуют продольные движения плазмы, то есть когда $\dot{b}(t) = 0$, $b(t) = 1$, и $\tilde{T}_2(t) = 0$ из уравнения (30) следует, что на плазму трубки действует сжимающая сила, направленная к ее оси, в том случае, если

$$\tilde{T}_1(a,t) < \frac{1}{a^2\beta}. \tag{50}$$

В точке $a = a^*$ пересечения кривых $\tilde{T}_1(a,t)$ и $1/(a^2\beta)$ (см. рис. 6) происходит смена знака ускорения плазмы. При этом, возможны два варианта ориентации кривой $\tilde{T}_1(a,t)$ по отношению к кривой $1/(a^2\beta)$, которые обозначены на рис. 6 цифрами 1 и 2. Случаю 1 соответствует более быстрое убывание функции $\tilde{T}_1(a,t)$ в точке a^* по сравнению с $1/(a^2\beta)$, что на языке аналогии с движением материальной точки (см. п. 3.2) означает существование минимума у эффективного потенциального рельефа и обуславливает возможность осцилляторного режима, тогда как в случае 2 возможны лишь режимы монотонной компрессии и декомпрессии. Например, если для случая 1 соответствующая начальным условиям $a(0) = a_0$ и $\tilde{T}_1(a_0,0) = \tilde{T}_{10}$ изображающая точка системы располагается на кривой $\tilde{T}_1(a,t)$ левее точки пересечения ее с зависимостью $1/(a^2\beta)$, то при нулевой начальной скорости ($\dot{a}(0) = 0$) действующая на плазму сила, обусловленная градиентом газокинетического давления, будет больше силы Лоренца и начнется эволюция системы в сторону увеличения значения a, сопровождаемая истечением плазмы из трубки и уменьшением $\tilde{T}_1$. Когда после прохождения точки пересечения функций $\tilde{T}_1(a,t)$ и $1/(a^2\beta)$ изображающая точка системы окажется под кривой $1/(a^2\beta)$, сила Лоренца, действующая на плазму, станет больше чем ∇p и появится возвращающая сила. Таким образом, создаются условия для осуществления режима осцилляций. Конкретный характер протекания этого режима и границы его существования определяются видом зависимости $\tilde{T}_1(a,t)$, определяемой уравнением (33). Аналогичные рассуждения, проводимые для случая 2, приводят к выводу, что при начальных условиях, когда изображающая точка системы находится на кривой $\tilde{T}_1(a,t)$ левее точки ее пересечения с кривой $1/(a^2\beta)$, в системе осуществляется режим монотонной компрессии, а когда правее, то монотонной декомпрессии.

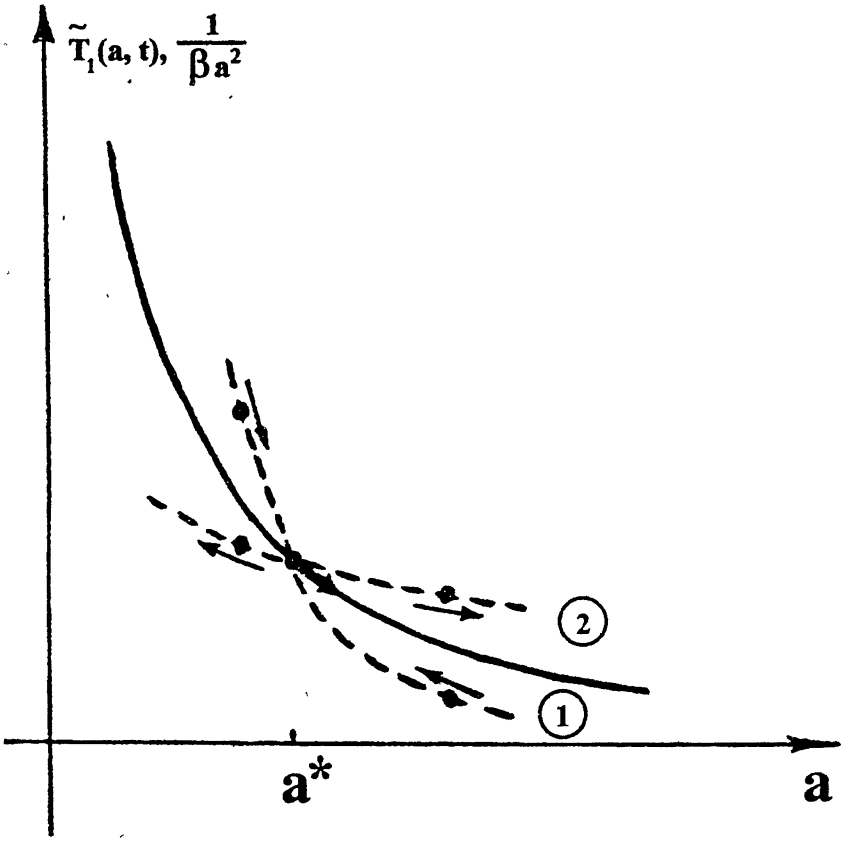

Рис. 6. Возможная взаимная ориентация кривых $\tilde{T}_1(a,t)$ и $1/(a^2\beta)$ в зависимости от характера поведения функции $\tilde{T}_1(a,t)$. В случае 1 в системе оказывается возможен осцилляторный режим, тогда как в случае 2 реализуются лишь режимы монотонной компрессии и декомпрессии.

Здесь необходимо отметить, что для адиабатической модели ($f_k = 0$, $k = 1, 2, 3, 4$) у зависимости $\tilde{T}_1(a,t)$ существует аналитическое выражение (46), и схематически изображенным на рис. 6 случаям 1 и 2 соответствуют ситуации с $\gamma \geq 1$ и $\gamma < 1$. Для неадиабатической модели, вследствие более сложной зависимости $\tilde{T}_1(a,t)$, координата, $a^*(t)$, пересечения соответствующей кривой с кривой $1/(a^2\beta)$ изменяется с течением времени, кроме того, изменяется и форма данной кривой, она как бы скользит вдоль линии $1/(a^2\beta)$, поворачиваясь при этом относительно точки их пересечения, что обуславливает динамические особенности и разнообразие режимов эволюции исследуемой системы. Наконец, на форму кривой $1/(a^2\beta)$ оказывают влияние начальные значения φ-й компоненты магнитного поля при $r = R^*$, $B_\varphi(r{=}R^*, t{=}0) = B_{10}$, и температуры плазмы на оси трубки $T_0(t{=}0)$, входящие в параметр модели β. В общем случае, когда учитывается возможность существования в магнитной трубке продольных течений плазмы ($\dot{b}(t) \neq 0$, $\tilde{T}_2(t) \neq 0$), подобная графическая интерпретация динамических режимов системы требует введения на рис. 6 дополнительной координаты, b. При этом, рассматривавшиеся выше линии $\tilde{T}_1(a,t)$ и $1/(a^2\beta)$ трансформируются в поверхности $\tilde{T}_1(a,b,t)$ и $1/(a^2 b\beta)$.

Касаясь применимости рассмотренной в данной работе динамической модели магнитной токовой трубки в условиях Солнца, необходимо отметить, что исследовавшиеся здесь автомодельные решения системы МГД уравнений описывают эволюцию магнитной трубки, заполненной плазмой, от некоторого начального состояния, определяемого начальными значениями магнитного поля, скорости плазмы, ее плотности и температуры. Установление этих начальных значений в каждом конкретном случае может происходить по-разному и зависит от предыстории исследуемой магнитной трубки и активной области в целом. Большую роль в этом процессе могут сыграть различные неустойчивости и быстрые по сравнению с временем $\tau = \min\{R^*, L\}/V_A$ нестационарные процессы, возникающие в активной области вблизи рассматриваемой магнитной трубки и приводящие к появлению распространяющихся возмущений, которые, в свою очередь, способствуют формированию в исходной стационарной магнитной трубке определенных начальных условий. Это могут быть также быстрые, с характерным временем порядка τ, нестационарные течения в фотосфере активной области, сопровождающие процесс ее перестройки и оказывающие влияние на возбуждение токов в магнитной трубке. В качестве триггера, запускающего рассмотренные выше динамические процессы в магнитной трубке, могут выступать еще и происходящие в данной или соседних активных областях вспышки. В этом случае, при формировании в рассматриваемой магнитной трубке соответствующих условий, в ней также может произойти вспышка в результате осуществления режима компрессии и нагрева. Подобное явление известно под названием симпатических вспышек.

Автор выражает благодарность В.В.Зайцеву за полезные советы и обсуждения. Данная работа была выполнена при частичной поддержке грантами Российского фонда фундаментальных исследований (No.93–02–3008, No.95–02–04272–а), а также грантами Южно-Европейской обсерватории (No.A–01–080) и Международного научного фонда (No.R92000, No.R92300).

ЛИТЕРАТУРА

1. Kippenhanh R. and Schltter A. Z. // Astrophysical Journal, 1957. V. 43. P. 36.
2. Anzer U. // Solar Physics, 1972. V. 24. P. 324.
3. Kuperus M. and Raadu M. A. // Astronomy and Astrophysics, 1974. V. 31. P. 189.
4. Malherbe J. M. and Priest E. R. // Astronomy and Astrophysics, 1983. V. 123. P. 80.
5. Anzer U. and Priest E. R. // Solar Physics, 1985. V. 95. P. 263.
6. Wu F. and Low B. C. // Astrophysical Journal, 1987. V. 312. P. 431 (paper I).
7. Dwmoulin P., Anzer U., and Priest E. R. // Astronomy and Astrophysics, 1989. V. 221. P. 36.
8. Anzer U. and Ballester J. L. // Astronomy and Astrophysics, 1990. V. 238. P. 365.
9. Fiedler R. A. S. and Hood A. W. // Solar Physics, 1993. V. 146. P. 297.
10. Priest E. R. and Ridgway C. // Solar Physics, 1993. V. 146. P. 277.
11. Rosner R., Tucker W. H., and Vaiana G. S. // Astrophysical Journal, 1978. V. 220. P. 643.
12. Hood A. W. and Priest E. R. // Astronomy and Astrophysics, 1979. V. 77. P. 233.
13. Wragg M. and Priest E. R. // Solar Physics, 1981. V. 20. P. 293.
14. She Z. S., Malherbe J. M., and Raadu M. A. // Astronomy and Astrophysics, 1986. V. 164. P. 364.
15. Pakkert J. W., Martens P. C. H., and Verhulst F. // Astronomy and Astrophysics, 1987. V. 179. P. 285.
16. Anzer U. // Solar Physics, 1969. V. 8. P. 37.
17. Wu F. // Astrophysical Journal, 1987. V. 320. P. 418.
18. Dwmoulin P. and Priest E. R. // Astronomy and Astrophysics, 1988. V. 206. P. 336.
19. Habbal S. and Rosner R. // Astrophysical Journal, 1979. V. 234. P. 1113.
20. Hood A. W. and Priest E. R. // Solar Physics, 1980. V. 35. P. 123.
21. Craig I. J. D. and McClymont A. N. // Astrophysical Journal, 1985. V. 289. P. 820.

22. Antiochos S.K., Shoub E., An C.-H., and Emslie G. // Astrophysical Journal, 1986. V.298. P.876.
23. Karpen J.T., Picone J.M., and Dahlburg R.B. // Astrophysical Journal, 1988. V.324. P.590.
24. Mok Y., Drake J.F., Schnack D.D., and Van Hoven G. // Astrophysical Journal, 1990. V.359. P.228.
25. Gan W.Q., Fang C., and Zhang H.Q. // Astronomy and Astrophysics, 1991. V.241. P.618.
26. Cally P.S. and Robb T.D. // Astrophysical Journal, 1991. V.372. P.329.
27. Antiochos S.K. and Klimchuk J.A. // Astrophysical Journal, 1991. V.378. P.372.
28. Stone J.M. and Norman M.L. // Astrophysical Journal, Suppliment Series, 1992. V.80. P.753.
29. Имшенник В.С., Сыроватский С.И. // ЖЭТФ, 1967. Т.52. С.990.
30. Bulanov S.V. and Olshanetsky M.A. // Physics Letters, 1984. V.100 A. P.35.
31. Куликовский А.Г. // Докл. Академии Наук СССР, 1958. Т.120. С.984.
32. Syrovatskii S.I. // Ann. Rev. Astron. Astrophys., 1981. V.19. P.163.
33. Буланов С.В. Динамика токовых слоев и физика солнечной активности. — Рига: Зинатне, 1982. С.24.
34. Sakai J.-I. and Koide S. // Solar Physics, 1992. V.137. P.293.
35. Sakai J.-I. // Solar Physics, 1989. V.120. P.117.
36. Sakai J.-I. and de Jager C. // Solar Physics, 1991. V.134. P.329.
37. Sakai J.-I., Chargeishvili B., and Zhao J. // Solar Physics, 1993 (submitted).
38. Sakai J.-I. and Ohsawa Y. // Space Sci. Reviews, 1987. V.46. P.113.
39. Sakai J.-I. and Washimi H. // Bull. Faculty Eng. Toyama University, 1985. V.36. P.47.
40. Sakai J.-I., Colin A., and Priest E.R. // Solar Physics, 1987. V.114. P.253.
41. Khodachenko M.L., Zaitsev V.V., and Bakhareva N.M. // Solar Physics, 1992. V.139. P.299.
42. Ходаченко М.Л., Зайцев В.В. // Астрономический Журнал, 1992. Т.69. С.159.
43. Murawski K. and Roberts B. // Solar Physics, 1993. V.143. P.89.
44. Murawski K. and Roberts B. // Solar Physics, 1993. V.144. P.255.
45. Spitzer L. Physics of Fully Ionized Gases. — New York: Interscience, 1962. (Спитцер Л. Физика полностью ионизированного газа. — М.: Мир, 1965).
46. Priest E.R. Solar magnetohydrodynamics. — Dordrecht, Holland: D.Reidel Publishing Company, 1982. (Прист Э.Р. Солнечная магнитогидродинамика. — М.: Мир, 1985).
47. Сыроватский С.И. // ЖЭТФ, 1968. Т.54. С.1422.

48. Forbes T. G. and Speiser T. W. // Journal of Plasma Physics, 1979. V. 21. P. 107.
49. Сыроватский С. И. // ЖЭТФ, 1966. Т. 50. С. 1133.

Институт прикладной физики
РАН, г. Н. Новгород

Поступила в редакцию
17 июля 1995 г.

ON THE PLASMA DYNAMICS IN A SOLAR MAGNETIC TUBE

M. L. Khodachenko

On the basis of known self-similar solutions of the MHD equations, describing plasma flows with a homogeneous deformation, the dynamical model of a solar magnetic loop was developed. A general form of the energy equation taking into account the Joule heating radiative losses, thermoconductivity and viscosity effects was considered in this model. Various dynamic regimes of the loop's evolution were investigated. Of great interest are the process of the plasma fast compression with heating, similar to the flare event, the process of the plasma cooling and compression, corresponding to the prominence formation in the loop, as well as a number of oscillatoric regimes and processes of plasma decompression accompained by its cooling or heating. Analytical treatment and numerical simulations of the model were made.

HIGH-FREQUENCY WAVE PACKETS IN INHOMOGENEOUS PLASMA WITH STRICTION NONLINEARITY

E. M. Gromov and V. I. Talanov

The study of the evolution of $1-D$ intense high-frequency (HF) packets in smoothly inhomogeneous plane-layer medium with local and nonlocal striction nonlinearities is reviewed. The role of the low-frequency (LF) radiation from the HF packet in inhomogeneous medium with nonlocal nonlinearity is discussed.

1. INTRODUCTION

It is known that the quasi monochromatic packets of the weak HF field $\psi(z,t)\exp(-it)$ in smoothly inhomogeneous media, described by the nonstationary Schrödinger Eq.

$$2i\frac{\partial\psi}{\partial t}+\frac{\partial^2\psi}{\partial z^2}-U(z)\psi=0 \tag{1}$$

behave as quasi particles, the mass center trajectories $\bar{z}$ of the which

$$\bar{z}=\frac{1}{N_0}\int\limits_{-\infty}^{+\infty} z|\psi|^2\,dz$$

(here $N_0=\int\limits_{-\infty}^{+\infty}|\psi|^2\,dz$ is the wave field energy in the packet) coincide with the classic trajectories of the motion of the material point in the potential $U(z)$

$$\frac{d^2\bar{z}}{dt^2}=-\frac{1}{2}\frac{\partial U(z)}{\partial z}\bigg|_{z=\bar{z}(t)}. \tag{2}$$

The role of the potential $U(z)$ for the Langmuir or electromagnetic (EM) wave packets in isotropic inhomogeneous plasma is played by plasma concentration. The Fig.1 gives the packet trajectories in the medium with the linear and parabolic profile of inhomogeneity $U(z)$ (Fig.a and b) at various initial packet group velocity values. The striction nonlinearity changes the packet motion in the inhomogeneous medium. The type of variations depends on striction nonlinearity type. At first let us consider the well-known evolution of HF packets in medium with the local striction nonlinearity.

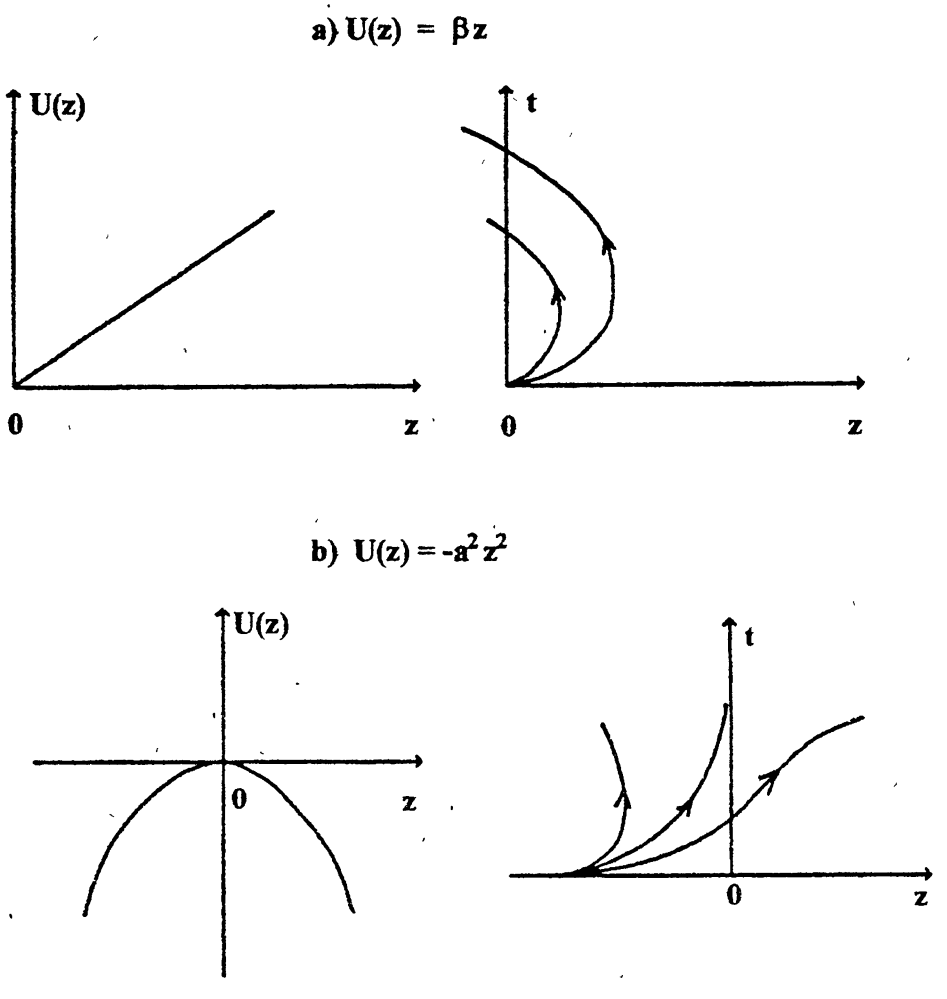

Fig. 1. Trajectories of the weak HF wave packet in the medium with linear (a) and parabolic potential barrier (b) at various initial velocities.

2. HF PACKETS IN THE LOCAL STRICTION NONLINEARITY MEDIUM

In this case the evolution of $1-D$ intense HF packet envelope $\psi(z,t)$ in plane-layer medium is described by well-known nonlinear Schrödinger Eq. (NSE)

$$2i\frac{\partial\psi}{\partial t}+\frac{\partial^2\psi}{\partial z^2}-U_{\text{eff}}\left(z,|\psi|^2\right)\psi=0 \tag{3}$$

with the effective potential

$$U_{\text{eff}}\left(z,|\psi|^2\right)=U(z)-|\psi|^2\,. \tag{4}$$

For the space localized HF packet its acceleration is described by the relationship

$$\frac{d^2\,\bar{z}}{dt^2} = -\frac{1}{2N_0}\int\limits_{-\infty}^{+\infty}\frac{\partial U(z)}{\partial z}\,|\psi|^2\,dz. \tag{5}$$

For the smoothly inhomogeneous medium, whose inhomogeneous scale L is much greater the packet extension Δ, we neglect in (5) the variation of the function $\partial U(z)/\partial z$ in the vicinity of the packet mass center $z(t)$

$$\frac{\partial U(z)}{\partial z} \simeq \left.\frac{\partial U(z)}{\partial z}\right|_{z=\overline{z(t)}}. \tag{6}$$

Then from (5) we get the relation (2), which follows that the intense HF packet mass center in a smoothly inhomogeneous medium with local striction nonlinearity moves along the classic geometrooptic traces corresponding to the weak HF field. The local nonlinearity affects only the HF packet envelope evolution and does not affect the packet motion trajectories as whole. The HF field evolution in the medium with the linear [1,2], and parabolic [3] profiles of inhomogeneity is studied most thoroughly in this case. We consider for example more detail strong HF packets in medium with the linear profile $U(z) = \beta z$. The HF packet envelope $\psi(z,t)$ in this case is described by the Eq.

$$2i\frac{\partial\psi}{\partial t} + \frac{\partial^2\psi}{\partial z^2} + |\psi|^2\psi - \beta z\psi = 0 \tag{7}$$

and admits the exact solution in the form of the uniformly accelerated moving Chen-soliton [1]. To demonstrate this solution in (7) we use the system of reference moving with constant acceleration:

$$\xi = z + \frac{\beta}{4}t^2,\ t' = t \tag{8}$$

and replace the function

$$\psi(z,t) = \Phi(\xi,t)\exp\left\{-i\frac{\beta}{2}\xi t\right\}. \tag{9}$$

For $\Phi(\xi,t)$ we get NSE

$$2i\frac{\partial\psi}{\partial t} + \frac{\partial^2\psi}{\partial z^2} + |\psi|^2\psi = 0, \tag{10}$$

one of the solution is the soliton

$$\Phi(\xi,t) = \frac{\Phi_0}{\cosh\left(\Phi_0\xi/\sqrt{2}\right)}\exp\left\{i\Phi_0^2 t\right\}. \tag{11}$$

In the initial coordinates the field $\psi(z,t)$ corresponding (11) has the form

$$\psi(z,t) = \frac{\Phi_0}{\cosh\left(\Phi_0\xi/\sqrt{2}\right)} \exp\left\{i\Phi_0^2 t - i\frac{\beta}{2}xt - \frac{\beta^2}{8}t^3\right\}, \qquad (12)$$

which is called Chen-soliton.

3. HF PACKETS IN NONLOCAL STRICTION NONLINEARITY MEDIUM

The evolution of HF packets $\psi(z,t)\exp(-it)$ in smoothly inhomogeneous medium with the nonlocal striction nonlinearity and small perturbations of the base inhomogeneous potential $U(z)$ is described by the Zakharov-type system Eq. [5]

$$2i\frac{\partial\psi}{\partial t} + \frac{\partial^2\psi}{\partial z^2} - n\psi - U(z)\psi = 0, \qquad (13)$$

$$\frac{\partial^2 n}{\partial t^2} - \frac{\partial^2 n}{\partial z^2} = \frac{\partial^2\left(|\psi|^2\right)}{\partial z^2}. \qquad (14)$$

Here n is the concentration perturbation. The given system of Eqs. describes the wave packets, for example, Langmuir or EM one in the approximation of the "parabolic" law of wave dispersion. The strong HF packet in inhomogeneous plasma with nonlocal nonlinearity was analyzed for the first time in [4] by the perturbation method. On particular, it was shown in [4] that HF packets in inhomogeneous plasma radiate ion-acoustic waves. However, in [4] the low-frequency (LF) radiation recoil to the HF packet core was not taken into account. Below we consider the motion of the HF packets in smoothly inhomogeneous plasma with nonlocal nonlilearity taken into account the LF radiation coursed the deviation the HF packets trajectory from the classic one. Assuming that the packet velocity equals $a(t)$ (by $a(t)$ we denote the HF field velocity), we pass the Eqs. (13), (14) to the reference system accompanying

$$\xi = z - \int_0^t a\left(\tilde{t}\right)d\tilde{t}, \qquad t' = t,$$

$$2i\left(\frac{\partial\psi}{\partial t} - a\frac{\partial\psi}{\partial\xi}\right) + \frac{\partial^2\psi}{\partial\xi^2} - \dot{n}\psi - U(\xi + z_c, t)\psi = 0, \qquad (15)$$

$$\left(a^2 - 1\right)\frac{\partial^2 n}{\partial\xi^2} + \frac{\partial^2 n}{\partial t^2} - 2a\frac{\partial^2 n}{\partial t\partial\xi} - \dot{a}\frac{\partial n}{\partial\xi} = \frac{\partial^2\left(|\psi|^2\right)}{\partial\xi^2}, \qquad (16)$$

where $z_c = \int_0^t a\left(\tilde{t}\right)d\tilde{t}$, $\dot{} \equiv d/dt$. We shall be interested in HF packets whose extend Δ is much less than the medium inhomogeneity scale

$L^{-}U\,(\partial U/\partial\xi)^{-1} \gg \Delta$, which permits to approximate the function U near the point $\xi = 0$

$$U\,(\xi + z_c, t) \simeq U\,(z_c, t) + \left.\frac{\partial U(\xi,t)}{\partial\xi}\right|_{\xi=0} \xi. \tag{17}$$

Changing the unknown searched field function

$$\psi\,(z,t) = \Phi\,(\xi,t) \exp\left\{ i\left[a\,(t)\,\xi + \frac{1}{2}\int_0^t \left(a^2 - \int_0^{\tilde{t}} U\left(z_c, \hat{t}\right) d\hat{t} \right) \right] \right\} \tag{18}$$

from (15) taken into account (17) and (18) we get

$$2i\frac{\partial\Phi}{\partial t} + \frac{\partial^2\Phi}{\partial\xi^2} - \left[n + \xi\left(2\,\dot{a} + \left.\frac{\partial U(\xi,t)}{\partial\xi}\right|_{\xi=0} \right) \right] \Phi = 0. \tag{19}$$

Now we refer to Eq. (16). We limit ourselves by the consideration of the wave packets whose velocity is small enough in comparison with the free LF perturbations $a \ll 1$. Here, neglecting in (16) the term of the order of a a, a^2, the second time derivation term and integrating the obtained relations over ξ from ξ to $+\infty$ provided $n\,(\xi \to +\infty, t) \to 0$ and $\Phi\,(\xi \to +\infty, t) \to 0$, we obtain from (16)

$$\dot{a}\,n + \frac{\partial n}{\partial\xi} = -\frac{\partial\left(|\Phi|^2\right)}{\partial\xi}. \tag{20}$$

The Eqs. system (19), (20) describes the evolution of the strong wave-packets in smoothly inhomogeneous plane-layer medium with nonlocal striction nonlinearity. The HF packet velocity $a\,(t)$ in this reference system has not been defined yet. The striction force in (20) will lead to the LF radiation. The arising LF radiation changes the effective potential profile $U_{\text{eff}}\left(\xi, |\Phi|^2\right)$ in the HF packet region and behind it (Fig.2). This gives rise to the LF radiation recoil, which causes the deviation of the motion trajectories from the classic ones. To analyze the value of the LF radiation recoil we express in (20) explicitly the concentration perturbation n via the field $|\Phi|^2$. To do this, multiplying (20) by $\exp\left(\dot{a}\,\xi\right)$ and integrating the obtained relation with respect to ξ from ξ to $+\infty$ under the conditions $n\,(\xi \to +\infty, t) \to 0$ and $\Phi\,(\xi \to +\infty, t) \to 0$, we yield

$$n\,(\xi,t) = -|\Phi|^2 - \dot{a}\exp\left(\dot{a}\,\xi\right) \int_{\xi}^{+\infty} |\Phi|^2 \exp\left(\dot{a}\,\xi\right) d\xi. \tag{21}$$

In particular, for wave packets, whose acceleration is small enough, that the relation $L \sim \left(\dot{a}\right)^{-1} \gg L_\Phi$ is fulfilled, where L_Φ is the scale of the inhomo-

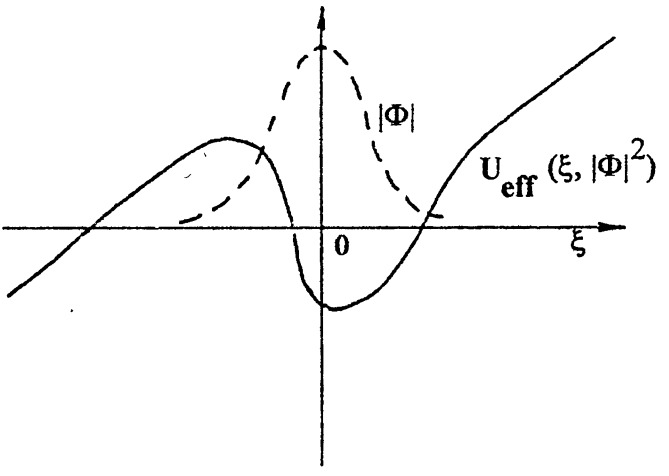

Fig. 2. The effective potential profile $U_{\text{eff}}(\xi, |\Phi|^2)$ of Eq. (23) $U_{\text{eff}}(\xi, |\Phi|^2 \equiv n$ (the solid curve) at $a < 0$ and the local distribution of the HF field modulus $|\Phi|$ (the dotted curve).

geneity Φ, we can neglect the exponential multipliers in (21). We get for n :

$$n(\xi, t) = -|\Phi|^2 - \dot{a} \int_{\xi}^{+\infty} |\Phi|^2 \, d\xi. \tag{22}$$

Substituting (22) into (19), we get for Φ the relation

$$2i\frac{\partial \Phi}{\partial t} + \frac{\partial^2 \Phi}{\partial \xi^2} - U_{\text{eff}}\left(\xi, |\Phi|^2\right)\Phi = 0 \tag{23}$$

with the effective potential

$$U_{\text{eff}}\left(\xi, |\Phi|^2\right) = \xi\left(2\dot{a} + \frac{\partial U(\xi, t)}{\partial \xi}\bigg|_{\xi=0}\right) - |\Phi|^2 - \dot{a}\int_{\xi}^{+\infty} |\Phi|^2 \, d\xi. \tag{24}$$

The Eq. (23) describes the evolution of the envelope of quasi localized strong wave packet, whose dumping is caused by the HF and LF wave radiation.

3.1. LF radiation

LF radiation is caused by the nonuniformity of the packet motion in the medium with nonlocal nonlinearity and leads to the modification of the effective potential profile U_{eff} (the latter term of (24)). Thus, at the braking of the packet $\dot{a} < 0$ LF radiation leads to increase of the effective potential after the wave packet core and near it (Fig. 2) thus decreasing the rolling down

force (produced by the inhomogeneous medium) affecting the HF core to the region of small values of the unperturbed potential. The polling down force proportional to the inclination of the effective potential, in the wave packet core center at $\xi = 0$ where $(\partial\Phi(\xi,t)/\partial t)\,|_{\xi=0} = 0$ from (24) equals

$$f \sim \left.\frac{\partial U_{\text{eff}}(\xi,t)}{\partial\xi}\right|_{\xi=0} = 2\,\dot{a} + \left.\frac{\partial U_{\text{eff}}(\xi,t)}{\partial\xi}\right|_{\xi=0} + \dot{a}\,|\Phi(\xi=0,t)|^2 . \qquad (25)$$

The latter term (25) takes into account the LF radiation recoil to the HF packet. In the reference system HF packet is stationary, i.e. $f = 0$. It follows that the LF radiation caused by the nonlocal character of nonlinearity changes the acceleration of the packet motion and leads to the trajectory deviation from the classic one $\dot{a}_{\text{cl}} = -0.5(\partial U(\xi,t)/\partial t)\big|_{\xi=0}$. Thus, for the packets, moving in the density gradient direction ($\partial U/\partial\xi > 0$) and radiating LF waves in the opposite direction, we yield from the condition $f = 0$: $|\dot{a}| < |\dot{a}_{\text{cl}}|$, i.e. quasi localized HF packets penetrate into more dense plasma layers in comparison with localized HF packets without of LF wave radiation. The Fig.3 shows the trajectories of strong and weak HF packets in smoothly inhomogeneous medium with nonlocal striction nonlinearity.

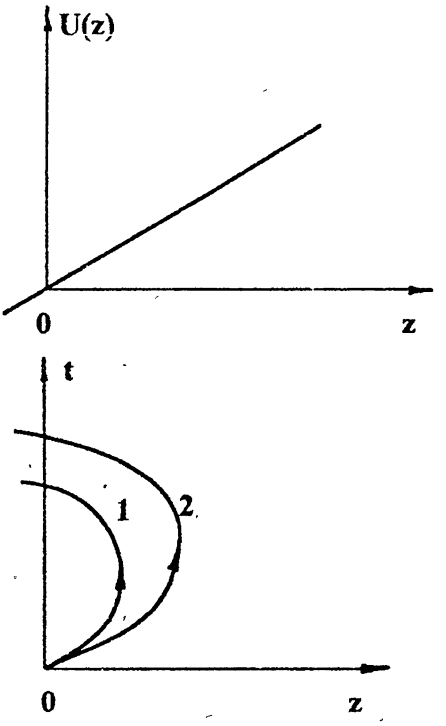

Fig. 3. Trajectories of the strong HF wave packets in the smoothly inhomogeneous medium at various amplitudes.

To analyze the given effect numerically we consider in Eqs. (23), (24) the linear profile of inhomogeneity $U(z) = \beta z$ ($\beta > 0$) and make the substitution

$$\eta = -\overset{\bullet}{a}\,\xi, \quad \tau = \left(\overset{\bullet}{a}\right)^2 t, \quad n = -\tilde{n}\frac{\lambda}{\overset{\bullet}{a}}, \quad \Phi = \varphi\sqrt{\lambda/\left(\overset{\bullet}{a}\right)}, \tag{26}$$

in which $\overset{\bullet}{a} = (\lambda - \beta)/2$. Here $\lambda/2$ is deviation of the packet real acceleration $\overset{\bullet}{a}$ from the classic one $-\beta/2$. In new variables Eq. (23) takes the form

$$2i\frac{\partial\varphi}{\partial\tau} + \frac{\partial^2\varphi}{\partial\eta^2} - q\left(\eta - |\varphi|^2 + \int\limits_{\eta}^{+\infty} |\varphi|^2\, d\eta\right)\varphi = 0, \tag{27}$$

where $q = \lambda/\left(-\overset{\bullet}{a}\right)^3$ is a new parameter. As the initial wave packet we consider the one-soliton solution of Eq. (27) for homogeneous medium with local nonlinearity:

$$\varphi(\eta, \tau = 0) = \frac{\varphi_0}{\cosh\left(\varphi_0\eta\sqrt{q/2}\right)}. \tag{28}$$

The Eq. (27) was analyzed at the dimensionless parameter $q = 10^3$ and various values of the initial amplitude φ_0. The Fig. 4 gives the distributions of the HF field intensity $|\varphi(\eta, \tau)|$ and the concentration n at different time moment τ. Fig. a) corresponds to the amplitude $\varphi_0 = 0.5$ b) — $\varphi_0 = 1.2247$ and c) — $\varphi_0 = 1.5$. The curves 1 correspond to the moment $\tau = 0$; 2 — $\tau = 2 \cdot 10^{-2}$; 3 — $\tau = 4 \cdot 10^{-2}$. It follows from simulation that there is the critical packet amplitude

$$\varphi_{0,c} \simeq 1.2247, \tag{29}$$

at which the packet is rest in the chosen reference system. This relation slightly differ from the critical packet amplitude $\varphi_{0,c} = 1$, obtained from Eq. (27) under the condition that the force affecting the packet core in the point $\eta = 0$ in the inhomogeneous medium with the nonlocal nonlinearity is equal to zero;

$$f(\eta = 0, \tau) \sim \left.\frac{\partial U(\eta, \tau)}{\partial\eta}\right|_{\eta=0} = q\left(1 - |\varphi_{0,c}(\eta = 0, \tau)|^2\right) = 0. \tag{30}$$

This yield that $\varphi_{0,c} = 1$. Such a deviation is caused by the finite packet extend in the presence of the inhomogeneous effective potential. Thus, taking into account (27) we obtain for the acceleration of packet mass center in the reference system moving with the velocity a

$$\frac{d^2\,\bar{\eta}}{dt^2} = -\frac{1}{2N_0}\int^{+\infty}\frac{\partial U}{\partial\eta}|\varphi|^2\, d\eta = -\frac{q}{2}\left(1 - \frac{N_1}{N_0}\right), \tag{31}$$

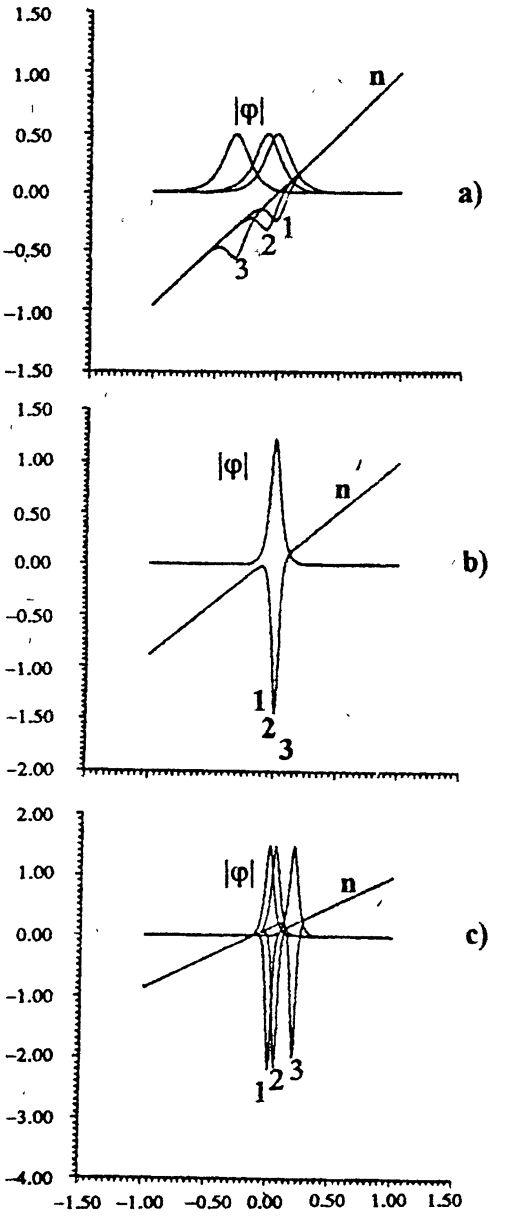

Fig. 4. The HF intensity $|\varphi(\tau, \eta)|$ and the concentration distribution n from Eq. (27) at $\varphi_0 = 0.5$; 1.2247 and 1.5 at various time moments: a) corresponds to $\varphi_0 = 0.5$; b) — $\varphi_0 = 1.2247$ and c) — $\varphi_0 = 1.5$. The curves 1 correspond to the initial time moment $\tau = 0$; 2 — $\tau = 2 \cdot 10^{-2}$; 3 — $\tau = 4 \cdot 10^{-2}$.

where $N_1 = \int_{-\infty}^{+\infty} |\varphi|^4 \, d\eta$. For the wave packets corresponding to the initial distribution (28) we have

$$\frac{d^2\overline{\eta}}{dt^2} = -\frac{q}{2}\left(1 - \frac{2}{3}\varphi_0^2\right). \tag{32}$$

It follows from (32) that the packet remains fixed in the reference system moving with the velocity a if the packet amplitude is equal $\varphi_{0,c} = \sqrt{3/2} \simeq 1.2247$. This value coincides with the simulation result (41). In this case the parameter q is as follows

$$q = \frac{8}{3}\frac{\Phi_0^2}{\beta^2}\left(1 + \frac{1}{3}\Phi_0^2\right)^2. \tag{33}$$

The packet acceleration in the laboratory reference system is

$$\dot{a} = -\frac{1}{2}\frac{\beta}{(1 + \Phi_0^2/3)}. \tag{34}$$

The shift of the reflection point Δz in the region of great values of the unperturbed potential constitutes

$$\Delta z = \frac{a_0^2\Phi_0^2}{3\beta}. \tag{35}$$

The value of the reflection point shift to the dense plasma increases with growth of the packet amplitude and its initial velocity.

3.2. HF radiation

The equilibrium of the HF packet in the moving reference system in the inhomogeneous media with the nonlocal nonlinearity is caused by the balance of the inhomogeneous medium force $f_{\text{inh}} \sim \partial U/\partial\xi$ and the LF radiation effect $f_{\text{LF}} \sim \dot{a}\,|\Phi|^2$. This is achieved at the inclination of the effective potential U_{eff} different from zero (which caused the HF radiation to the region of small values $U(\xi)$ (Fig.2). Thus the effective potential U_{eff} (24) for the packet which are stationary in the tracking system and at $\Phi_0^2 \ll 1$ will take the form

$$U_{\text{eff}} = \frac{\xi\beta}{3}\Phi_0^2 - |\Phi|^2 + \frac{\beta}{2}\int_{\xi}^{+\infty} |\Phi|^2 \, d\xi, \tag{36}$$

where $\beta = (\partial U/\partial\xi)\big|_{\xi=0}$. The power of the HF radiation from the packet core proportional to the inclination of the effective potential U_{eff} (the first term in (36)) increases with the increase of the HF packet amplitude and the decrease of the medium inhomogeneity scale.

3.3. HF wave packets in inhomogeneous media with the significant variation of the potential $U(z)$

The model Eqs. (13), (14) are applicable only at rather small variations of the frequency of nonlinear wave packets $\Delta\omega \ll \omega$. As packets move in the smoothly inhomogeneous plasma with the significant variation of the electron concentration, the frequency of the pulse also changes significantly: $\Delta\omega \sim \omega$.

We consider this effect using as the example the self-consistent $1-D$ intense EM field in plane-layer isotropic plasma with nonlocal striction nonlinearity. We assume that the wave vector of EM waves are collinear to the direction of the plasma gradient. In this case the Eqs. for the EM field vector-potential $\vec{A} = A \cdot \vec{x_0}$ ($\vec{x_0}$ is the unit vector in the axis x direction and the plasma concentration perturbation N_{NL} caused by the EM field action) in plasma with the parabolic barrier of the unperturbed concentration

$$N(z) = N_0 \left(1 - \left(\frac{z}{\Delta}\right)^2\right), \tag{37}$$

in dimensionless variables

$$t_n = \frac{c}{\Delta}t,\ z_n = \frac{z}{\Delta},\ A_n = \frac{\omega_p(0)\,A}{\alpha\sqrt{16\pi N_0 T_e}},\ \omega_n(t) = \frac{\omega(t)}{\omega_p(0)},\ n = \frac{N_{NL}}{N_0}, \tag{38}$$

(below we omit the index "n") have the form

$$\frac{\partial^2 A}{\partial z^2} - \frac{\partial^2 A}{\partial t^2} - \alpha^2\left(1 - z^2 + n\right)A = 0, \tag{39}$$

$$g^2\frac{\partial^2 n}{\partial t^2} - \frac{\partial^2 n}{\partial z^2} = \frac{1}{\alpha^2}\frac{\partial^2}{\partial z^2}\left(\left|\frac{\partial A}{\partial t}\right|^2\right), \tag{40}$$

where

$$\omega_p^2(0) = \frac{4\pi e^2 N_0}{m_e},\ \alpha = \frac{\omega_p(0)}{c}\cdot\Delta,\ g = \frac{c}{c_s},$$

T_e is the electron temperature, m_e is the electron mass, e is its charge. Passing to the reference system accompaning the packet

$$\xi = z - \int_{t_0}^{t} a\left(\bar{t}\right)d\bar{t}, \qquad t' = t, \tag{41}$$

we neglect the terms of the order $\partial^2/\partial t^2$ in the newly obtained Eqs., which corresponds to the slow enough rearrangement of the packet parameters. We present the solution (39), (40) in the form

$$A(z,t) = \frac{\Phi(\xi,t)}{\sqrt{\omega}}\exp\left\{i\int_0^t \Omega\left(\xi,\bar{t}\right)d\bar{t}\right\}, \tag{42}$$

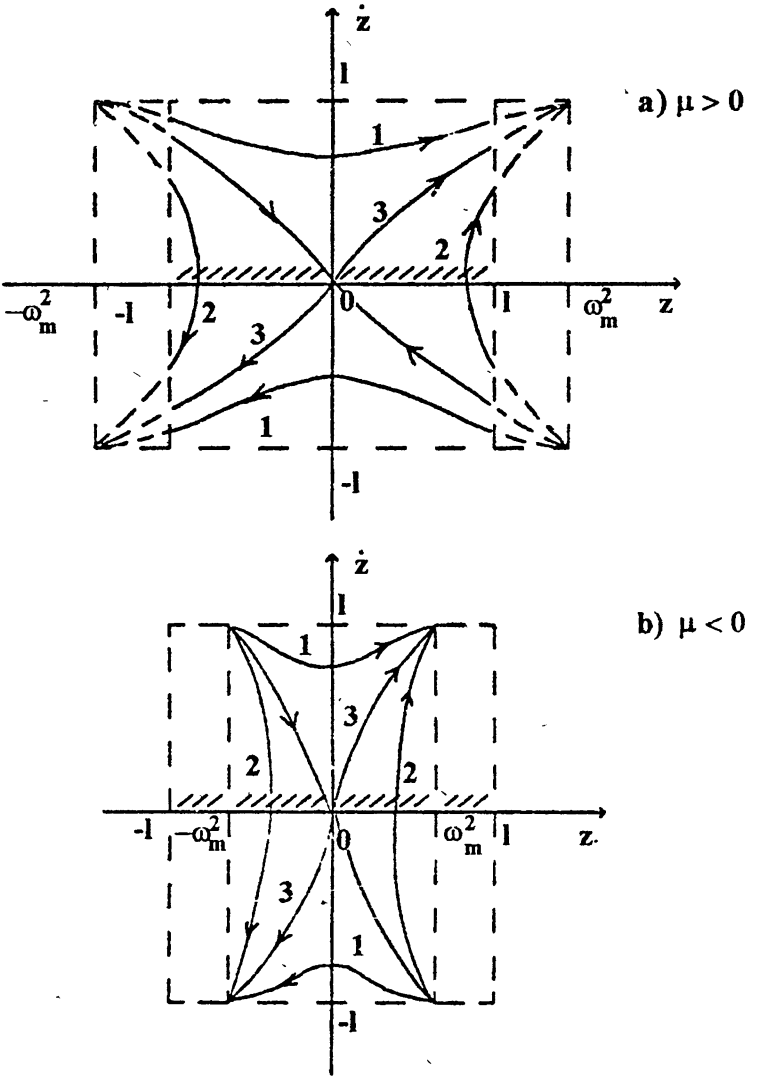

Fig. 5. Phase plane of Eqs. (44), (45) which describes the intense EM packet motion in a plasma wich a parabolic density profile: a) corresponds to $\mu > 0$; b) — $\mu < 0$. The curve 1 correspond to the passage, 2 corresponds to the packet reflection from the density barrier, 3 corresponds to packet "draving in" "rolling doun" from the barrier top.

where

$$\Omega(\xi, t) = \alpha \left[\omega - \frac{1}{2} \frac{\omega a^2}{(1 - a^2)} - \frac{\mu}{2\omega} - \frac{d}{dt} \left(\frac{\omega a}{1 - a^2} \right) \right]. \qquad (43)$$

We are interested in the wave packets, whose frequency $\omega(t)$, the velocity $a(t)$ and position $z(t)$ satisfy the relations

$$\omega^2(t) - \omega_p^2(t) = \mu, \qquad (44)$$

$$z(t) - \omega \frac{d}{dt}\left(\frac{\omega a}{1-a^2}\right) = 0, \tag{45}$$

where $\omega_p(t) = \sqrt{1-z^2(t)}$ is the unperturbed plasma frequency in the wave packet center at $\xi = 0$. In this case the Eqs. for envelope of the packet Φ and concentration n will be following

$$\left(1-a^2\right)\frac{\partial^2\Phi}{\partial\xi^2} - 2i\alpha\omega\frac{\partial\Phi}{\partial t} + \alpha^2\left(\xi^2 - n\right)\Phi = 0, \tag{46}$$

$$\left(a^2g^2 - 1\right)\frac{\partial n}{\partial\xi} - \frac{1}{n}\frac{\partial}{\partial t}\left(an^2\right) = \omega\frac{\partial}{\partial\xi}\left(|\Phi|^2\right). \tag{47}$$

The analyze of the packet motion Eqs. (44) and (45) shows that at $\mu > 0$ the packet trajectories achieve the plasma layer $|z| \leq 1$, not achieving its boundaries. The Fig. 5 shows the phase plane of Eqs. (44) and (45). The Fig. a) corresponds to the values $\mu > 0$, b) — $\mu < 0$. The curve 1 correspond to the passage of the EM packet through the density barrier, the curve 2 — to the reflection from it, the curve 3 — to divining regimes of "drawing in" and "rolling down" the packets from the density barrier crest. The obtained Eqs. are thoroughly analyzed in the approximation $\alpha \ll 1$ in [7]. Note that the nonlinear HF packets may transport the energy of the strong EM field through super critical plasma layers.

This work was supported by International Science Foundation and Ministry for Science of Russia (Grant No R8V300).

REFERENCES

1. Chen H.H. and Liu C.S. // Phys. Fluids, 1978. V.21. P.377.
2. Gupta M.R., Som B.K., and Dasgupta B. // Phys. Lett., 1978. V.A69. P.172.
3. Gromov E.M. and Talanov V.I. // Izv. VUZov. Radiofizika, 1993. V.30. P.601.
4. Chucbar R.V., Yan'kov V.V. // Fizika plazmy, 1978. V.3. P.1496.
5. Zakharov V.E. // ZhETF, 1978. V.61. P.1496.
6. Gromov E.M., Piskunova L.V., Talanov V.I. // ZhETF, 1995. V.108. N 7.
7. Gromov E.M., Nakaryakov V.M., Talanov V.I. // ZhETF, 1991. V.97. P.1745.

Институт прикладной физики
РАН, г.Н.Новгород

Поступила в редакцию
2 октября 1995 г.

MODELLING OF STOCHASTIC FORCES IN TURBULENT SPACE PLASMAS

C.-V. Meister

A model of a Langevin-equation for electrons in turbulent, almost collision-free magnetoactive plasmas is developed, which can form the starting point for particle simulations, especially in regions with reconnection of magnetic field lines. The mean wave force is expressed by a friction force and a velocity-derivative of the intensity of the stochastic force. The obtained expression for the Langevin force is in consistency with the kinetic theory in polarization approximation.

The intensity of the stochastic force corresponds to the velocity diffusion tensor of the electrons, which is estimated for plasmas with ion-acoustic turbulence using two different methods. One method is based on the direct calculation of the space-time spectral density of the wave energy. The second way uses approximations of quasi-linear plasma theory. The estimates for the intensities of the stochastic forces found within the two methods differ by orders.

A table of parameters of ion-acoustic waves, electron-wave collision frequencies and intensities of the stochastic wave forces on electrons in solar flares, in the solar wind, as well as in different regions of the earth's magnetosphere is presented. Results are given for the whole intervals of available experimental data for the mean magnetic induction, mean plasma temperatures and mean particle densities.

1. INTRODUCTION

Recently two methods are applied to investigate the influence of turbulence on the macroscopic dynamics of space plasmas — resistive magnetohydrodynamic modelling and particle simulation studies. These methods demand for good expressions for the wave-particle collision frequencies and corresponding anomalous resistivities or hyperresistivities, and for the wave forces on the charges. First mathematical formulae for stochastic forces on electrons in space plasma with ion-acoustic waves are obtained in [1]. There a Langevin-equation for electrons was developed, which is in consistency with the kinetic equation for plasmas with electrostatic turbulence [2]. But the influence of the magnetic field on the time-dynamics of the wave-particle collision operator was neglected. Considering waves with frequencies $|\omega|$ above the cyclotron frequencies $|\omega_{La}|$ of the plasma charges such an approximation is possible. But for plasmas with strongly magnetized ($|\omega| \lesssim |\omega_{La}|$) charges this approximation should be improved. Thus here a Langevin equation for electrons in plasmas with ion-acoustic turbulence is derived, which is again consistent with the kinetic equation for plasmas with wave-particle collisions in polarization approximation. But particle motion in the mean magnetic field is partially

taken into account in the wave-particle collision operator. Application is done for the solar flare and solar wind plasmas, and for the bow shock, the plasma sheet boundary layer and the polar cusp of the earth's magnetosphere.

2. LANGEVIN-EQUATION

The Langevin-equation for turbulent magnetoactive plasmas reads

$$m_a \frac{d\vec{v}}{dt} = q_a \left(\vec{E}_o(\vec{r}) + [\vec{v} \times \vec{B}_o(\vec{r})] \right) + \vec{F}_a(x,t), \quad \frac{d\vec{r}}{dt} = \vec{v}, \quad x = \{\vec{r}; \vec{v}\}. \tag{1}$$

q_a, n_a, m_a, and T_a are the charge, density, mass, and temperature of particles of type a. The index e denotes the electrons and i designates the ions. $\vec{E}_o(\vec{r})$ and $\vec{B}_o(\vec{r})$ are the electrical field strength and the magnetic induction of the plasma averaged over small length scales and time intervals below the inverse wave numbers $1/k$ and inverse wave frequencies $1/|\omega|$ of the considered electrostatic waves with field strength $\delta\vec{E}(\vec{r},t)$. $\vec{E}_o(\vec{r}) = \vec{E}(\vec{r},t) - \delta\vec{E}(\vec{r},t)$, $\vec{B}_o(\vec{r}) = \vec{B}(\vec{r},t) - \delta\vec{B}(\vec{r},t)$. The force of the waves on the particles $\vec{F}_a$ is divided in a mean ensemble average $\langle \vec{F}_a(x) \rangle$ and a stochastic force $\delta\vec{F}_a(x,t)$,

$$\vec{F}_a(x,t) = \langle \vec{F}_a(x) \rangle + \delta\vec{F}_a(x,t). \tag{2}$$

The stochastic force does not influence the mean motion of the plasma,

$$\langle \delta\vec{F}_a(x,t) \rangle = \int \delta\vec{F}_a(x,t) f_{N_a}(X,t)\, dX = 0, \quad \{X\} = \{x_1, x_2, ..., x_{N_a}\}. \tag{3}$$

N_a is the number of particles of kind a and f_{N_a} the N_a -particle distribution function.

Assuming a Gaussian distributed stochastic force

$$f_{\delta\vec{F}_a}(\delta\vec{F}_a) = \frac{1}{\sqrt{2\pi}\sigma_a} \exp\left\{ -\frac{(\delta\vec{F}_a)^2}{2\sigma_a^2} \right\} \tag{4}$$

the correlation functions of the stochastic force of odd order are zero, and the correlation functions of even order can be expressed by functions of second order given by

$$\langle \delta F_{ai}(x,t_1) \delta F_{aj}(x,t_2) \rangle = 2\delta_{ij}\delta(t_1 - t_2) D^a_{ij}(x). \tag{5}$$

That means, components of the stochastic force in different space directions and at different moments of time are assumed to be uncorrelated. As suggested in [3] the mean wave force on the particles is expressed by a friction force $-\gamma^*_a(x)v_i$ and a second tensor contribution, which has to be found regarding consistency with kinetic theory

$$\langle F_{ai}(x) \rangle = -\gamma^*_a(x) v_i + \sum_j \frac{\partial R^a_{ij}(x)}{\partial v_j}. \tag{6}$$

Instead of solving the Langevin equation (1) for given initial conditions $x_o = x(t_o)$ and to find the probability of the solutions, it is possible to develop an equation of motion for the one-particle distribution function $f_a(x)$ corresponding to the Langevin equation, and to solve the equation for $f_a(x,t)$. If the plasma processes are suggested to be Markovian, that means, if there exist time intervals Δt much larger than a few inverse effective collision frequencies $1/\nu_{\text{eff}}$ and smaller than the dissipation time of the considered plasma process t_d,

$$\frac{1}{\nu_a^{\text{eff}}} \ll \Delta t < t_d, \tag{7}$$

then the equation for $f_a(x,t)$ is the Fokker–Planck–equation

$$\frac{\partial}{\partial t} f_a(x,t) + \vec{v}\frac{\partial}{\partial \vec{r}} f_a(x,t) + \frac{q_a}{m_a}\left(\vec{E}_o(\vec{r}) + [\vec{v}\times\vec{B}_o(\vec{r})]\right)\frac{\partial}{\partial \vec{v}} f_a(x,t) =$$

$$= \frac{1}{m_a}\frac{\partial}{\partial \vec{v}}\left(\gamma_a^*(x)\vec{v} f_a(x,t)\right) + \frac{1}{m_a^2}\sum_i \frac{\partial}{\partial v_i} D_{ii}^a(x)\frac{\partial}{\partial v_i} f_a(x,t). \tag{8}$$

In (8) only diagonal elements of the velocity diffusion tensor appear, which is the consequence of the assumption of Gaussian stochastic forces used to obtain convergence of the Kramers–Moyal series of $f_a(x,t)$ for small Δx developing the Fokker–Planck equation. Besides, the Fokker–Planck equation can be only written in the usual form (8) if the relation $m_a R_{ii}^a(x) = D_{ii}^a$ is valid.

Comparing (8) with the kinetic equation for plasmas with large-scale electrostatic fluctuations with wave numbers $|k| < \text{Min}\,\{1/r_{De}; 1/r_{Le}\}$ ($r_{De} = \sqrt{\varepsilon_o k_B T_a/n_a}/q_a$ — Debye radius) [2] the friction coefficient γ_a^* can be expressed by the imaginary part of the dielectric function

$$\gamma_a^* v_i = \frac{q_a^2}{2\pi^2 V}\sum_{m=-\infty}^{\infty}\int \delta(\omega - k_{\|}v_{\|} - m\omega_{La})\frac{k_i}{k^2} J_m^2\left(\frac{k_\perp p_\perp}{\omega_{La}}\right)\cdot \tag{9}$$

$$\cdot\frac{\text{Im}\varepsilon(\omega,\vec{k})}{|\,\varepsilon(\omega,\vec{k})\,|^2} d\omega d\vec{k}, \quad \omega_{La} = \frac{q_a B_o}{m_a}$$

and the intensity of the stochastic force σ_a is given by the space-time spectral density of the energy $\left(\delta\vec{E}\delta\vec{E}\right)_{\omega\vec{k}}$ of the large-scale plasma fluctuations, which are represented by the electrostatic waves,

$$\sigma_a = \sqrt{2D_{ii}^a(x)\delta(t_1 - t_2)}, \tag{10}$$

$$D_{ij}^a(x) = \frac{q_a^2}{16\pi^3 V}\sum_{m=-\infty}^{\infty}\int \frac{k_i k_j}{k^2}\delta(\omega - k_{\|}v_{\|} - m\omega_{La})\cdot \tag{11}$$

$$\cdot J_m^2\left(\frac{k_\perp p_\perp}{\omega_{La}}\right)\left(\delta\vec{E}\delta\vec{E}\right)_{\omega\vec{k}}\,d\omega d\vec{k}.$$

J_m is the Bessel function defined by

$$\exp\{iz^*\sin\phi\} = \sum_{m=-\infty}^{\infty} J_m(z^*)\exp\{im\phi\}. \qquad (12)$$

In the applied type of kinetic equation the (large–scale) space and time fluctuations $\delta f_e(x,t)$ of the electron distribution are assumed to have smaller scales than the changes of the mean distribution $f_e(x,t)$ (given by t_d), which are a consequence of the reaction of the fluctuations δf_e. And even this assumption is equivalent to the condition (7). Of course, equation (11) is a very complicated expression, and there is much to do to calculate D_{ij}^a for a special type of wave turbulence. In the following first approximations are found for D_{ij}^a for space plasmas with ion-acoustic turbulence. Solar flares (SF), the solar wind (SW), as well as the bow shock (BS), the plasma sheet boundary layer (PSBL) and the polar cusp (PC) of the earth's magnetosphere are considered. In Table 1 for these plasma regions the following parameters are presented: electron density n_e, particle temperatures T_a, mean magnetic induction B_o, electric field strength E_o, Debye radii r_{Da}, skin depth δ, Larmor radii $r_{La} = v_a/\omega_{La}$, mean free path of electrons l_e, Larmor frequencies $f_{La} = \omega_{La}/2\pi$, plasma frequencies $f_{pa} = \omega_{pa}/2\pi$, lower-hybrid frequency $f_{LH} = \omega_{LH}/2\pi$, collision frequency of the electrons with the charged particles ν_e, ion-sound velocity c_s, Alfvén velocity v_A, thermal velocities v_a, $\vec{E}_o \times \vec{B}_o$-drift velocity v_D, plasma-β and density of the magnetic energy $W_m = B_o H_o/2$.

3. GENERAL CHARACTERISTICS OF ION–ACOUSTIC TURBULENCE

The certainly best investigated and rather effective plasma instability is the ion-acoustic (IA) one. It seems to appear in different regions of the sun, e.g. in solar flares where electrons can be heated up to $T_e \approx 4T_i$ [4]. In the solar wind IA waves were detected by Helios and Voyager satellites [5]. In the shock front (bow shock) of the earth's magnetosphere they also appear, but according to [6] they are not intensive enough to influence the macroscopic structure. And, in general, in the earth's magnetosphere itself their generation is only possible in regions with $T_e > T_i$, that means at lower altitudes, or in cases with additional preceding electron heating. In the high-altitude auroral region and the polar cusp strong IA turbulence was obtained during the EISCAT-VHF (224 MHZ) radar experiment at altitudes above 600 km [7] and below 300 km as well as a little above 300 km ($2 \lesssim T_e/T_i \lesssim 3$) [8].

As usual, here IA turbulence excited by electron drifts $\vec{V}_e^o \| \vec{n}_z$ is considered. Thus one can describe the electron distribution in the initial state at

the beginning of the wave generation by a shifted in z-direction Maxwellian function,

$$f_e^o(\vec{v}) = \frac{n_e}{\pi^{3/2} v_e^3} \exp\left\{-\frac{v_x^2 + v_y^2 + (v_z - V_e^o)^2}{v_e^2}\right\}. \tag{13}$$

The ions are assumed to be Maxwellian. Suggesting further rather cold ions with $|\omega/kv_i| > 1$ and relatively warm electrons, $|(\omega - \vec{k}\vec{V}_e^o)/kv_e| < 1$, the dielectric function of the plasma containing fluctuations of the electric field with complex frequency

$$\omega = \omega_r + i\gamma, \quad \omega_r = \mathrm{Re}\{\omega\}, \quad \gamma = \mathrm{Im}\{\omega\} \tag{14}$$

and wave vector $\vec{k}$ reads ($|\gamma| < |\omega_r|$, $z_e < 1$)

$$\varepsilon(\vec{k}, \omega) = 1 + \varepsilon_o^{(e)} + \varepsilon_o^{(i)} =$$

$$= 1 + \frac{1}{k^2 r_{De}^2}\left(1 + \left[\frac{i\sqrt{\pi}(\omega_r - \vec{k}\vec{V}_e^o)}{|k_z| v_e} - \frac{2(\omega_r - \vec{k}\vec{V}_e^o)^2}{|k_z|^2 v_e^2}\right](1 - z_e)\right) -$$

$$- \frac{\omega_{pi}^2}{\omega_r^2}\left(1 + \frac{3k^2 v_i^2}{2\omega_r^2}\right) + \frac{i\sqrt{\pi}\omega_r}{k^3 v_i r_{Di}^2} \exp\left\{-\frac{\omega_r^2}{k^2 v_i^2}\right\}, \tag{15}$$

$$z_e = \frac{k_\perp^2 k_B T_e}{m_e \omega_{Le}^2} = k_\perp^2 \rho_e^2 = \frac{c^2 k_\perp^2 \beta_e}{2\omega_{pe}^2}, \quad \omega_{pa} = q_a \sqrt{\frac{n_a}{\varepsilon_o m_a}}. \tag{16}$$

From (15) follows, that the plasma is unstable, if the electron drift satisfies

$$V_e^o > V^{\mathrm{crit}} = \frac{c_s}{(1 - z_e)\sqrt{1 + k^2 r_{De}^2}} \cdot \tag{17}$$

$$\left[1 - z_e + \left(\frac{m_i T_e^3}{m_e T_i^3}\right)^{1/2} \exp\left\{-\frac{3}{2} - \frac{T_e}{2T_i(1 + k^2 r_{De}^2)}\right\}\right], \quad c_s^2 = \frac{k_B T_i}{m_e}.$$

Thus, the stronger the influence of the magnetic field, the larger V_e^o has to be. If $k^2 r_{De}^2 \ll 1$, the ratio V^{crit}/c_s has a maximum at $T_e \approx 3T_i$. The large scale fluctuations generated under the conditions

$$T_i/T_e + k^2 r_{Di}^2 \ll 1 \quad \text{and} \quad k^2 r_{De}^2 \ll 1 \tag{18}$$

with frequencies

$$\omega_r^2 = k^2 c_s^2 \left(1 + \frac{3T_i}{T_e}\right), \tag{19}$$

Table 1

	SF	SW	BS	PSBL	PC
n_e [cm^{-3}]	E10-E11	5	20	0.1	E4-E5
T_e [K]	E7-3E7	E5	E6	5E6	5800
T_i [K]	E7-3E7	4E4	5E5	E7	5800
B_o [nT]	2E7-3E7	5	10	20	100
E_o [V/m]		3E-3	2E-3	E-4	$E_{o\parallel}$ =0.1
v_D [km/s]		400	210	5	
r_{De} [m]	7E-4-4E-3	10	15	490	0.02-0.05
r_{Di} [m]	7E-4-4E-3	6	15	690	0.02-0.05
δ [m]	0.02-0.05	2400	1200	1.7E4	20-50
r_{Le} [m]	4E-3-8E-3	1900	3100	3400	24
r_{Li} [m]	0.1-0.4	5.4E4	9.6E4	2.2E5	1000
l_e [m]	5.6E4-2.5E6	5.1E10	1.2E12	4.7E12	1.4E4-1.3E5
f_{Le} [Hz]	5.6E8-8.4E8	140	280	560	2800
f_{Li} [Hz]	3.3E5-4.4E5	7.6E-2	0.15	0.3	1.5
f_{pe} [Hz]	9E8-2.8E9	2E4	4E4	2800	9E5-2 8E6
f_{pi} [Hz]	2.1E7-6.6E7	470	940	66	2.1E4-6.6E4
f_{LH} [Hz]	1E7-2E7	3.4	6.7	13	65-66
ν_{ee} [Hz]	7.0-320	2E-5	2.8E-6	1.5E-9	1.9-18
ν_{ei} [Hz]	5.0-220	1.4E-5	2.0E-6	1.1E-9	1.3-13
ν_e [Hz]	12-540	3.4E-5	4.7E-6	2.5E-9	3.3-30
ν_{ii} [Hz]	0.16-7.4	1.7E-6	1.8E-7	1.3E-11	0.04-0.41
c_s [km/s]	300-500	29	91	200	6.9
v_A [km/s]	1400-6500	49	49	1400	7-22
v_e [km/s]	2E4-3E4	1700	5500	1.2E4	420
v_i [km/s]	470-710	26	91	410	9.7
β	8E-3-0.5	0.97	10	0.13	0.4-4
W_m [J/m^3]	160-360	E-11	4E-11	1.6E-10	4.0E-9
V^{crit} [km/s]	2000-3400	340	1000	730	47
ω_M [Hz]	7.6E7-2.4E8	1700	3400	240	7.6E4-2.4E5
$\gamma_M(V^{crit})$ [Hz]	5E6-1.6E7	200	370	8.5	5100-1.6E4
k_M [1/m]	190-1000	7.2E-2	4.6E-2	1.4E-3	14-44
a	5.3E-8-7.7E-7	1E-8	6.4E-10	1.1E-8	1.5E-5-4.2E-5
$\nu_e^{WP}(V^{crit})$ [Hz] (34)	8.8E6-2.8E7	870	1300	7.5	9000-2.8E4
$E_{ox}(V^{crit})$ [V/m]	60-910	1.7E-3	7.3E-3	3.1E-5	2.4E-3-7.6E-3
$\nu_B(V^{crit})$ [Hz]	4.0E7-1.0E9	1.9E4	2.7E4	51	1.2E5-3.6E5
ν_N [Hz]	1.3E7-4.1E7	740	1200	21	1.3E4-4.1E4
h	5.80	10.8	10.0	2.05	5.80
$A_o(V^{crit})$	-0.32 - -24	-27	-22	-5.9E-2	-4.9
$C_o(V^{crit})$	0.47-1.3	1.4	1.3	4.3	0.80
$W/(k_BT_en_e)$ (31)	0.37-4.7	8.6	8.2	$\approx$0.5	0.32-1.2
$\nu_e^{WP}(W)$ [Hz] (31,33)	8.3E5-3.4E7	420	800	3.6	720-8.9E3
$k_BT_en_e$ [J/m^3]	1.4-41	6.9E-12	2.8E-10	6.9E-12	8.0E-10-8.0E-9
D_{xx}^e [kg^2m^2/s^3] (42)	E-45-2E-42	2E-53	2E-53	2E-56	E-49-E-48
D_{xx}^e [kg^2m^2/s^3] (47)	E-41-(2E-36)	-	-	2E-45	6E-47-E-43
D_{xx}^e [kg^2m^2/s^3] (48)	E-40-2E-35	E-44	3E-43	E-45	E-46-2E-42
σ_e [kgm/s^2] (10,48)	2E-20-6E-18	2E-22	7E-22	5E-23	E-23-2E-21

growth rates

$$\gamma = -\sqrt{\frac{\pi}{8}} k c_s \left[\left(\sqrt{\frac{m_e}{m_i}} - \sqrt{2} \frac{\vec{k}\vec{V}_e^o}{k v_e} \right) (1 - z_e) + \sqrt{\frac{m_e}{m_i}} h \right], \tag{20}$$

and usually finite values

$$h = \left(\frac{m_i T_e^3}{m_e T_i^3} \right)^{1/2} \exp\left\{ -\frac{3}{2} - \frac{T_e}{2T_i} \right\} \tag{21}$$

are the so-called ion-acoustic waves. The term proportional to h in γ describes the damping by the ions.

Davidson and Krall [14] found within quasi-linear plasma theory at maximum wave growth and $c_s \ll V_e^o \ll v_e$

$$\gamma_M \approx \frac{1}{3} \sqrt{\frac{\pi m_e}{6 m_i}} \frac{V_e^o}{c_s} \omega_{pi}, \quad \omega_M \approx \frac{\omega_{pi}}{\sqrt{3}}, \quad k_M \approx \frac{1}{\sqrt{2} r_{De}}. \tag{22}$$

In Table 1 the threshold $V^{\rm crit}$ (17) for the excitation of electrostatic waves and the characteristics of IA waves at maximum wave growth in solar flares, the solar wind at 1AE, the bow shock, the plasma sheet boundary layer in the tail and the polar cusp of the earth's magnetosphere are presented. For the plasma sheet boundary layer $T_i = 2T_e$ is assumed, so that the condition (18) cannot be satisfied and (20)–(22) are extremely rough. Nevertheless estimates are made.

In [15] the energy spectrum $(\delta\vec{E}\delta\vec{E})_{\vec{k}}$ was obtained within quasi-linear theory for the case of stationary IA turbulence. There it was assumed, that the waves are first scattered by the ions, so that their wave numbers decrease. And then, second, the waves with the long wavelengths saturate by ion-ion collisions. In this case the energy spectrum can be factorized,

$$(\delta\vec{E}\delta\vec{E})_{\vec{k}} = \Phi(g)(\delta\vec{E}\delta\vec{E})_k, \quad g = \cos\theta, \quad \theta = \angle(\vec{k}\vec{E}_o) \tag{23}$$

and the wave-number dependence is (exact result in the case of absence of Non-Maxwellian tails of particle distributions)

$$(\delta\vec{E}\delta\vec{E})_k = \frac{8\pi^5 \omega_\tau^4 V}{v_i^2 \omega_{pi}^2 \varepsilon_o} \sqrt{\frac{\pi m_e}{2 m_i}} \frac{\ln(k r_D)}{k^5} n_e k_B T_e, \tag{24}$$

$r_D^{-2} = r_{De}^{-2} + r_{Di}^{-2}$. In the case of weak electric fields the angular dependence can be approximated by ($g^2 \geq g_o^2$, $\vec{E}_{oz}$ is antiparallel to $\vec{n}_z$)

$$\Phi(g) = \frac{4\nu_E}{3\pi\nu_N g} \frac{d}{dg} \frac{g(g^2 - g_o^2)^{3/2}}{1 - g + h + A_o}, \quad g_o^2 = \frac{\nu_{ei}}{\nu_E}(1 + h + A_o) \leq 1, \tag{25}$$

$$\nu_E = \sqrt{\frac{9\pi}{8}}\frac{q_e E_{oz}}{m_e c_s} > 0, \quad \nu_N = v_e \int_o^{1/r_{De}} \frac{k^3}{(2\pi)^2}\frac{(\delta\vec{E}\delta\vec{E})_k}{n_e k_B T_e} dk \approx \frac{\omega_{pi}}{4\sqrt{2\pi}}\frac{T_e}{T_i}, \tag{26}$$

$$A_o \approx \frac{4\nu_E}{3\pi\nu_N}\ln\left(\frac{3\pi\nu_N}{4\nu_E}\right) \ll 1 - h. \tag{27}$$

As a consequence of Landau damping the waves do not propagate parallel to the electron drift $\vec{V}_e^o$, but waves with larger θ are less intensive. The total wave energy can be estimated with the help of [15]

$$W = \int W(\vec{k})d\vec{k} = \frac{\sqrt{2m_e}n_e k_B T_e^2 \nu_E}{\sqrt{9\pi m_i T_i}\nu_N(A_o + h)}\ln^2 a, \quad a = \sqrt{\frac{m_i}{m_e}}\frac{\nu_{ii}T_i}{\omega_{pi}T_e}. \tag{28}$$

$$W(\vec{k}) = \frac{\varepsilon_o}{2V(2\pi)^3}\frac{\partial(\omega\varepsilon(\omega,\vec{k}))}{\partial\omega}(\delta\vec{E}\delta\vec{E})_{\vec{k}}. \tag{29}$$

But if the electric field is relatively large and $A_o \gtrsim 1$ or $A_o < 0$, then A_o has to be neglected in the first line of (25) and $\Phi(g)$ can be approximated by [15]

$$\Phi(g) \approx \frac{16\nu_E g^2}{3\pi\nu_N C_o}\left[1 - 3g^2 + 2g^4\right], \quad C_o \approx 0.27\sqrt{\frac{\nu_E}{\nu_N}} \approx 0.117\frac{V_e^o}{c_s}. \tag{30}$$

Thus, the total wave energy is

$$W = 6.5\ 10^{-3}\frac{4\pi\sqrt{m_e\nu_E}n_e k_B T_e^2}{\sqrt{m_i\nu_N T_i}}\ln^2 a. \tag{31}$$

The expressions (29), (31) are valid for $k \gtrsim k_{\min} = a/r_{De}$.

Within quasi-linear plasma theory here certainly to high wave energy values are considered. Nevertheless it is clear that in the studied space regions with $T_e \gtrsim T_i$ (and $T_e \lesssim T_i$!) the electron-wave collision frequencies at critical electron drift $V_e^o \approx V^{\text{crit}}$ are many orders larger than the electron-particle collision frequencies. From the velocity momentum balance in z-direction and the quasi-linear approximation for the electron-wave collision frequency (34) follows $E_{oz} \approx n_e q_e V_{ez}^o/\sigma_{zz}^{(e)}(\omega = 0) \approx 0.01 m_e T_e \omega_{pi} V_{ez}^{o2}/(q_e c_s T_i)$ and $\nu_E \approx 0.01\sqrt{9\pi/8}T_e\omega_{pi}V_{ez}^{o2}/(c_s^2 T_i)$. $\sigma_{zz}^{(e)}$ is the field-aligned electrical conductivity of the electrons. Thus here negative values of A_o appear ($h > 1$), which were neglected in [15].

Within kinetic theory in polarization approximation Belyi et al. [16] found for the wave-particle collision frequencies of plasmas with ion-acoustic turbulence

$$\nu_a^{WP} = \frac{\omega_{pa}^2}{4(2\pi)^{7/2}n_a k_B T_a v_a j_a^2}\int_{k<1/r_{Di}} \frac{(\vec{k}\vec{j}_a)^2}{k^3}(\delta\vec{E}\delta\vec{E})_{\vec{k}}d\vec{k}, \tag{32}$$

which corresponds under the condition $k \approx 1/r_{De}$ to the results of Galeev and Sagdeev [15]

$$\nu_e^{WP} = \frac{\omega_{pa} W}{4(2\pi)^{7/2} n_a k_B T_a}, \tag{33}$$

(1973)

$$\nu_e^{WP} \approx 0.01 \omega_{pi} \frac{V_e^o}{c_s} \frac{T_e}{T_i}. \tag{34}$$

Here estimating the mean electrical field E_{oz} only the angular-averaged expression for the z-component of the electrical conductivity was used

$$\sigma_{zz}^{(a)} \approx \frac{q_a^2 n_a}{m_a} \frac{1}{\nu_a^{\text{eff}} - i\omega}. \tag{35}$$

ν_a^{eff} designates the sum of the wave-particle collision frequency ν_a^{WP} and the electron-ion collision frequency ν_{ei}.

From (25)–(27) and (30) it can be seen, that, as in space plasmas $\vec{V}_e^o$ is mostly directed along $\vec{B}_o$, IA waves with larger angles θ with respect to $\vec{B}_o$, which should mainly cause magnetic reconnection, are less intensive.

In the discussed space plasma regions the angular-averaged electron-wave collision frequencies are generally large. But in solar flares and in the plasma sheet boundary layer they are only of the order of the maximum growth rate of the waves (22). That means, at least at the very initial stage of the wave growth, when only some waves with maximum growth rate γ_M are of importance, the coordinate space and velocity diffusion in these space plasma regions cannot be considered as Markovian processes ((7) is not valid). But the frequency spectra of the waves are rather broad-band (guaranteeing the possibility of a statistical description), so that after a short time interval many wave modes determine the diffusion process. Moreover, γ_M decreases with the time as the energy spectra saturate. Thus the dissipation time t_d in (7) can be expected to be about one order of magnitude larger than the inverse maximum growth rate, so that the electron distribution in all considered space plasma regions can nevertheless be estimated with the help of a Fokker-Planck-equation. And as $k \ll \text{Min}\{1/r_{De}; 1/r_{Le}\}$, the system of equations (6), (9)–(11) can be used to find the wave force.

4. ESTIMATE OF THE VELOCITY–DIFFUSION TENSOR FOR ION-ACOUSTIC TURBULENCE

To calculate the intensity of wave forces on electrons one way is first to determine the space-time spectral density of the wave energy $(\delta\vec{E}\delta\vec{E})_{\omega\vec{k}}$, which is a parameter of the here used theory. As shown in [2] $(\delta\vec{E}\delta\vec{E})_{\omega\vec{k}}$ can be

expressed by the dielectric function $\varepsilon(\omega,\vec{k})$ and a spectral function $A_a(\omega,\vec{k})$,

$$(\delta\vec{E}\delta\vec{E})_{\omega\vec{k}} = V|\varepsilon(\omega,\vec{k})|^{-2}\sum_{a=e,i}A_a(\omega,\vec{k}). \tag{36}$$

For nonmagnetized Maxwellian ions drifting with velocity V_i^o follows

$$A_i(\omega,\vec{k}) = \frac{2\pi m_i\omega_{pi}^2}{\varepsilon_o n_i k^2}\int d\vec{v}\delta(\omega-\vec{k}\vec{v})f_i^o(\vec{v}) =$$

$$= \frac{2\pi^{1/2}m_i\omega_{pi}^2}{\varepsilon_o v_i k^2|k|}\exp\left\{-\frac{(\omega-\vec{k}\vec{V}_i^o)^2}{k^2v_i^2}\right\}, \tag{37}$$

and for the Maxwellian magnetized electrons with shift V_e^o the expression

$$A_e(\omega,\vec{k}) = \frac{2\pi m_e\omega_{pe}^2}{\varepsilon_o n_e k^2}\sum_{m=-\infty}^{\infty}\int d\vec{v}\delta(\omega-k_{\|}v_{\|}-m\omega_{Le})J_m^2\left(\frac{k_\perp v_\perp}{\omega_{Le}}\right)f_e^o(\vec{v}) =$$

$$= \frac{2\pi^{1/2}m_e\omega_{pe}^2}{\varepsilon_o v_e k^2|k_z|}\exp\left\{-\frac{(\omega-\vec{k}\vec{V}_e^o-m\omega_{Le})^2}{k_z^2v_e^2}\right\}\exp\left\{-\frac{k_\perp^2v_e^2}{2\omega_{Le}^2}\right\}I_m\left(\frac{k_\perp^2v_e^2}{2\omega_{Le}^2}\right), \tag{38}$$

$$I_m\{z_a\} = \left(\frac{z_a}{2}\right)^m\sum_{k=0}^{\infty}\frac{(z_a^2/4)^k}{k!(m+k)!},\quad \sum_{m=-\infty}^{\infty}I_m\{z_a\} = e^{z_a} \tag{39}$$

can be found. Substituting (37), (38) into (11), taking into account, that at maximum wave growth only the imaginary part of $\varepsilon(\omega,\vec{k})$ is of importance, and considering only Bessel functions J_o, I_o of first order (as $z_e \approx (1-g^2)\omega_{pe}^2/(2\omega_{Le}^2) < 1$ at maximum wave growth) one obtains for the velocity–diffusion component D_{xx}^e perpendicular to the mean magnetic induction and the electron drift $\vec{V}_e^o$

$$D_{xx}^e(\vec{v}) \approx \frac{q_e^2m_e\omega_{pe}^2}{8\varepsilon_o\pi^2\sqrt{\pi}}\int_{-1}^{1}dg(1-g^2)\int_o^{\infty}dkk^3J_o^2\left(\frac{kv_\perp\sqrt{1-g^2}}{\omega_{Le}}\right)\cdot$$

$$\cdot\left[\frac{1}{v_i}\exp\left\{-\frac{g^2v_{\|}^2}{v_i^2}\right\}+\frac{1}{v_e|g|}\exp\left\{-\frac{(v_{\|}-V_e^o)^2}{v_e^2}\right\}\exp\left\{-\frac{k^2v_e^2(1-g^2)}{2\omega_{Le}^2}\right\}\cdot\right.$$

$$\left.\cdot I_o\left(\frac{k^2v_e^2(1-g^2)}{2\omega_{Le}^2}\right)\right]\left[\frac{(v_{\|}-V_e^o)g}{v_er_{De}^2\,|\,g\,|}+\frac{v_{\|}g}{v_ir_{Di}^2}\exp\left\{-\frac{g^2v_{\|}^2}{v_i^2}\right\}\right]^{-2}. \tag{40}$$

Further, neglecting the ion-damping contribution in (40) (second term in third line) and considering the limits of the wave numbers and angles of ion-acoustic waves, in lowest order with respect to $z_e < 1$ follows

$$D^e_{xx}(\vec{v}) \approx \frac{q_e^2 m_e v_e^4 r_{De}^2}{8\varepsilon_o \pi^2 \sqrt{\pi}(v_\parallel - V_e^o)^2} \int\limits_{g_o}^{1} dg(1-g^2) \int\limits_{k_{\min}=a/r_{De}}^{1/r_{De}} dk k^3 \cdot$$

$$\cdot \left(1 - \frac{k^2 v_\perp^2 (1-g^2)}{4\omega_{Le}^2}\right)^2 \left[\frac{1}{v_i} \exp\left\{-\frac{g^2 v_\parallel^2}{v_i^2}\right\} + \frac{1}{v_e|g|} - \frac{k^2 v_e (1-g^2)}{2\omega_{Le}^2 g}\right]. \qquad (41)$$

Approximating $\int_{g_o}^1 F(g)dg$ by $(F(1)+F(g_o))(1-g_o)/2$ and $\int_{k_{\min}}^{1/r_{De}} F(k)dk$ by $(1-a)(F(1/r_{De})+F(a/r_{De}))/(2r_{De})$ the final expression for the electron velocity-diffusion component D^e_{xx} in a plasma with ion-acoustic waves is

$$D^e_{xx}(\vec{v}) \approx \frac{q_e^2 m_e v_e^2 \omega_{pe}^2 (1-a)(1-g_o)}{16\varepsilon_o \pi^2 \sqrt{\pi}(v_\parallel - V_e^o)^2} [H(a=1) + H(a)], \qquad (42)$$

$$H(a) = a^3(1-g_o^2)\left[\frac{1}{v_i}\exp\left\{-\frac{g_o^2 v_\parallel^2}{v_i^2}\right\} + \frac{v_\parallel}{v_e c_s} - \frac{a^2 v_e v_\parallel (1-g_o^2)}{2\omega_{Le}^2 r_{De}^2 c_s}\right] \cdot$$

$$\cdot \left[1 - \frac{a^2 v_\perp^2 (1-g_o^2)}{4\omega_{Le}^2 r_{De}^2}\right]^2. \qquad (43)$$

Immediately using, that in the case $|\omega_r| > |\gamma|$ the space-time spectral density of the wave energy can be approximated by

$$(\delta\vec{E}\delta\vec{E})_{\omega\vec{k}} = \pi(\delta\vec{E}\delta\vec{E})_{\vec{k}}[\delta(\omega - \omega_r(\vec{k})) + \delta(\omega + \omega_r(\vec{k}))] \qquad (44)$$

(with the help of (44) one changes from Fourier presentation to the integration over plasma frequencies and wave vectors!), one finds from (11), (23) introducing spherical coordinates $\vec{k} = \{k, \theta, \varphi\}$ and integrating over ω and φ

$$D^e_{xx}(\vec{v}) = \frac{q_e^2}{16V\pi|v_\parallel|} \int\limits_{g_o}^{1} dg\Phi(g) \int\limits_{k_{\min}}^{1/r_{De}} dk k^2 J_o^2\left(\frac{kv_\perp\sqrt{1-g^2}}{\omega_{Le}}\right) \cdot$$

$$\cdot (\delta\vec{E}\delta\vec{E})_k \left[\delta(kg + \frac{\omega_r}{v_\parallel}) + \delta(kg - \frac{\omega_r}{v_\parallel})\right]. \qquad (45)$$

Here the conditions (18) and $g \geq g_o$ for the wave vector are used. Approximating the frequency of the ion-acoustic waves by kc_s and integrating over the angular dependence one finds from (24), (25), (45)

$$D^e_{xx}(\vec{v}) \approx -\frac{4\pi^4 q_e^2 \nu_E \sqrt{m_e} c_s^3 n_e k_B T_e \sqrt{c_s^2 - g_o^2 v_\parallel^2}}{3\varepsilon_o \sqrt{\pi 2 m_i} \nu_N v_\parallel^2 v_i^2 \omega_{pi}^2} \left\{ \frac{3c_s^2 - g_o^2 v_\parallel^2}{v_\parallel (1 + h + A_o) - c_s} + \right.$$

$$\left. + \frac{c_s^3 - c_s g_o^2 v_\parallel^2}{[v_\parallel (1 + h + A_o) - c_s]^2} \right\} \int\limits_{a/r_{De}}^{1/r_{De}} dk \ln(kr_D) J_o^2 \left(\frac{k v_\perp \sqrt{v_\parallel^2 - c_s^2}}{|v_\parallel| \omega_{Le}} \right) \qquad (46)$$

for very low E_{oz}. Finally, approximating the integral $\int_{k_{\min}}^{r_{De}} dk \ln(kr_D) J_o^2$ by $(\ln[r_D/r_{De}] - 1 - a \ln[a r_D/r_{De}] + a)/r_{De} J_o^2$ it follows

$$D^e_{xx}(\vec{v}) \approx \frac{\pi^4 q_e^2 \nu_E m_e v_e n_e T_e r_{De}^3 \sqrt{c_s^2 - g_o^2 v_\parallel^2}}{3\varepsilon_o \sqrt{\pi} \nu_N v_\parallel^2 T_i} \left(1 - \frac{v_\perp^2 (v_\parallel^2 - c_s^2)}{4 v_\parallel^2 r_{De}^2 \omega_{Le}^2} \right)^2 \cdot$$

$$\cdot \left[1 + \ln \left(\sqrt{1 + T_e/T_i} \right) - a - a \ln \left(\frac{\sqrt{1 + T_e/T_i}}{a} \right) \right] \cdot$$

$$\cdot \left\{ \frac{3c_s^2 - g_o^2 v_\parallel^2}{v_\parallel (1 + h + A_o) - c_s} + \frac{c_s^3 - c_s g_o^2 v_\parallel^2}{[v_\parallel (1 + h + A_o) - c_s]^2} \right\}. \qquad (47)$$

But if the electric field E_{oz} is relatively large and the angular dependence of the energy spectrum of the waves has to be estimated by (30), then one has

$$D^e_{xx}(\vec{v}) \approx -\frac{q_e^2 \nu_E \sqrt{m_e} c_s^4 n_e k_B T_e r_{De}^2 (2\pi)^{9/2}}{\varepsilon_o \pi \sqrt{m_i} \nu_N |v_\parallel^3| v_i^2 C_o} \left\{ 1 - 3\frac{c_s^2}{v_\parallel^2} + 2\frac{c_s^4}{v_\parallel^4} \right\} \cdot$$

$$\cdot \int\limits_{a/r_{De}}^{1/r_{De}} dk \ln(kr_D) J_o^2 \left(\frac{k v_\perp \sqrt{v_\parallel^2 - c_s^2}}{|v_\parallel| \omega_{Le}} \right) \approx$$

$$\approx \frac{q_e^2 \nu_E \sqrt{m_e} c_s^4 n_e k_B T_e r_{De}^3 (2\pi)^{9/2}}{12\varepsilon_o \pi \sqrt{m_i} \nu_N |v_\parallel^3| v_i^2 C_o} \left\{ 1 - 3\frac{c_s^2}{v_\parallel^2} + 2\frac{c_s^4}{v_\parallel^4} \right\} \left(1 - \right.$$

$$\left. - \frac{v_\perp^2 (v_\parallel^2 - c_s^2)}{4 v_\parallel^2 r_{De}^2 \omega_{Le}^2} \right)^2 \left[1 + \ln \left(\sqrt{1 + T_e/T_i} \right) - a - a \ln \left(\frac{\sqrt{1 + T_e/T_i}}{a} \right) \right], \qquad (48)$$

which is about $2[1 + h + A_o - c_s/v_{||}]/(3C_o)$ times the tensor D^e_{xx} given in (47). Values of the electron velocity-diffusion tensor calculated according to (42), (47) and (48) are compared in Table 1. The results for $D^e_{xx}(\vec{v})$ found via the spectral function A_e seem to be underestimated and the corresponding approximations have to be improved in future. On the other hand, the values basing on approximation (44) seem to give an overestimate. The rather good coincidence of the results (47) and (48) reflects, that the parameters ν_E and ν_N are of the same order in the considered space plasma regions.

5. DISCUSSION

A model of a Langevin-equation for electrons in almost collision-free weakly magnetoactive plasmas with ion-acoustic turbulence is developed, which can form the starting point for particle simulations to investigate the influence of microturbulence on macroscopic space plasmas parameters.

Estimates of wave characteristics at maximum possible wave growth, electron-wave collision frequencies, electron-velocity diffusion tensors, and the intensities of the wave forces on the electrons in solar flares, the solar wind as well as in different regions of the earth's magnetosphere are made.

Generally two ways are used to find the velocity diffusion tensor of the electrons in the turbulent plasmas. One possibility is based on a first attempt at estimating the space-time spectral-density of the wave energy. This corresponds to a parameter theory and it is not necessary to know the saturation mechanisms of plasma instabilities. But the calculations are extremely complicated and the here obtained results are yet very rough and probably too low. In future a lot of numerical work has to be done to improve these results.

The second way is only applicable, if the plasma turbulence is weak ($|\gamma| \ll |\omega_r|$) and if measurements or theoretical expressions for the wave energies exist. This is fortunately the case for ion-acoustic turbulence. But the up to now existing handable quasi-linear results for the energy spectrum of ion-acoustic waves used in this paper seem to have a too small region of applicability. Besides the amount of the wave energy strongly depends on the wave saturation mechanism. Here for the saturation of ion-acoustic waves a special well-known mechanism basing on ion-ion collisions is assumed. And the corresponding expressions for the wave energy taken from quasi-linear theory seem to give overestimates. Thus the presented results are at most estimates of the order of the effects.

Further, calculating the diffusion tensors using both mentioned ways several additional approximations were introduced. In the case of ion-acoustic turbulence the parameter $z_e \approx \sin^2\theta\omega^2_{pe}/(2\omega^2_{Le})$ is certainly often small as intensive waves propagate mainly quasiparallel to the electron drift and their

propagation angle θ is small. Thus calculating the diffusion tensor one can in first order neglect Bessel functions of higher orders as done in this work. But in some cases, especially in the bow shock and in the polar cusp, also waves with small angle θ can be of importance, because the relation $\omega_{pe}^2 \gg \omega_{Le}^2$ is valid. Besides, in (40) ion-damping contributions were neglected calculating the diffusion tensor. And the rather weak dependence of the diffusion tensor on the strength of the mean magnetic field E_{oz} is estonishing. But, what is most important, ion-acoustic wave dispersion is also approximately considered for plasmas with $T_e \lesssim T_i$, although it is shown that this is unrealistic. The aim was first to find the general orders of the intensities of wave forces in different space plasma regions. Now, for cases with $T_e \lesssim T_i$, the presented non-linear plasma theory is applied to other more relevant types of electrostatic turbulence.

Finally it should be mentioned that with the help of the obtained electron diffusion tensors both, contributions to mean wave forces and to stochastic wave forces on electrons in turbulent plasmas can be calculated. And it is shown in general, that rather strong electron magnetization with $z_e < 1$ decreases the velocity-diffusion of the electrons and the friction force of the waves.

REFERENCES

1. Meister C.-V., Nikutowski B., Schindler K., Arendt U. // Contrib. Plasma Phys., 1991. V. 31 (2). P. 95.
2. Klimontovich Ju. L. Statistical physics. — Moscow: Nauka, 1982, transl. by Springer.
3. Klimontovich Ju. L. Turbulent motion and structure of chaos. A new approach to the statistical theory of open systems. — Moscow: Nauka, 1990; Harwood Academic Publishers, Lordrecht, 1991.
4. Boiko A. Ya., Livshits M. A. Influence of impulsive heating on the gasodynamic characteristics of the atmosphere: Two-temperature approximation // Astronomy Reports, 1995. No. 2.
5. Gurnett D. A., Marsch E., Pilipp W., Schwenn R., Rosenbauer H. // J. Geophys. Res. 1979. V. 84. P. 2029.
6. Gurnett D. A. //In: Collisionless shocks in the Heliosphere /Eds. Tsurutani B. T. and Stone R. G. — Washington: Edition of the American Geophys. Society, 1985. P. 207–224.
7. Collis P. N., Häggström I., Kaila R., Rietveld M. T. // Geophys. Res. Lett., 1991. V. 18. P. 1031.
8. Rietveld M. T., Collis P. N., St.-Maurice J.-P. // Geophys. Res. Lett., 1991. V. 96. P. 19291.
9. Isliker H., Benz A. O. // Astron. Astrophys. Ser., 1994. V. 104. P. 145.
10. Gershman B. N., Erukhimov L. M., Jashin Yu. Ya. Wave phenomena in the ionosphere and in the cosmical plasma. — Moscow: Nauka, 1984.

11. Avanov L., Leibov A., Němeček Z., Šafranková J., Vaisberg O., Yermolaev Yu., and Zastenker G. //In: Intershock project. /Ed. Fisher S., Publications of the Astron. Inst. of the Czechoslovak Academy of Sci., Ondřejov, 1985. V. 60. P. 39–59.
12. Lui A. T. Y. //In: Magnetotail physics. /Ed. Lui A. T. Y. — Baltimore: J. Hopkins Univ. Press, 1987. P. 3–9.
13. Curtis S. A., Hoegy W. R., Brace L. H., and Winningham J. D. // J. Geophys. Res., 1985. V. 90. P. 4415.
14. Davidson R. C., Krall N. A. // Nucl. Fusion, 1977. V. 17. P. 1313.
15. Galeev A. A. and Sagdeev R. Z. //In: Handbook of Plasma Physics, Supplement to Vol. 2. /Eds. Galeev A. A. and Sudan R. — Moscow: Energoatomizdat, 1984. P. 5–37 (transl. into English).
16. Belyi V. V., Klimontovich Ju. L., Nalivaiko V. P. // Fizika Plazmy, 1982. V. 8 (5). P. 1063.

Germany, Potsdam University,
WIP-Project Space Plasma Physics

Поступила в редакцию
15 декабря 1995 г.

THEORETICAL MODELING OF RADIATION–DRIVEN PLASMA TURBULENCE IN AN UNMAGNETIZED PLASMA

L.-H. Li, M. Matsuoka

Radiation–driven plasma turbulence problem is in essence an application problem of electrodynamics. In electrodynamics, electromagnetic fields at any point are determined by all charges and currents in the underlying physical system, fields' history and physical constraints. Starting from this standpoint, we have proved that radiation–driven electromagnetic turbulence in a plasma can be studied in the same way we study the electrostatic turbulence excited by electromagnetic waves in the plasma by means of two-fluid approximation, two-timescale technique and two-spacescale technique. The main difference between electromagnetic turbulence model equations and the Zakharov equations governing electrostatic turbulence is that a driving term appears in the former. The physical origin of this driving term is the current that emits the radiation which supplies the free energy source that gives rise to both electromagnetic and electrostatic turbulences. Simulated electromagnetic emissions, large scale density disturbation and anomalous absorption can be calculated quantitatively based on the electromagnetic turbulence model equations.

I. INTRODUCTION

Microwave–plasma interaction, laser–plasma interaction and ionospheric HF–heating experiments have revealed that radiations can excite plasma turbulence. Radiation–driven plasma turbulence manifests itself not only in the form of electrostatic turbulence, as probed by the incoherent scattering radar (ISR) technique, but also in the form of electromagnetic turbulence, as revealed by the SEE (stimulated electromagnetic emission) technique. Thidé et al. [1] have discovered experimentally that a powerful elctromagnetic wave incident upon the ionospheric plasma may stimulate plasma electromagnetic emissions in ionospheric modification experiments at Tromsø, Norway. The frequency spectra not only contain the expected plasma reflection component at the incident frequency, but also the unexpected rich sideband components [2]. Later on, Leyser et al. [3, 4] found that the character of the SEE spectra changed stronly when the incident frequency approaches an integer multiple of the electron gyrofrequency. Combined anamolous absorption and SEE measurements porformed recently at Tromsø have revealed that the rich SEE sideband features are closely related to anomolous absorption [5, 6]. It seems to us that dependence of the observed SEE properties on geomagnetic field can be attributed to their dependence on cyclotron absorption of electromagnetic waves: the closer the pump frequency to the harmonics of the

gyrofrequency, the stronger the cyclotron damping, the lower the excited level of electromagnetic waves, and thus the lower the excited level of upper hybrid waves. As a result, the more outstanding the gyrofeatures [6]. Otherwise, the more prominent the universal features. Therefore, electromagnetic turbulence effects must be important in these experiments.

Plasma turbulence is usually described by plasma waves, which are in essence electromagnetic fields generated by collective motion of charged particles in the plasma. In radiation–driven plasma turbulence, electromagnetic force exserted by the radiation field is the cause of collective motion of plasma particles. Therefore, if the induced electromagnetic waves in a plasma are considered to be emitted by electron motions forced by the incident electromagnetic wave rather than conserdered to be propagating from the outer of the plasma with the plasma taken as a medium, electromagnetic turbulence of plasmas can be studied in the same way Langmuir turbulence is studied [7, 8, 9], as has been shown in our previous work [10]. Our numerical simulations demonstrated that excited electromagnetic waves and density profile modifications depend on plasma state parameters, heating parameters and the excited plasma waves. Such a dependence may qualitatively explain the following ionosphere modification experiment facts: overshoot, dependence of plasma line enhancement on pulse length, preconditioning, large scale density profile modification, altitude characteristics of plasma turbulence excited by superheater at Tromsø, Norway, difference of thermal effects between Arecibo and Tromsø experiments, below–threshold excitation, direct conversion, solitary free mode spectral peak, intermittency of plasma turbulence and stimulated electromagnetic emissions. Therefore, studies on electromagnetic turbulence is very important in order to understand the variety of observational facts in both laboratory and ionospheric modification experiments.

Although plasams are rare on the earth, most part of (99%) matter in the Universe exists in the plasma state. They encompass distinguishable scales ranging from the atomic to the galactic and their density and temperature can vary substantially within ten orders of magnitude or more. It is well known that radiation is one of the basic release forms of nuclear reaction energy and gravitational potential energy under astrophysical circumstances, radiation–driven plasma turbulence is common from the astrophysical point of view and thus must have something to do with some basic astrophysical processes, for example, origin of cosmic magnetic fields, solar neutrino problem. If the magentic pressure caused by radiation–generated magnetic field and/or electromagnetic turbulence pressure in the core of the sun is sufficiently high, the core temperature of the sun need not be so high and thus the predicted rate of solar neutrino capture by ^{37}Cl by the standard solar model [11] will decrease. Recent numerical simulations by Wilks et al. [12] of the interaction of an ultraintense laser pulse with an overdense plasma target have revealed extremely high self–generated magnetic fields about 250 MG in the overdense

plasma, which may be high enough to solve solar neutrino problem if there exists such intense a self–generated magnetic field in the solar core where nuclear reactions take place.

All these show that it is worth–while to study radiation–driven electromagnetic turbulence of plasmas. In our previous work [10], we have outlined how to model such a plasma turbulence. Because of its importance and deviation from the conventional approach to this problem, it is necessary to work out the details. In this paper, we are about to prove our model equations governing electromagnetic turbulence starting from the basic dynamical plasma equations.

II. BASIC DYNAMICAL PLASMA EQUATIONS

The Boltzmann equations for charged particles and the Maxwell equations for electromagnetic fields are the basic dynamical plasma equations. Before writting them down we have to know the distribution of electric charges and currents in the underlying physical system. For the ionospheric modification experiments, charges and currents distribute on the transmission antenna (there is no net charge thereon, $\mathbf{J}_A$) and in the ionosphere:

$$\rho_I = \sum_\alpha q_\alpha \int f_\alpha d\mathbf{V}, \tag{1}$$

$$\mathbf{J}_I = \sum_\alpha q_\alpha \int \mathbf{V} f_\alpha d\mathbf{V}, \tag{2}$$

where α sdands for species of charged particles in the ionosphere. When all charges and currents in the physical system are included in, the fields appeared in the basic dynamical equations are the total ones. Therefore, these equations can be written explicitly as follows:

$$\frac{\partial f_\alpha}{\partial t} + (\mathbf{V}\cdot\nabla) f_\alpha + \frac{q_\alpha}{m_\alpha}[\mathbf{E}_{tot} + V_\alpha \times \mathbf{B}_{tot}]\frac{\partial f_\alpha}{\partial \mathbf{V}} = \left(\frac{\partial f_\alpha}{\partial t}\right)_c, \tag{3}$$

$$\nabla\cdot\mathbf{E}_{tot} = \frac{\rho_I}{\varepsilon_0}, \tag{4}$$

$$\nabla\times\mathbf{E}_{tot} = -\frac{\partial \mathbf{B}_{tot}}{\partial t}, \tag{5}$$

$$\nabla\times\mathbf{B}_{tot} = \frac{1}{c^2}\frac{\partial \mathbf{E}_{tot}}{\partial t} + \mu_0(\mathbf{J}_A + \mathbf{J}_I), \tag{6}$$

$$\nabla\cdot\mathbf{B}_{tot} = 0. \tag{7}$$

Here $(\partial f_\alpha/\partial t)_c$ is the contribution of particle collision to the change rate of particle distribution functions.

Since the antenna is far away from the ionosphere, we can neglect influences of the ionosphere on the antenna. As a result, we can write down the Maxwell equations that determine the field caused by only the source current density on the antenna as follows:

$$\nabla \cdot \mathbf{E}_A = 0\,, \tag{8}$$

$$\nabla \times \mathbf{E}_A = -\frac{\partial \mathbf{B}_A}{\partial t}\,, \tag{9}$$

$$\nabla \times \mathbf{B}_A = \frac{1}{c^2}\frac{\partial \mathbf{E}_A}{\partial t} + \mu_0 \mathbf{J}_A\,, \tag{10}$$

$$\nabla \cdot \mathbf{B}_A = 0\,. \tag{11}$$

Subtracting (8), (9), (10) and (11) from (4), (5), (6) and (7), respectively, we obtain

$$\nabla \cdot \mathbf{E}_I = \frac{\rho_I}{\varepsilon_0}\,, \tag{12}$$

$$\nabla \times \mathbf{E}_I = -\frac{\partial \mathbf{B}_I}{\partial t}\,, \tag{13}$$

$$\nabla \times \mathbf{B}_I = \frac{1}{c^2}\frac{\partial \mathbf{E}_I}{\partial t} + \mu_0 \mathbf{J}_I\,, \tag{14}$$

$$\nabla \cdot \mathbf{B}_A = 0\,, \tag{15}$$

which are the Maxwell equations that determine the self-consistent fields $\mathbf{E}_I$ and $\mathbf{B}_I$ in the inosphere, where $\mathbf{E}_I = \mathbf{E}_{tot} - \mathbf{E}_A$ and the same for $\mathbf{B}_I$.

The designer of the transmitter antenna is able to determine the vacuum electromagnetic fields emitted by the their antenna from Eqs. (8), (9), (10), (11) and special boundary conditions designed by them. Therefore, $\mathbf{E}_A$ is assumed to be given in radiation-driven plasma turbulence experiments. As a result, Eqs. (12), (13), (14), (15), and (3) become the basic dynamical equations governing ionospheric modification by the transmitter.

From differential equation theory we know that it is true that the solution will be determined by the differential equations, initial conditions and boundary conditions as well, but they are independent. Physically, differential equations embody natural laws, which should not be affected by concrete boundary conditions and initial conditions. What are affected by the latter are the concrete results. Therefore, it will not lead to more complicated boundary conditions to separate the vacuum field generated by the antenna. In addition, although these equations are derived from the original equations especially for the case of ionospheric modification experiments, they should be valid for any radiation-driven plasma turbulence.

III. SIMPLIFIED DYNAMICAL PLASMA EQUATIONS

In order to simplify the dynamical plasma equations and obtain the dynamical equations that describe strongly nonlinear wave–wave interactions (WWI's) and wave–particle interactions (WPI's) in the simplest way, we take plasma waves as quasi–particles so that we can explicitly express the effects of waves on particle distribution functions in the Boltzmann equations. The collision interations between particles are able to change particle distribution functions, so are WPI's, which can be represented in terms of the growth rate γ_α and damping rate ν_α of waves. The former cause decrease of momentum of α species particle, while the latter cause increase of its momentum. Therefore, Eq. (3) can be rewritten as follows:

$$\frac{\partial f_\alpha}{\partial t} + (\mathbf{V}\cdot\nabla)f_\alpha + \frac{q_\alpha}{m_\alpha}[\mathbf{E}_{tot} + V_\alpha \times \mathbf{B}_{tot}]\frac{\partial f_\alpha}{\partial \mathbf{V}} = \gamma_\alpha^k - \nu_\alpha^k - \nu_c^k . \qquad (16)$$

The main advantage to rewrite Eqs. (3) as (16) is that we can take assembly average over Eq.(16) to simplify it substantially and take some important WPI's into account at the same time.

A. Two–fluid approximation

The dynamical plasma equations are microscopic equations. Macroscopic equations can be derived from Eq. (16) by multiplying it by some functions of particle velocities and by averaging the result over all possible velocities. Such equations are called as (velocity) moment equations. They are an infinite hierachy. Nevertheless, only the first three moment equations that correspond to physical conservation quantity equations are meaningful [13].

The lowest order conservation quantity equations are the particle conservation equations

$$\frac{\partial n_\alpha}{\partial t} + \nabla\cdot(n_\alpha \vec{V}_\alpha) = 0, \qquad (17)$$

the second ones are the momentum transport equations

$$\frac{d\mathbf{V}_\alpha}{dt} = \frac{q_\alpha}{m_\alpha}[\mathbf{E}_{tot} + \mathbf{V}_\alpha \times \mathbf{B}_{tot}] - \frac{\lambda_\alpha}{m_\alpha n_\alpha}\nabla(n_\alpha T_\alpha) - (\gamma_\alpha - \nu_\alpha - \nu_c)\cdot\mathbf{V}_\alpha, \qquad (18)$$

where we have defined the convolution product $\gamma_\alpha \cdot \mathbf{V}_\alpha = \int \gamma_\alpha(t,\vec{r}')\mathbf{V}_\alpha(t,\vec{r}-\vec{r}')d\vec{r}' \equiv \int \gamma_\alpha^k(t,\vec{r},\mathbf{V})\mathbf{V}d\mathbf{V}$, λ_α is the ratio of specific heat at constant pressure over that at constant volume, which can be determined phenomenologically. The third moment equations are the energy transport equations, which can be represented by the following thermal energy balance equations [13]:

$$\frac{3}{2}n_p\frac{dT_e}{dt} = Q_e - \nabla\cdot(\kappa_e\nabla T_e) - n_p\nu_{ei}(T_e - T_i) - n_p\nu_{en}T_e, \qquad (19)$$

$$\frac{3}{2}n_p\frac{dT_i}{dt} = Q_i - \nabla\cdot(\kappa_i\nabla T_i) - n_p\nu_{ie}(T_i - T_e) - n_p\nu_{in}T_i, \tag{20}$$

where $\nu_{ei} = \nu_{ee}$, $\nu_{ie} = 2(m/M)\nu_{ee}$, $\kappa_e = \frac{5}{2}n_pT_e/(m\nu_e)$ and $\kappa_i = \frac{5}{2}n_pT_i/(M\nu_i)$ are the electron–ion collision frequency, ion–electron collision frequency, thermal conductivity coefficients of electron fluid and ion fluid, respectively, with $\nu_e \equiv \nu_{ee} + \nu_{ei} \approx 2\nu_{ee}$ and $\nu_i \equiv \nu_{ii} + \nu_{ie} \approx \nu_{ii} = \frac{1}{\sqrt{2}}(m/M)^{1/2}(T_e/T_i)^{3/2}\nu_{ee}$,

$$\nu_{ee} = (4\pi\varepsilon_0)^2\frac{4\sqrt{2\pi}n_e e^4}{3m_e^{1/2}T_e^{3/2}}\ln\Lambda, \tag{21}$$

in which we have assumed that the charge number of an ion is unity, $\Lambda = 4\pi(\varepsilon_0T_e)^{3/2}/(n_e^{1/2}e^3)$ is the plasma parameter. Q_e and Q_i represent wave energy absorbed by electrons and ions.

Eqs. (12), (13), (14), (15), (17), (18), (19) and (20) are the two–fluid approximation to the basic dynamical plasma equations. The boundary condition now reduces to the outgoing–wave condition, a natural boundary condition. Consequently, it is not necessary for us to pay much attention to the boundary condition, which makes it much easier to deal with nonlinear problems. Besides, these equations can be substantially simplified through distinguishing the ion time scale and the electron time scale provided by the plasma itself.

B. Two–timescale technique

We assume $m_i >> m_e$, so the time scale of motion of ions $\tau_i \sim \omega_{pi}^{-1}$ is much larger than that of electrons $\tau_e \sim \omega_{pe}^{-1}$. Consequently, when the plasma turbulence is well–developed, the ion fluid has only slow–time–scale motion,

$$n_i = n_{i,s}\,, \quad \mathbf{V}_i = \mathbf{V}_{i,s}\,, \tag{22}$$

however, the electron fluid has both slow– and fast–time–scale motions,

$$n_e = n_{e,s} + n_f\,, \quad \mathbf{V}_e = \mathbf{V}_{e,s} + \mathbf{V}_f\,. \tag{23}$$

In general, both induced electric and induced magnetic fields have two time-scale components,

$$\mathbf{E}_I = \mathbf{E}_s + \mathbf{E}_f\,, \quad \mathbf{B}_I = \mathbf{B}_s + \mathbf{B}_f\,. \tag{24}$$

Because $\tau_i >> \tau_e$, the time–average of the fast–time–scale components over the slow time period τ_i must vanish,

$$\langle A_f\rangle = 0\,, \tag{25}$$

where $A = \{n, \mathbf{V}, \mathbf{E}, \mathbf{B}\}$, angle brackets indicate time averaging. In addition, the quasineutrality condition for the slow–time–scale motions must hold, which yields

$$n_{i,s} \approx n_{e,s} \equiv n_s \,. \tag{26}$$

Therefore, the slow–timescale charge density vanishes, i.e.,

$$\rho_s \sim 0 \,. \tag{27}$$

Substituting (22), (23) and (26) into (17), then taking time–average over the slow period τ_i, we obtain

$$\frac{\partial n_s}{\partial t} + \nabla \cdot (n_s V_{e,s} + \langle n_f \mathbf{V}_f \rangle) = 0 \,, \tag{28}$$

$$\frac{\partial n_s}{\partial t} + \nabla \cdot (n_s \mathbf{V}_{i,s}) = 0 \,, \tag{29}$$

which yield

$$\mathbf{V}_{i,s} = \mathbf{V}_{e,s} + \frac{\langle n_f \mathbf{V}_f \rangle}{n_s} \,. \tag{30}$$

Thus we can calculate the slow–timescale current $\vec{J}_s$,

$$\begin{aligned} \vec{J}_s &= \sum_\alpha \langle q_\alpha n_\alpha \mathbf{V}_\alpha \rangle = \\ &= q_i n_s \mathbf{V}_{i,s} + q_e n_s \mathbf{V}_{e,s} + q_e \langle n_f \mathbf{V}_f \rangle = \\ &= e[n_s(\mathbf{V}_{i,s} - \mathbf{V}_{e,s}) - \langle n_f \mathbf{V}_f \rangle] = \\ &= 0 \,. \end{aligned} \tag{31}$$

Here e is the absolute value of an electron charge. With (27) and (31) taken into account, it can be seen that the slow–timescale Maxwell equations are homogeneous and thus we can set $\mathbf{E}_s = 0$ and $\mathbf{B}_s = 0$. Therefore, it is no need to consider spontaneous excitation of the slow–time–scale magnetic fields. It should be pointed out that we have assumed $\mathbf{V}_{i,s} = \mathbf{V}_{e,s}$ in [14], which is not consistent with the quasineutrality assumption. Therefore, we have to forgo the quasineutrality assumption (26) for the slow–time–scale motions in order to study spontaneous excitation of quasisteady magnetic fields by a pump wave. We shall pursue this topic separately. As a result, the slowly varying components can be simplified substantially. To demonstrate this, we define

$$\mathbf{V}_s = \frac{m_i \mathbf{V}_{i,s} + m_e \mathbf{V}_{e,s}}{m_i + m_e} \,. \tag{32}$$

Eqs. (28) and (29) thus reduce to

$$\frac{\partial n_s}{\partial t} + \nabla \cdot (n_s \mathbf{V}_s) = -\frac{m_e}{m_i + m_e} \nabla \cdot \langle n_f \mathbf{V}_f \rangle \,. \tag{33}$$

Similarly, we get the slow–timescale equation for $\mathbf{V}_s$:

$$\frac{d\mathbf{V}_s}{dt} = -C_s^2\frac{\nabla n_s}{n_s} - \frac{m_e}{m_i+m_e}\left\{\langle(\mathbf{V}_f\cdot\nabla)\mathbf{V}_f\rangle + \right.$$
$$\left. + \frac{e}{m_e}\langle\mathbf{V}_f\times\mathbf{B}_{Af}\rangle\right\} + \nu_i\cdot\mathbf{V}_s\,, \tag{34}$$

where $C_s^2 = (\lambda_e T_e + \lambda_i T_i)/(m_e+m_i)$. By substracting corresponding time–average equations from the original equations, we obtain the fast–timescale equations:

$$\frac{\partial n_f}{\partial t} + \nabla\cdot(n_s\mathbf{V}_f + n_f\mathbf{V}_s + n_f\mathbf{V}_f - \langle n_f\mathbf{V}_f\rangle) = 0\,, \tag{35}$$

$$\frac{\partial\mathbf{V}_f}{\partial t} = (\gamma_e-\nu_e-\nu_c)\cdot\mathbf{V}_f - \frac{\varepsilon_0\lambda_e T_e}{em_e n_s}\nabla\nabla\cdot\mathbf{E}_f\frac{e}{m_e}[\mathbf{E}_{Af} +$$
$$+\mathbf{V}_s\times\mathbf{B}_{Af} + \mathbf{V}_f\times\mathbf{B}_{Af} - \langle\mathbf{V}_f\times\mathbf{B}_{Af}\rangle] -$$
$$-(\mathbf{V}_s\cdot\nabla)\mathbf{V}_f - (\mathbf{V}_f\cdot\nabla)\mathbf{V}_s - (\mathbf{V}_f\cdot\nabla)\mathbf{V}_f +$$
$$+\langle(\mathbf{V}_f\cdot\nabla)\mathbf{V}_f\rangle\,, \tag{36}$$

$$\frac{\partial^2\mathbf{E}_f}{\partial t^2} + c^2\nabla\times\nabla\times\mathbf{E}_f = \frac{e}{\varepsilon_0}\frac{\partial}{\partial t}(n_s\mathbf{V}_f + n_f\mathbf{V}_{e,s} + n_f\mathbf{V}_f - \langle n_f\mathbf{V}_f\rangle)\,, \tag{37}$$

where $\mathbf{E}_{Af} = \mathbf{E}_A + \mathbf{E}_f$, and the same for $\mathbf{B}_{Af}$, ν_i and ν_e are the damping rates of LF and HF waves respectively, γ_e is the growth rate of the HF waves.

Too many nonlinear terms in our two–timescale equations make them very complicated. However, not all the nonlinear terms contribute equally. When the condition $W_f k/k_D << 1$, $W_s k/k_D << \mu \equiv m_e/m_i$ is satisfied, where $W_f \equiv E_f^2/4\pi n_0 T_e$, $W_s \equiv E_s^2/4\pi n_0 T_e$, k is characteristic wavenumber of waves that have been excited and k_D is the Debye wavenumber, through making comparisons among nonlinear terms and neglecting the much smaller nonlinear terms, as has been done in our previous work [14], we get

$$\frac{\partial n_s}{\partial t} + \nabla\cdot(n_s\mathbf{V}_s) = 0\,, \tag{38}$$

$$\frac{\partial\mathbf{V}_s}{\partial t} = -C_s^2\frac{\nabla n_s}{n_s} - \frac{\mu}{2}\nabla\langle|\mathbf{V}_f|^2\rangle + \nu_i\cdot\mathbf{V}_s\,, \tag{39}$$

$$\frac{\partial n_f}{\partial t} + \nabla\cdot(n_s\mathbf{V}_f) = 0\,, \tag{40}$$

$$\frac{\partial\mathbf{V}_f}{\partial t} = -\frac{e}{m_e}\mathbf{E}_{Af} - \frac{\varepsilon_0\lambda_e}{em_e n_0}\nabla(T_e\nabla\cdot\mathbf{E}_f) + (\gamma_e-\nu_e-\nu_c)\cdot\mathbf{V}_f\,, \tag{41}$$

$$\frac{\partial^2\mathbf{E}_f}{\partial t^2} + c^2\nabla\times\nabla\times\mathbf{E}_f = \frac{en_s}{\varepsilon_0}\frac{\partial\mathbf{V}_f}{\partial t}\,. \tag{42}$$

These equations are still difficult to deal with analytically and numerically since both fast–timescale quantities $A_f = \{n_f, \mathbf{V}_f, \mathbf{E}_f\}$ and slow–timescale quantities $\{n_s, \mathbf{V}_s\}$ show up in these equations at the same time. We [14] have shown that the mixed time–scale problem can be resolved by coarse–graining all fast timescale quantatities if we are able to find out a fast characteristic frequency ω_m so that all fast varying components can be expressed like this:

$$A_f = \frac{1}{2}[A(\vec{r}, t)\exp(-i\omega_m t) + c.c.], \tag{43}$$

where A is the slowly varying envelope ($\partial A/\partial t << \omega_m A$) of A_f. This condition was named as the quasimonochoromatic wave approximaton. From Eqs.(41) and (42), we obtain dispersion relations for HF Langmuir and electromagnetic waves by linearization and ignoring the source term $\mathbf{E}_A$ therein:

$$\omega_l^2 = \omega_{pe}^2 + \lambda_e V_{Te}^2 k^2, \tag{44}$$

$$\omega_t^2 = \omega_{pe}^2 + c^2 k^2, \tag{45}$$

where ω_{pe} stands for the local plasma frequency, $V_{Te} = (T_e/m_e)^{1/2}$. If the radiation frequency of the source is ω_0, frequency of the Langmuir and electromagnetic waves excited by the radiation will not substantially deviate from the driven frequency. In this case, if we set $\omega_m = \omega_0$, the quasimonochoromatic approximation will be met with.

Substituting (43) with $\omega_m = \omega_0$ into (42), we obtain

$$\mathbf{V} = a\mathbf{E}_m, \tag{46}$$

where $a = -ie/m_e\omega_{pe}$, $\mathbf{E}_m = \mathbf{E} + \mathbf{E}_0\exp(i\mathbf{k}_0 \cdot \mathbf{x})$ is the complex envelope of $\mathbf{E}_{Af}$ in which $\mathbf{k}_0 = \omega_0/c$ is the wavelength of the radiation field in vacuum. It should be noted that the plasma is considered to be free charges distributed in vacuum rather than a medium in the dynamical plasma equations. Taking use of this relation, we can express the time–averaging term in terms of the coarse–graining quantitaties as follows:

$$\langle|\mathbf{V}_f|^2\rangle = \frac{1}{2}|\mathbf{V}|^2 = \frac{1}{2}|a|^2|\mathbf{E}_m|^2. \tag{47}$$

From (42) and (41) with (43) substituted in, we get the envelope equation of the HF field as follows:

$$\frac{2i}{\omega_0}\frac{\partial \mathbf{E}}{\partial t} + \frac{3V_{Te}^2}{\omega_0^2}\nabla\nabla\cdot\mathbf{E} - \frac{c^2}{\omega_0^2}\nabla\times\nabla\times\mathbf{E} + \left[1 - \frac{\omega_{pe}^2}{\omega_0^2} - i\frac{1}{\omega_0}(\gamma_e - \nu_e - \nu_c)\right]\cdot\mathbf{E} = \frac{\omega_{pe}^2}{\omega_0^2}\mathbf{E}_0\exp(i\mathbf{k}_0\cdot\mathbf{x}) - \frac{3V_{Te}^2}{c^2}\frac{\nabla T_e}{T_e}\nabla\cdot\mathbf{E}, \tag{48}$$

where $\omega_{pe} \doteq n_p e^2/\varepsilon_0 m_e$, $n_p = n_0(z) + n^t(z,t) + n^l(z,t)$ and we have assumed $|n^t + n^l| << n_0$ and inhomogeneity is in the z-axis. From (38), (39) and (47) we obtain the slow–timescale equation:

$$\left(\frac{\partial^2}{\partial t^2} + \nu_i \cdot \frac{\partial}{\partial t} - C_s^2 \nabla^2\right)(n^t + n^l) = n_0 \varepsilon_0 \nabla^2 \frac{|\mathbf{E}|^2}{4 m_i n_p} . \tag{49}$$

These two equations are the model equations [Eqs. (1) and (2)] used in our previous work [10] with uniform temperature approximation assumed. They and with Eqs. (19) and (20) together can be used to study nonuniform temperature effects.

C. Two–spacescale technique

There is not only the two–timescale problem solved above but also two–spacescale problem in radiation–driven plasma turbulence. The latter can be seen from (44) and (45): if $\omega_t \sim \omega_l \approx \omega_0$, $k_t/k_l \sim V_{Te}/c$, i.e., the typical wavelength of electromagnetic waves is much larger than that of the Langmuir waves. This problem can be solved by using a two–spacescale technique that is similar to the widely used two–timescale technique described above. The key point is that $\mathbf{E}$ in the envelope field equation can be decomposed into the electromagnetic waves $\mathbf{E}^t$ and Langmuir waves $\mathbf{E}^l$:

$$\mathbf{E} = \mathbf{E}^t + \mathbf{E}^l , \quad \langle \mathbf{E}^t \rangle \approx \mathbf{E}^t , \quad \langle \mathbf{E}^l \rangle = 0 , \tag{50}$$

where bracket represents space averaging. This decomposition implies that the space scale over which the average is made should be much larger than the characteristic wavelength of Langmuir waves so that $\langle \mathbf{E}^l \rangle = 0$ and should be much smaller than the characteristic wavelength of the electromagnetic waves so that $\langle \mathbf{E}^t \rangle = \mathbf{E}^t$ at the same time. Taking space–averaging over Eq. (48), we have the large spacescale envelope field equations:

$$\frac{2i}{\omega_0}\frac{\partial \mathbf{E}^t}{\partial t} - \frac{c^2}{\omega_0^2}\nabla \times \nabla \times \mathbf{E}^t + \left(i\frac{\nu_e}{\omega_0} - \frac{Z}{L} - \frac{n^t}{n_c}\right)\mathbf{E}^t = \\ = \mathbf{E}_0 + \frac{1}{L}\langle z\mathbf{E}^l \rangle + \frac{1}{n_c}\langle n^l \mathbf{E}^l \rangle , \tag{51}$$

$$\left(\frac{\partial^2}{\partial t^2} + \nu_i \cdot \frac{\partial}{\partial t} - C_s^2 \nabla^2\right) n^t = \frac{n_0 \varepsilon_0}{4 m_i n_p} \nabla^2 |\mathbf{E}^t|^2 , \tag{52}$$

where we have assumed $n_0(z) = n_c(1 + z/L)$, here L is the scalelength of the inhomogeneous plasma at the critical density n_c. We have also ignored the term caused by the temperature gradient. The space average $\langle(\omega^2 - \omega_p^2)(\mathbf{E}^t + \mathbf{E}^l)\rangle = Z\mathbf{E}^t/L + n^t\mathbf{E}^t/n_c + \langle z\mathbf{E}^l\rangle/L + \langle n^l\mathbf{E}^l\rangle/n_c$ with n^t and

$\mathbf{E}^t$ understood as functions of the macroscopic coordinates such as Z. In contrast, z represents the microscopic coordinate. This idea originates from DuBois et al. [15]. These authors also have pointed out that $\langle n^l \mathbf{E}^l \rangle$ embodies anomalous absorption, which will be determined by short spacescale envelope field equations:

$$\frac{2i}{\omega_0}\frac{\partial \mathbf{E}^l}{\partial t} + \frac{3V_{Te}^2}{\omega_0^2}\nabla\nabla\cdot\mathbf{E}^l + \left(i\frac{\nu_e}{\omega_0} - \frac{z}{L} - \frac{n^t}{n_c} - \frac{n^l}{n_c}\right)\mathbf{E}^l = \\ = \left(\frac{z-Z}{L} + \frac{n^l}{n_c}\right)\mathbf{E}^t - \frac{1}{L}\langle z\mathbf{E}^l\rangle - \frac{1}{n_c}\langle n^l\mathbf{E}^l\rangle, \tag{53}$$

$$\left(\frac{\partial^2}{\partial t^2} + \nu_i\cdot\frac{\partial}{\partial t} - C_s^2\nabla^2\right)n^l = \frac{n_0\varepsilon_0}{4m_i n_p}\nabla^2|\mathbf{E}^l + \mathbf{E}^t|^2, \tag{54}$$

which can be obtained by subtracting the space–averaged envelope field equation from the original one.

IV. CONCLUSION AND DISCUSSION

Radiation–driven plasma turbulence is in essence an application problem of electrodynamics. In electrodynamics, electromagnetic fields at any point are determined by all charges and currents, fields' history and physical constraints imposed on the underlying physical system. Starting from this standpoint, we have proved that radiation–driven electromagnetic turbulence in a plasma can be studied in the same way we study the electrostatic turbulence excited by electromagnetic waves in the plasma. The most important difference between electromagnetic turbulence model equations and the Zakharov equations governing electrostatic turbulence is that a driving term appears in the former. The physical origin of this driving term is the current that emits the radiation which supplies the free energy source that gives rise to both electromagnetic and electrostatic turbulences.

It has been shown that the source term is consistent with the basic dynamical plasma equations, the basic equations governing radiation–driven plasma turbulence experiment system. It has also been found out that the physical origin of that source term as stated above. It has been shown that the widely used driving Zakharov equations can be obtained by means of spacescale–separating technique from our source–term–contained spacescale–fixed envelope field equations. Of cause, electromagnetic turbulence model equations have also been obtained. Primary numerical simulations based on the electromagnetic turbulence model equations have shown that many ionospheric modification experiments may be explained by such a turbulence mechanism. Numerical simulations have also shown that the linear results are in agreement

with propagating theory of electromagnetic waves in nonuniform plasmas, except for an indefinity of amplitude, which is allowed in any linear theory. Therefore, it seems to us that we don't have reason to rule out that source term. Morales et al. [16] have found out this source term, too.

Boundary conditions should be mentioned here. Unlike laboratory plasmas such as those contained in Tokamaks, boundarys are free for space plasmas because there is no physical constraint as met in laboratory. Therefore, periodic boundary conditions are plausible if we carefully select the numerical boundarys, for example, using sufficiently large system size and placing the numerical upper boundary far above the critical layer and the numerical lower boundary far below the critical layer, because in this case, the boundary fields approximately vanish and meet with each other.

From differential equation theory we know that it is true that the solution will be determined by the differential equations, initial conditions and boundary conditions as well, but they are independent. Physically, differential equations embody natural laws, which should not be affected by concrete boundary conditions and initial conditions. What are affected by the latter are the concrete results. Therefore, our model equations will not be ruined by any boundary problem.

ACKNOWLEDGMENTS

One of the authors (L.H. Li) greatly acknowledges Prof. V.L. Ginzburg for his confirming me that Eqs. (3), (12), (13), (14) and (15) are correct, Prof. E. Mjølhus for his showing me how to separate different spacescale fields and Prof. B. Thidé for his advice at ISS'95. Li also wants to thank M. Matsuoka for providing partial economical support and for the kind hospitality met during my year–long stay at RIKEN, where this work was completed.

REFERENCES

1. Thidé B., Kopka H., and Stubbe P. // Phys. Rev. Lett., 1982. V. 49. P. 1561.
2. Stubbe P., Kopka H., Thidé B., and Derblom H. // J. Geophys. Res., 1984. V. 89. P. 7523.
3. Leyser T.B., Thidé B., Derblom H., Hedberg Å., and Lundborg B. // J. Geophys. Res., 1990. V. 95. P. 17233.
4. Leyser T.B., Thidé B., Goodman S., Waldenvik M., Frolov V.L., Grach S.M., Karashtin A.N., Komrakov G.P., and Kotik D.S. // J. Geophys. Res., 1993. V. 98. P. 17597.
5. Stocker A.J., Honary F., Robinson T.R., Jones T.B., and Stubbe P. // J. Geophys. Res., 1993. V. 98. P. 13627.

6. Stubbe P., Stocker A.J., Honary F., Robinson T.R., and Jones T.B. // J. Geophys. Res., 1994. V.99. P.6233.
7. Zakharov V.E. //Sov. Phys. JETP, 1972. V.35. P.908. [Zh. Eksp. Teor. Fiz., 1972. V.62. P.1745].
8. DuBois D.F., Rose H.A., and Russel D. // J. Geophys. Res., 1990. V.95. P.21221.
9. Hanssen A., Mjølhus E., DuBois D.F., and Rose H.A. // J. Geophys. Res., 1992. V.92. P.12073.
10. Li L.H., Matsuoka M., and Zhang H.Q, Excitation of plasma waves by an externally applied electromagnetic wave to a nonuniform classical plasma. // Radiophysics and Quantum Electrons, in press.
11. Bahcall J.N., Pinsonneault M.H. // Rev. Mod. Phys., 1992. V.64. P.885.
12. Wilks S.C., Kruer W.L., Tabak M., and Langdon A.B. Phys. Rev. Lett., 1992. V.69. P.1383.
13. Ma T.C., Hu X.W., and Chen Y.H. Principles of Plasma Physics. — Hefei: UCTC press, 1986.
14. Li L.H. // Phys. Fluids, 1993. V.B 5. P.350.
15. DuBois D.F., Hanssen A., Rose H.A., and Russell D. J. Geophys. Res., 1993. V.98. P.17543.
16. Morales G.J. and Lee Y.C. // Phys. Fliuds, 1977. V.20. P.1135.

The Institute of Physical and Chemical Research, Hirosawa, Japan

Поступила в редакцию
8 декабря 1995 г.

DISPERSION PROCESS OF ELECTROMAGNETIC WAVES IN A MOVING MEDIUM

E. D. Lopez

The propagation of electromagnetic waves in a moving isotropic plasma and in a moving magnetoactive plasma is considered using the invariant methods of tensor analysis. The expressions for the dielectric tensor of permittivity, the dispersion equations and the refractive indexes of the electromagnetic waves in these mediums are determinated. Using these results it is possible to establish corrections to the angular displacement which occurs when the radiation is passing trought moving electron plasma.

1. INTRODUCTION

The appearance and propagation of different kinds of electromagnetic waves in plasma depends basically on material configuration of the system and electric and magnetic fields distribution; this information about the physical state of the system is described by a dielectric tensor of permittivity. The dielectric tensor of permittivity plays an important role in the theory of the waves propagation. For instance, the variation of anisotropy of a media can be described by changes in the components of the permittivity tensor. These changes in general are small but important because they cause qualitative modifications of optical properties of the plasma and consequently of the propagation of the electromagnetic waves.

The pass of radiation through material substances located along the path of the electromagnetic waves was studied by some authors. For example, the angular displacement of radiation coming from a far radio sources and intersecting a magnitoactive plasma, was estimated by Bastian [1] (the case of a gradient of the electron density in the plasma) and by Gnedin and Lopez [2] (the case of a simultaneouse gradient of the electron density and of the external magnetic field).

When the radiation traverses a globally moveing plasma some additional physical effects appear due to the influence of the plasma velocity. For example, an isotropic system becomes anisotropic. In this case, the refraction and the wave propagation depends on the direction of the ray path. The anisotropy of a moving plasma is reflected in the dielectric tensor of the permittivity $\varepsilon_{ij}(w, \vec{k})$. When an external magnetic field is present in the plasma (magnetoactive plasma), plasma is initially anisotropic due to the presence of the field. The global movement of the plasma increases the grade of anisotropy and the complexity of the system.

In this work general expressions for the dielectric tensor of the permittivity $\varepsilon_{ij}(w,\vec{k})$, the dispersion equations and the relations for the refractive indexes of the electromagnetic waves passing through both an isotropic plasma and an anisotropic plasma (in the presence of an external magnetic field) are deduced taking into account the global movement of the plasma. These results are obtained using the method of the invariant tensor representation. The diad–representation gives a simple method to find solutions of dispersion equations. Elude the use of a definite coordinate system, the involved mathematics becomes very simple and gains evident physical meaning, and thus the difficulties of coordinate methods disappear.

2. THE DIELECTRIC TENSOR IN A MOVING MEDIUM

In this section the results obtained for the dielectric permittivity tensor are presented for two cases: moving plasma without external magnetic field and moving plasma immersed in an external magnetic field.

The components of the dielectric tensor can be obtained using the Maxwell's equations and the electron kinetic theory with a distribution function in which the system displacement is taken into account. An additional method explained in [3] consits in carrying out the direct transformation of the dielectric permittivity tensor from the rest coordinate system to the moving system using the traditional relations for the coordinate system transformations and the continuity equation. The relation between tensors in different coordinate systems is given by:

$$\begin{aligned}\varepsilon_{ij} &= \delta_{ij}\Big(1-\frac{w'^2}{w^2}\Big)+\frac{w'^2}{w^2}\varepsilon'_{ij}+\frac{w'^2}{w^2}\frac{v_i k_\mu \varepsilon'_{\mu j}}{w'}-\frac{w'^2}{w^2}\frac{v_i k_j}{w'}+\\ &+\frac{w'}{w}\frac{k_\nu v_j \varepsilon'_{i\nu}}{w}-\frac{w'}{w}\frac{k_i v_j}{w}+\frac{w'}{w}\frac{v_i v_j}{w'w}(k_\mu \varepsilon'_{\mu\nu}k_\nu-k^2),\end{aligned}\qquad(1)$$

where $\varepsilon_{ij}(w,\vec{k})$ is the permittivity tensor in the laboratory system (xyz), $\varepsilon'_{ij}(w',\vec{k}')$ is the permittivity tensor in the rest system $(x'y'z')$, w the wave frequency in the system xyz, w' the frequency in the system $x'y'z'$, $\vec{k}$ is the wave vector in the system xyz, $\vec{k}'$ the wave vector in the system $x'y'z'$ and $v(x,y,z)$ is the system velocity.

Now, for an isotropic plasma, i.e. when the dielectric tensor is considered in the rest system, the expression for it has the form $\varepsilon'_{ij}=\varepsilon'\delta_{ij}$, and the previous formulae becomes:

$$\varepsilon_{ij}(w,\vec{k})=\left(1-\frac{w_p^2}{w^2}\right)\delta_{ij}-\frac{w_p^2}{w^2}\frac{(v_i k_j+k_i v_j)}{w'}-\frac{w_p^2}{w^2}\frac{k^2 v_i v_j}{w'^2},\qquad(2)$$

this relation suggests that the anisotropy appears in the system due to the movement of the plasma, moreover simultaneously with the temporal dispersion of electromagnetic wave (w dependence) the spatial dispersion takes place ($\vec{k}$ dependence). The equation (2) represents the general expression for the dielectric permittivity tensor ε_{ij} in a moving isotropic electron plasma.

In the rest frame the tensor ε'_{ij} for a magnetoactive plasma can be described in the common form:

$$\varepsilon' = \begin{pmatrix} \varepsilon_\perp & ig & 0 \\ -ig & \varepsilon_\perp & 0 \\ 0 & 0 & \varepsilon_\parallel \end{pmatrix}, \tag{3}$$

where:

$$\varepsilon_\perp = 1 - \frac{w_p^2}{w^2 - w_b^2}, \quad g = \frac{-w_p^2 w_b}{w(w^2 - w_b^2)}, \quad \varepsilon_\parallel = 1 - \frac{w_p^2}{w^2}$$

w_p is the plasma frequency, and w_b gyrofrequency.

The substitution of previous expression for the tensor ε'_{ij} into general equation (1) lets us to obtain the different components of the dielectric tensor of permittivity ε_{ij} in the laboratory system, which can be written as:

$$\begin{aligned} \varepsilon_{xx} &= 1 + \frac{w'^2}{w^2}(\varepsilon_\perp - 1) + 2\frac{w'^2}{w^2}\frac{v_x k_x}{w'}(\varepsilon_\perp - 1) + \\ &+ \frac{w'^2}{w^2}\frac{v_x^2}{w'^2}(\varepsilon_\perp k_\perp^2 + \varepsilon_\parallel k_z^2 - k^2); \end{aligned} \tag{4}$$

$$\begin{aligned} \varepsilon_{yy} &= 1 + \frac{w'^2}{w^2}(\varepsilon_\perp - 1) + 2\frac{w'^2}{w^2}\frac{v_y k_y}{w'}(\varepsilon_\perp - 1) + \\ &+ \frac{w'^2}{w^2}\frac{v_y^2}{w'^2}\left[(k_x^2 + k_y^2)\varepsilon_\perp + k_z^2\varepsilon_\parallel - k^2\right]; \end{aligned} \tag{5}$$

$$\begin{aligned} \varepsilon_{zz} &= 1 + \frac{w'^2}{w^2}(\varepsilon_\parallel - 1) + 2\frac{w'^2}{w^2}\frac{v_z k_z}{w'}(\varepsilon_\parallel - 1) + \\ &+ \frac{w'^2}{w^2}\frac{v_z^2}{w'^2}\left[(k_x^2 + k_y^2)\varepsilon_\perp + k_z^2\varepsilon_\parallel - k^2\right]; \end{aligned} \tag{6}$$

$$\begin{aligned} \varepsilon_{xy} &= \frac{w'^2}{w^2}ig + \frac{w'^2}{w^2}\frac{ig}{w'}(v_x k_x + v_y k_y) + \frac{w'^2}{w^2}\frac{(\varepsilon_\perp - 1)}{w'}(v_x k_y + v_y k_x) + \\ &+ \frac{w'^2}{w^2}\frac{v_x v_y}{w'^2}\left[(k_x^2 + k_y^2)\varepsilon_\perp + k_z^2\varepsilon_\parallel - k^2\right]; \end{aligned} \tag{7}$$

$$\varepsilon_{yx} = -\frac{w'^2}{w^2}ig - \frac{w'^2}{w^2}\frac{ig}{w'}(v_x k_x + v_y k_y) + \frac{w'^2}{w^2}\frac{(\varepsilon_\perp - 1)}{w'}(v_x k_y + v_y k_x) +$$

$$+ \frac{w'^2}{w^2}\frac{v_x v_y}{w'^2}\left[(k_x^2 + k_y^2)\varepsilon_\perp + k_z^2\varepsilon_\parallel - k^2\right]; \quad (8)$$

$$\varepsilon_{xz} = \frac{w'^2}{w^2}\frac{v_x k_z}{w'}(\varepsilon_\parallel - 1) + \frac{w'}{w}\frac{k_x v_z}{w}(\varepsilon_\perp - 1) + ig\frac{w'}{w}\frac{v_z k_y}{w} +$$

$$+ \frac{w'^2}{w^2}\frac{v_x v_z}{w'^2}\left[(k_x^2 + k_y^2)\varepsilon_\perp + k_z^2\varepsilon_\parallel - k^2\right]; \quad (9)$$

$$\varepsilon_{xx} = \frac{w'^2}{w^2}\frac{v_x k_z}{w'}(\varepsilon_\parallel - 1) + \frac{w'}{w}\frac{k_x v_z}{w}(\varepsilon_\perp - 1) - ig\frac{w'}{w}\frac{v_z k_y}{w} +$$

$$+ \frac{w'^2}{w^2}\frac{v_x v_z}{w'^2}\left[(k_x^2 + k_y^2)\varepsilon_\perp + k_z^2\varepsilon_\parallel - k^2\right]; \quad (10)$$

$$\varepsilon_{yz} = \frac{w'^2}{w^2}\frac{v_y k_z}{w'}(\varepsilon_\parallel - 1) + \frac{w'}{w}\frac{k_y v_z}{w}(\varepsilon_\perp - 1) - ig\frac{w'}{w}\frac{v_z k_x}{w} +$$

$$+ \frac{w'^2}{w^2}\frac{v_y v_z}{w'^2}\left[(k_x^2 + k_y^2)\varepsilon_\perp + k_z^2\varepsilon_\parallel - k^2\right]; \quad (11)$$

$$\varepsilon_{zy} = \frac{w'^2}{w^2}\frac{v_y k_z}{w'}(\varepsilon_\parallel - 1) + \frac{w'}{w}\frac{k_y v_z}{w}(\varepsilon_\perp - 1) + ig\frac{w'}{w}\frac{v_z k_x}{w} +$$

$$+ \frac{w'^2}{w^2}\frac{v_y v_z}{w'^2}\left[(k_x^2 + k_y^2)\varepsilon_\perp + k_z^2\varepsilon_\parallel - k^2\right], \quad (12)$$

as it can be seen in these relations, the dielectric tensor in the laboratory system forms a hermitic matrix ($\varepsilon = \varepsilon^H$). Moreover, due to the global movement of the plasma the anisotropic character of the system increases and wave-plasma processes change.

3. THE INVARIANT REPRESENTATION

Using the diada operation any hermitic dielectric tensor of permittivity can be written in the invariant representation as [4]:

$$\varepsilon^{-1} = a + b(C_1 \cdot C_2^* + C_2 \cdot C_1^*) \quad (13)$$

where:

$$C_1 = \left(\frac{a_1}{\sqrt{2}}, -i\frac{a_1}{\sqrt{2}}, a_3\right) \qquad C_2 = \left(\frac{-a_1}{\sqrt{2}}, i\frac{a_1}{\sqrt{2}}, a_3\right)$$

$$a_1 = \sqrt{\frac{\alpha_2 - \alpha_1}{\alpha_3 - \alpha_1}} \qquad a_3 = \sqrt{\frac{\alpha_3 - \alpha_2}{\alpha_3 - \alpha_1}}$$

$a = \alpha_2$, $b = (\alpha_3 - \alpha_1)/2$, C_1 and C_2 are the denominated axes of the tensor ε^{-1} and $\alpha_1, \alpha_2, \alpha_3$ are the corresponding eigenthvalues.
Working with the general expression for the Frenel dispersion [3] and with the dielectric tensor of permittivity in its invariant representation (13) it is not difficult now to deduce the expression for the refractive index in the invariant representation [5]:

$$\frac{1}{n_\pm^2} = a + b\left([\vec{n}C_1][\vec{n}C_2^*] \pm \sqrt{[\vec{n}C_1]^2[\vec{n}C_2]^2}\right). \tag{14}$$

Moreover, probable directions for the magnetic field in the electromagnetic radiation will be defined by the following expressions:

$$H_+ \parallel \left(\frac{[\vec{m}C_1]}{\sqrt{[\vec{m}C_1]^2}} + \frac{[\vec{m}C_2]}{\sqrt{[\vec{m}C_2]^2}}\right) \tag{15a}$$

$$H_- \parallel \left(\frac{[\vec{m}C_1]}{\sqrt{[\vec{m}C_1]^2}} - \frac{[\vec{m}C_2]}{\sqrt{[\vec{m}C_2]^2}}\right) \tag{15b}$$

where $\vec{m} = n\,\vec{n}$, n is the refractive index and $\vec{n}$ is the direction of the wave propagation.

The general formulaes given above represent the solution of the dispersion equation in invariant representation for a plasma with two optical axes. We have called "optical axes" those directions along which the refractive index has only one value. Obviously for this case the equation (14) must satisfy the condition $[\vec{n}C_1]^2 = 0$ or $[\vec{n}C_2]^2 = 0$. On the other hand equations (15) present the orientation of the magnetic field in the wave and consequently let us to know its state of polarization. For instance, in systems transparent along these directions, the electromagnetic wave does not have any definite polarization condition, and the direction of the magnetic field H remains indeterminate. In absorbing systems these directions are characterized by a circular polarization. Therefore, the condition for concurrence of the refractive indexes is equivalent to the condition for the presence of circular polarization in the radiation.

4. DISPERSION EQUATIONS

In this section the expressions for dispersion equations for electromagnetic waves propagating in a moving plasma both with (anisotropic case) and without (isotropic case) an external magnetic field are presented. We assume that the system is moving along the axis x, the magnetic field is located along z

axis ann the waves are propagating in the xz plane. With this assumptions the reverse dielectric tensor of permittivity ε_{ij}^{-1} is expressed in the standart invariant form (13). The refractive indexes and the dispersion equations are derived the same way as above.

4.1. Isotropic Plasma

If the magnetic field is negleted the electron plasma in the rest frame may be considered isotropic and the permittivity dielectric tensor in the laboratory system is defined by the formulae (2). Consequently the axes of the inverse tensor ε_{ij}^{-1} are given in this case by:

$$C_1 = \frac{1}{\sqrt{1+\mathcal{A}^2}}(a_1+a_3\mathcal{A}, 0, a_1\mathcal{A}-a_3) \quad C_2 = \frac{1}{\sqrt{1+\mathcal{A}^2}}(-a_1+a_3\mathcal{A}, 0, -a_1\mathcal{A}-a_3)$$

where

$$\mathcal{A} = \frac{(\varepsilon_{yy}-\varepsilon_{xx}+B)}{2\varepsilon_{xz}}, \quad B = \sqrt{(\varepsilon_{yy}-\varepsilon_{xx})^2+4\varepsilon_{xz}^2},$$

the eigenthvalues have the following form:

$$\alpha_1 = \frac{2}{(\varepsilon_{xx}+\varepsilon_{yy})+B}, \quad \alpha_2 = \frac{1}{\varepsilon_{yy}}, \quad \alpha_3 = \frac{2}{(\varepsilon_{xx}+\varepsilon_{yy})-B}.$$

From these expressions and from the formulae (14) the dispersion equations in the isotropic case can be obtained in the form:

$$2\frac{v}{c}\sin\theta\Big(1-\frac{w_p^2}{w^2}\cos^2\theta\Big)n_+^3 - \Big(1-\frac{w_p^2}{w^2}\Big)n_+^2 -$$

$$-2\frac{v}{c}\Big(1-\frac{w_p^2}{w^2}\Big)\sin\theta n_+ + \Big(1-\frac{w_p^2}{w^2}\Big)^2 = 0; \tag{16}$$

$$2\frac{v}{c}\sin\theta\Big(1+\frac{w_p^2}{w^2}\cos^2\theta\Big)n_-^3 - \Big(1-\frac{w_p^2}{w^2}\Big)n_-^2 -$$

$$-2\frac{v}{c}\Big(1-\frac{w_p^2}{w^2}\Big)\sin\theta n_- + \Big(1-\frac{w_p^2}{w^2}\Big)^2 = 0 \tag{17}$$

where n_+ and n_- are the refractive indexes. It is neccesary to note that for each direction of propagation of the radiation, there is a definite dielectric tensor of permittivity. Consequently the interaction of electromagnetic waves with the plasma and the polarization state of the waves depends on the direction of wave propagation $\vec{n}$. The equations (16) and (17) had been evaluated for two particular cases: transversal propagation and longitudinal propagation.

For the transversal propagation perpendicular to direction of the plasma displacement ($\theta = \frac{\pi}{2}$) the first optical axis was found, it corresponds to the refractive index

$$n_+^2 = n_-^2 = 1 - \frac{w_p^2}{w^2}. \tag{18}$$

For the longitudinal propagation along the plasma velocity direction ($\theta = 0$), the second optical axis is characterized by:

$$n_+^2 = n_-^2 = 1 - \frac{w_p^2}{w^2}. \tag{19}$$

The results show, that in these directions we have presence of optical axes, and the movement of the system does not influence the propagation of the waves, and therefore only ordinary waves are propagating. This is known in the literature as Frenel's effect.

4. 2. Anisotropic Plasma

For a plasma moving in an external magnetic field the vector that defines the directions of the axes of the tensor ε_{ij}^{-1} can be written as:

$$C_1 = \left(\frac{a_1}{\sqrt{1+\mathcal{A}^2}}, i\frac{a_1\mathcal{A}}{\sqrt{1+\mathcal{A}^2}}, a_3\right) \qquad C_2 = \left(\frac{-a_1}{\sqrt{1+\mathcal{A}^2}}, -i\frac{a_1\mathcal{A}}{\sqrt{1+\mathcal{A}^2}}, a_3\right)$$

where

$$\mathcal{A} = -\frac{\varepsilon_{yy} - \varepsilon_{xx} + \sqrt{(\varepsilon_{yy} - \varepsilon_{xx-})^2 + 4G^2}}{2G},$$

$$G = \frac{w'^2}{w^2} g\left(1 + \frac{vk}{w'}\right), \quad B = \sqrt{(\varepsilon_{yy} - \varepsilon_{xx})^2 + 4G^2}$$

$$\alpha_1 = \frac{1}{2}(\varepsilon_{xx} + \varepsilon_{yy} + B) \qquad \alpha_2 = \frac{1}{2}(\varepsilon_{xx} + \varepsilon_{yy} - B) \qquad \alpha_3 = \varepsilon_{zz}.$$

The eigenvalues and eigenvectors of the dielectric tensor of permittivity are as following:

$$\varepsilon^{-1}(C_1 - C_2) = \lambda_1(C_1 - C_2)$$

$$\lambda_1 = \alpha_2 - \frac{(\alpha 3 - \alpha_1)}{2}(1 - C_1 C_2^*)$$

$$\varepsilon^{-1}[C_1C_2] = \lambda_2[C_1C_2]$$
$$\lambda_2 = \alpha_2$$

$$\varepsilon^{-1}(C_1 + C_2) = \lambda_3(C_1 + C_2)$$
$$\lambda_3 = \alpha_2 + \frac{(\alpha 3 - \alpha_1)}{2}(1 + C_1C_2^*)$$

For the transversal propagation perpendicular to the external magnetic field $\theta = \frac{\pi}{2}$ the dispertion equation and refractive index are as following:

$$n_+^2 = 1 - \frac{w_p^2}{w^2} \tag{20a}$$

$$2\frac{v}{c}n^3 - \left[1 - \frac{(w_b^2 + w_p^2)}{w^2}\right]n^2 - 2\frac{v}{c}\left(1 - \frac{w_p^2}{w^2}\right)n + \left[\left(1 - \frac{w_p^2}{w^2}\right)^2 - \frac{w_b^2}{w^2}\right] = 0. \tag{20b}$$

The solution of this equation, in the case of a rarefied plasma $n \approx 1$, can be written in the form:

$$n_-^2 = 1 - \frac{w_p^2\left(1 - \frac{w_p^2}{w^2} - \frac{v}{c}\right)}{w^2\left(1 - \frac{w_b^2}{w^2} - \frac{w_p^2}{w^2} - \frac{2v}{c}\right)}, \tag{21}$$

For the longitudinal propagation along of the external magnetic field ($\theta = 0$) we have:

$$n_+^2 = 1 - \frac{w_p^2}{w(w + w_b)}$$
$$n_-^2 = 1 - \frac{w_p^2}{w(w - w_b)} \tag{22}$$

where n_+, n_- are the solutions for the refractive index.
In this direction an optical axis is present. The general motion of the plasma does not influence the propagation of the electromagnetic waves and the wave is refracting following the ordinary refraction law.

In the preceding paragraphs the solution of the dispertion equations was discussed only for some particular directions of waves propagation. However we had derived similar expressions for the case of arbitrary propagation of electromagnetic waves in respect to the external magnetic field and plasma velocity directions. These results with applications to the solar corona and solar wind will be presented in additional papers which are now in work.

The suggested model describes the interaction of electromagnetic waves with a space plasma and can be applied for an estimation of the angular deflexion of the radiation coming to the observer from a far radio source and passing trought a plasma located in the ray path. It is possible to estimate corrections to the values of the gradients in the magnetic field and electron density distributions mesuaring this angular displacement and taking into account the general movement of the dispersive medium.

REFERENCES

1. Bastian T.S. // Astrophys. Jorn. 1995. V. 426. № 2. P. 774.
2. Gnedin Y.N., and Lopez E.D. // Solar Physics. 1995. (in press).
3. Ginsburg V.L. Propagation of electromagnetic waves in plasma. — M.: Science, 1967.
4. Fedorov F.I. // Optica and Spectr. 1956. V. 1. P. 926.
5. Fedorov F.I. // Optica and Spectr. 1957. V. 2. P. 775.
6. Zheleznyakov V.V. Electromagnetic waves in the space plasma. — M.: Science, 1977.
7. Zheleznyakov V.V. Radio radiation of sun and planets. — M.: Science, 1964.
8. Gnedin Y.N. // Soviet Astron. Lett. 1987. V. 13. № 2. P. 105.

Central Astronomical Observatory
at Pulkovo,
Escuela Politecnica Nacional,
Ecuador

Поступила в редакцию
4 декабря 1995 г.